USAAEFA PROJECT NO. 77-38

(12) LEVEL II

PRODUCTION VALIDATION TEST-GOVERMENT KAMAN K747 IMPROVED MAIN ROTOR BLADE

FINAL REPORT

VERNON L. DIEKMANN
PROJECT OFFICER

TOM P. BENSON
SENIOR PROJECT ENGINEER

FRAME J. BOWERS
CPT, ARMOR
US ARMY
PROJECT ENGINEER

RALPH WORATSCHEK
PROJECT ENGINEER

GEORGE M. MULLEN
MAJ, IN
US ARMY
PROJECT PILOT

JOHN S. TULLOCH
CW4, USA
US ARMY
PROJECT PILOT

OCTOBER 1979

Approved for public release; distribution unlimited.

UNITED STATES ARMY AVIATION ENGINEERING FLIGHT ACTIVITY
EDWARDS AIR FORCE BASE, CALIFORNIA 93523

DISCLAIMER NOTICE

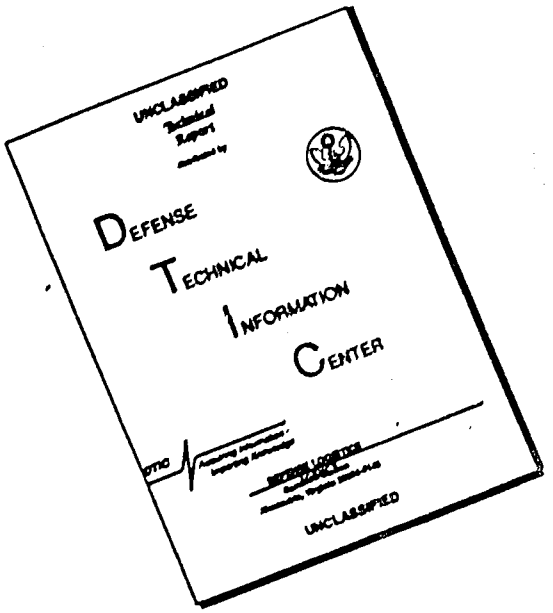

THIS DOCUMENT IS BEST QUALITY AVAILABLE. THE COPY FURNISHED TO DTIC CONTAINED A SIGNIFICANT NUMBER OF PAGES WHICH DO NOT REPRODUCE LEGIBLY.

DISCLAIMER NOTICE

The findings of this report are not to be construed as an official Department of the Army position unless so designated by other authorized documents.

DISPOSITION INSTRUCTIONS

Destroy this report when it is no longer needed. Do not return it to the originator.

TRADE NAMES

The use of trade names in this report does not constitute an official endorsement or approval of the use of the commercial hardware and software.

UNCLASSIFIED
SECURITY CLASSIFICATION OF THIS PAGE (When Data Entered)

REPORT DOCUMENTATION PAGE

READ INSTRUCTIONS BEFORE COMPLETING FORM

1. REPORT NUMBER: USAAEFA PROJECT NO. 77-38
2. GOVT ACCESSION NO.
3. RECIPIENT'S CATALOG NUMBER: Final Rept.

4. TITLE (and Subtitle): PRODUCTION VALIDATION TEST -- GOVERNMENT KAMAN K747 IMPROVED MAIN ROTOR BLADE
5. TYPE OF REPORT & PERIOD COVERED: September–December 1978
6. PERFORMING ORG. REPORT NUMBER: USAAEFA PROJECT NO. 77-38

7. AUTHOR(s): Vernon L. Diekmann, Tom P. Benson, CPT Frame J. Bowers, Ralph Woratschek, MAJ George M. Mullen, CW4 John S. Tulloch
8. CONTRACT OR GRANT NUMBER(s)

9. PERFORMING ORGANIZATION NAME AND ADDRESS: US ARMY AVIATION ENGINEERING FLIGHT ACTIVITY, EDWARDS AIR FORCE BASE, CALIFORNIA 93523
10. PROGRAM ELEMENT, PROJECT, TASK AREA & WORK UNIT NUMBERS: 1K-8-ET-M17-02-1K-EC

11. CONTROLLING OFFICE NAME AND ADDRESS: US ARMY AVIATION ENGINEERING FLIGHT ACTIVITY, EDWARDS AIR FORCE BASE, CALIFORNIA 93523
12. REPORT DATE: OCTOBER 1979
13. NUMBER OF PAGES

14. MONITORING AGENCY NAME & ADDRESS (if different from Controlling Office)
15. SECURITY CLASS. (of this report): UNCLASSIFIED
15a. DECLASSIFICATION/DOWNGRADING SCHEDULE

16. DISTRIBUTION STATEMENT (of this Report)

Approved for public release; distribution unlimited.

17. DISTRIBUTION STATEMENT (of the abstract entered in Block 20, if different from Report)

18. SUPPLEMENTARY NOTES

19. KEY WORDS (Continue on reverse side if necessary and identify by block number)

Acoustical Characteristics
Hover and Level Flight Performance
K747 Improved Main Rotor Blades (IMRB)
Production Validation Test - Government

20. ABSTRACT (Continue on reverse side if necessary and identify by block number)

The United States Army Aviation Engineering Flight Activity conducted a Production Validation Test - Government of the Kaman K747 improved main rotor blades (K747 IMRB) installed on a Bell Helicopter Company Production AH-1S helicopter from September through December 1978. A special test of the in-flight acoustical characteristics of the K747 IMRB was conducted in conjunction with the National Aeronautics and Space Administration (NASA) and the Aeromechanics Laboratory, US Army Research and Technology Laboratories, US Army Aviation Research and Development Command during October 1978. The performance testing consisted of out-of-ground-effect (OGE) hover and level flight in California at Bishop (4120-foot elevation), Coyote Flats (9950-foot

DD FORM 1 JAN 73 1473 EDITION OF 1 NOV 65 IS OBSOLETE

UNCLASSIFIED
SECURITY CLASSIFICATION OF THIS PAGE (When Data Entered)

elevation). Bakersfield (488-foot elevation), and Edwards AFB (2302-foot elevation). Hover and level flight performance and acoustic characteristics of the AH-1S were evaluated for both K747 IMRB and the B540 main rotor blades (B540 MRB). The K747 IMRB demonstrated a 3.3 percent (310 lb increase in gross weight at Army hot day conditions) improvement in OGE hover performance. The AH-1S configured with the K747 IMRB required slightly more power in level flight for coefficient of thrust (C_T) less than approximately 0.0054 and significantly less power required for C_T's more than approximately 0.0054 when compared to the B540 MRB configuration. A C_T of 0.0054 corresponds to a gross weight of 8780 pounds at 324 rpm, 4000 feet pressure altitude (H_p), 35°C or a gross weight of 10,000 pounds at 324 rpm, 2840 feet H_p, standard day. High-speed impulsive noise was determined by personnel of the Aeromechanics Laboratory to be considerably lower with the K747 IMRB. Two shortcomings, the excessive shift in airspeed position error with power application and the large deviation in airspeed position errors throughout the level flight airspeed envelope, were identified neither of which were attributed to the blade type. Two equipment performance reports (EPR) on the K747 IMRB maintenance and repair procedures were submitted. Two EPR's were submitted on the AH-1S.

DEPARTMENT OF THE ARMY
HQ, US ARMY AVIATION RESEARCH AND DEVELOPMENT COMMAND
4300 GOODFELLOW BOULEVARD, ST. LOUIS, MO 63120

DRDAV-D

SUBJECT: Directorate for Development and Qualification Position on the Final Report of USAAEFA Project No. 77-38, Production Validation Test - Government Kaman K747 Improved Main Rotor Blade, Oct 79

SEE DISTRIBUTION

1. The Directorate for Development and Qualification position on USAAEFA's report is provided herein. Paragraph numbers from the subject report are provided for reference.

a. Paragraph 8, 9, and 21 - The desired (R.F.Q.) hover performance improvement with the Improved Main Rotor Blade (IMRB) was 6 percent increase in Out of Ground Effect (OGE) hover gross weight at 4000 feet and 95°F at military rated power. The hover performance of the B540 and K747 rotors were both estimated by analytical methods and the hover performance improvement stated in the detail specification was established as the difference between the estimated performance of the two rotors. The detail specification for the Kaman IMRB states, "The AH-1S configured with the improved blade shall have the capability to hover out of ground effect at a gross weight 8.7 percent greater than the AH-1S configured with main rotor blades P/N 540-011-250-1, for conditions of military rated power (T53-L-703 engine), 4000 feet pressure altitude and 95°F ambient temperature."

Early flight testing with the prototype K747 IMRB indicated a 3% increase in OGE hover gross weight and it was anticipated that the production blades would provide an additional one percent increase in OGE hover gross weight due to leading edge contour clean up. As stated in paragraph 21, the production K747 IMRB demonstrated a 3.4 percent increase in OGE hover gross weight at the Army hot day conditions. The 3.3 percent value given in paragraphs 8 and 9 is in error.

b. Paragraphs 13, 14, and 21 - Although not anticipated, there is considerable difference in the power required in forward flight between the B540 and K747 rotors. The difference in power required is a function of gross weight and density altitude. The power required with the K747 blades is significantly reduced over that of the B540 blades at high gross weights and high altitudes, however; the power required with the K747 blades at low altitudes and low gross weight is slightly increased. These differences in power required result in variations in fuel consumption and speed capabilities. For the high altitude (10,000 ft) high gross weight (10,000 lbs) example of paragraph 14 the K747 rotor provides an increase in maximum specific range of 25 percent and 22 knots increase in maximum speed. For the low altitude (sea level) low gross weight (8,700 lbs) example the K747 rotor reduces maximum specific range only 5 percent and decreases maximum speed only 5 knots.

DRDAV-D
SUBJECT: Directorate for Development and Qualification Position on the Final Report of USAAEFA Project No. 77-38, Production Validation Test - Government Kaman K747 Improved Main Rotor Blade, Oct 79

c. Paragraphs 20, 22b, and 22c - As noted in paragraph 20, the excessive shift in airspeed with power application is a shortcoming and a more accurate airspeed system is desirable. The performance data presentation of the operator's manual is in terms of level flight indicated airspeed; therefore, the level flight errors do not constitute a severe operational problem. Because the operator's manual data is based on the assumption that the position error is the same for climb as level flight a relatively large error (up to 15 knots) in best climb speed will result. This error in climb speed will reduce the maximum rate of climb up to 3 percent and will result in a reduction in specific range in climb up to 30 percent. Unless some simple method can be found to correct the position error in climb without a drastic change in the level flight position error it would not be cost effective since the expected benefits are small and a change in level flight airspeed calibration would require a substantial operator's manual change. Should the AH-1S be qualified for flight under instrument meteorological conditions (IMC) the position error will become a significant problem, possibly requiring correction.

2. Although not covered by this testing, other primary objectives of the IMRB program were to provide improvements in survivability, reliability, maintainability, erosion protection, and retirement life. Significant improvements were achieved in all of these areas by the K747 IMRB, especially the retirement life which is almost unlimited (10,000 hrs) compared to 1100 hours for the B540 blades.

FOR THE COMMANDER:

CHARLES C. CRAWFORD, JR.
Director of Development
and Qualification

PREFACE

Special thanks are offered to Mr. Steve Strom of Sierra Pacific Airlines (Bishop), Mr. Rick English, the Mobil Oil distributor (Bakersfield), and Mr. Jim Glass of CALTRANS, all of whom provided valuable assistance and the use of their facilities during those portions of the test conducted at Bakersfield and Bishop, California. In addition, the cooperation and courtesies offered by Mr. Everett J. Julkowski, manager of Meadows Field (Bakersfield), and by Mr. William L. Young, manager of the Bishop Airport, proved invaluable.

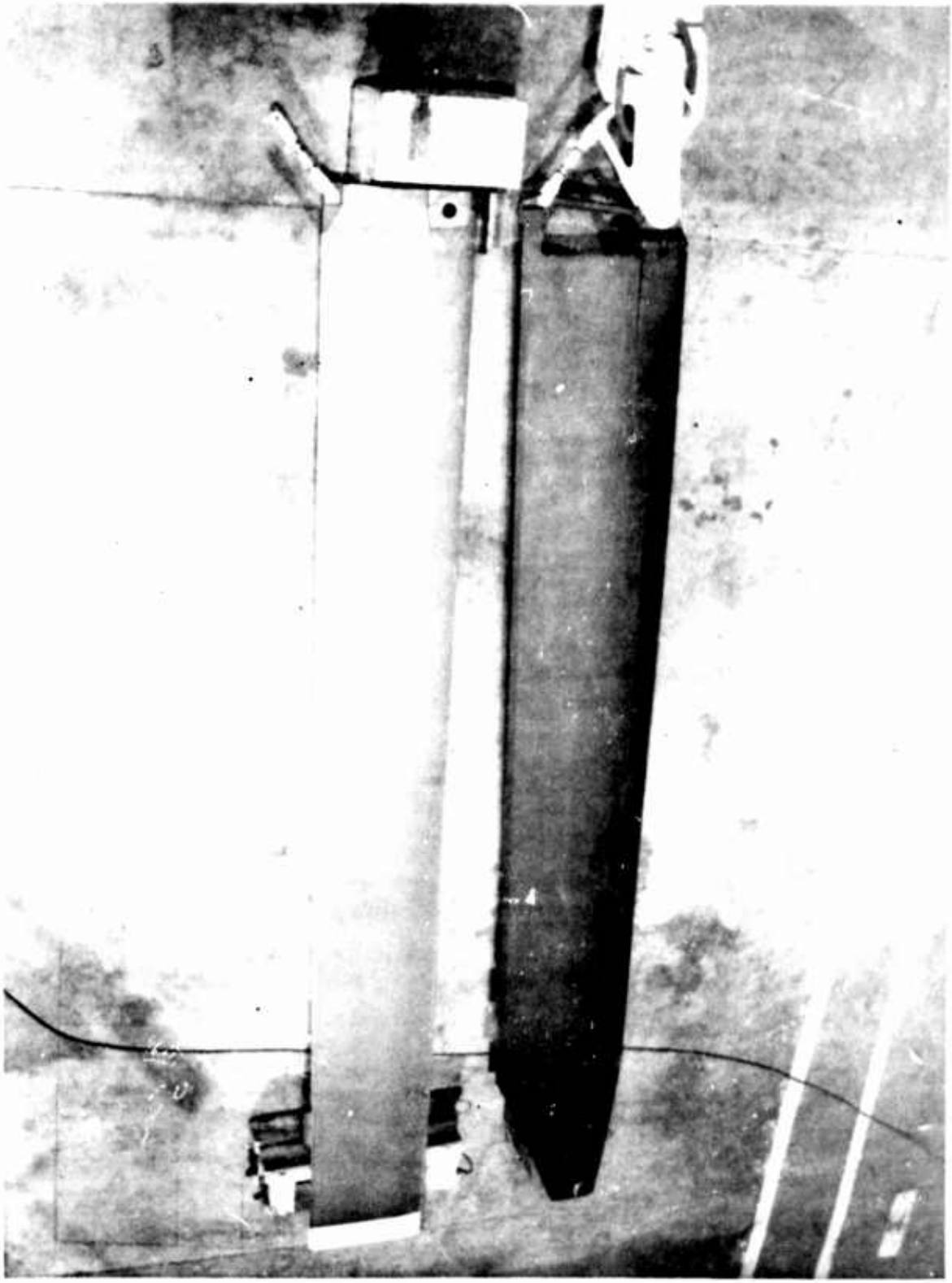

TABLE OF CONTENTS

THIS PAGE INTENTIONALLY BLANK

INTRODUCTION

BACKGROUND

1. The K747 improved main rotor blades (K747 IMRB) featuring an advanced design airfoil, tapered tip planform, composite material construction, and a multi-cell ballistically tolerant spar were developed by the Kaman Aerospace Corporation (KAC). The blade was designed to improve hover performance, maintainability and reliability while reducing ballistic vulnerability. The prototype K747 IMRB were evaluated during a preliminary airworthiness evaluation (ref 1, app A) and airworthiness and flight characteristics evaluation (ref 2). Data obtained from these previous tests indicated that the K747 IMRB did not achieve the government's desired level of increased performance when compared to the standard Bell Helicopter Textron (BHT) B540 main rotor blades (B540 MRB). The US Army Aviation Engineering Flight Activity (USAAEFA) was tasked by the Army Aviation Research and Development Command (AVRADCOM) to conduct a Production Validation Test - Government of an AH-1S (PROD) helicopter equipped with production K747 IMRB. The AH-1S was also tested with B540 MRB to provide baseline data. AVRADCOM also tasked USAAEFA to conduct in-flight acoustic testing to compare the K747 IMRB and the B540 MRB sound level in various flight profiles. A test plan was submitted (ref 3) in August 1978, and an airworthiness release (ref 4) was issued in October 1978.

TEST OBJECTIVES

2. The test objectives were:

a. Quantify the hover and level flight performance capability of the K747 IMRB and compare with the B540 MRB installed on a AH-1S (PROD) helicopter.

b. Quantify the acoustic signature characteristics of the K747 IMRB and B540 MRB.

DESCRIPTION

3. The standard B540 MRB, manufactured by BHT, has an aluminum spar and skin and nomex honeycomb core. The rectangular planform incorporates a negatively twisted leading edge and constant chord symmetrical airfoil cross section with a special symmetrical blade tip. The K747 IMRB have a multi-cell filament wound spar, nomex core, fiberglass skin and Kevlar trailing edge. Design of the K747 IMRB includes combining two nonsymmetrical airfoil cross sections with a tapered blade tip. The K747 IMRB was designed to be similar to the B540 MRB in dynamic characteristics. A detailed description of these blades is contained in appendix B.

4. The test aircraft, serial number 76-22573 was a production AH-1S. This helicopter is powered by a Lycoming T53-L-703 engine rated at 1800 shaft horsepower (shp) at sea level standard day conditions. Engine operation is transmission limited to 1134 shp continuous and 1290 shp for 30 minutes. At airspeeds greater than 100 KIAS engine operation is limited to 1134 shp. Distinctive features of this helicopter include a flat plate canopy and model 212 tail rotor. A more complete description is presented in the operator's manual (ref 5, app A).

TEST SCOPE

5. Evaluation of the K747 IMRB was conducted in California at Bishop (4120-foot elevation), Coyote Flats (9980-foot elevation), Bakersfield (488-foot elevation), and Edwards AFB (2302-foot elevation) and consisted of out-of-ground-effect (OGE) hover and level flight performance testing. The acoustic characteristics were measured using a NASA Ames Research Center YO-3A aircraft for forward and descending flight profiles at Edwards Air Force Base. Performance and acoustic testing during the evaluation period of 1 September to 31 December 1978 consisted of 47 flights and 38 productive flight hours. Acoustical measurement, data reduction and evaluation were performed by Aeromechanics Laboratory, US Army Research and Technology Laboratories, AVRADCOM.

6. The same AH-1S was used for all testing, and the limits of the operator's manual as modified by the airworthiness release were observed. General test conditions are listed in table 1.

Table 1. Test Conditions[1]

Type of Test	Blade Type	Gross Weight (LB)	Density Altitude (FT)	Trim True Airspeed (KT)	Referred Rotor Speed (RPM)
Hover performance	K747[2]	7740 to 8200	1180 to 10,580	Zero	294 to 330
	B540[3]	7920 to 8080	900 to 4500	Zero	293 to 333
Level flight performance	K747[2]	7980 to 9300	2180 to 11,340	35 to 150	324
	B540[3]	8140 to 9100	1300 to 11,700	34 to 150	324

[1]Forward longitudinal center-of-gravity location (FS 193.7-194.8) clean configuration used for all tests.

[2]Rotor blade serial numbers A2016 and A2025

[3]Rotor blade serial numbers AMR00021 and AMR50107

TEST METHODOLOGY

7. The methods for testing hover and level flight performance are described in appendix D. Acoustic characteristics were measured for both K747 IMRB and B540 MRB. Sound levels and frequency spectrum were measured and recorded through sensitive microphones positioned on the wings and tail of the YO-3A. The AH-1S was flown in formation with the YO-3A at specific relative azimuths, distances, airspeeds, and rates of descent. Sound data were analyzed by the Aeromechanics Laboratory. All flight test data were obtained from on-board instrumentation and recorded on magnetic tape on the test aircraft or telemetered to a ground station. Parameters measured are specified in appendix C.

RESULTS AND DISCUSSION

GENERAL

8. Hover and level flight performance, and acoustic characteristics of the AH-1S (PROD) were evaluated for both K747 IMRB and the B540 MRB. The K747 IMRB demonstrated a 3.3 percent (310 lb increase in gross weight at 4000 feet pressure altitude and 35°C) improvement in OGE hover performance. The AH-1S configured with the K747 IMRB required slightly more power in level flight for a thrust coefficient (C_T) less than approximately 0.0054 and significantly less power for C_T's more than approximately 0.0054 when compared to the B540 MRB configuration. A C_T of 0.0054 corresponds to a gross weight of 8780 pounds at 324 rpm, 4000 feet pressure altitude (H_p), 35°C or a gross weight of 10,000 pounds at 324 rpm, 2840 feet H_p, standard day. High-speed impulsive noise was determined by personnel of the Aeromechanics Laboratory to be considerably lower with the K747 IMRB. Two shortcomings not related to the blade type were identified. Two equipment performance reports (EPR) were submitted on the K747 IMRB and two on the AH-1S.

PERFORMANCE

Hover Performance

9. OGE hover testing was accomplished at test sites with ground elevations of 488, 2302, and 9980 feet above mean sea level. The test conditions are presented in table 1. The tethered hover method was used in all points except the free hover points used to gather minimum thrust data. An OGE hover performance summary is presented in figure 1, appendix E. Nondimensional hover performance of the AH-1S configured with the B540 MRB is presented in figure 2 and with K747 IMRB is presented in figure 3.

10. Hover performance of the aircraft equipped with K747 IMRB was improved over the B540 MRB at all C_T's tested. At the Army hot day condition (35°C, 4000 feet pressure altitude) and military rated power, the maximum OGE hover weight was 9375 pounds with the K747 IMRB. At the same conditions, the maximum OGE hover weight with B540 MRB installed was 9065 pounds. This is a gross weight increase of 310 pounds (3.3 percent improvement) with the K747 IMRB.

Level Flight Performance

11. Level flight performance testing was conducted at the conditions shown in table 1 with the aircraft in the clean configuration using both K747 IMRB and B540 MRB. Power required for level flight, fuel flow, and specific range as functions of airspeed were determined. Additionally, recommended airspeed for long range cruise (V_{cruise}), airspeed for maximum endurance ($V_{max\ end}$), and maximum airpseed for level flight (V_H) were determined. Data were obtained in stabilized level flight (zero sideslip) at incremental airspeeds from 30 knots calibrated airspeed (KCAS) to V_H using the methods described in appendix D.

12. Nondimensional level flight performance summaries are presented in figures 4 through 6, appendix E, for the B540 MRB and figures 7 through 9 for the K747

IMRB. Figures 10 through 19 are dimensional plots of the individual level flight performance tests accomplished. Aircraft specific range, $V_{max\ end}$ and V_{cruise}, and V_H in level flight are summarized in figures 20 through 23.

13. The change in level flight performance of the AH-1S caused by the K747 IMRB varied with C_T. The AH-1S configured with the K747 IMRB required slightly more power for C_T's less than 0.0054 and significantly less power for C_T's more than 0.0054 when compared to the B540 MRB configuration. A C_T of 0.0054 corresponds to a gross weight of 8780 pounds at 324 rpm, 4000 feet H_p, 35°C or a gross weight of 10,000 pounds at 324 rpm, 2840 feet H_p, standard day.

14. Figure A shows a level flight performance comparison at the specific conditions of 10,000 pounds gross weight, 10,000 feet pressure altitude, and standard day. At this condition (C_T = 0.006725), there is an increase in recommended cruise airspeed of approximately 17 knots true airspeed (KTAS) and an improvement in endurance for the K747 IMRB. Figure B shows a level flight performance comparison at a lightly loaded condition (8700 pounds gross weight, sea level, standard day, C_T = 0.004320). This figure shows degraded performance with the K747 IMRB throughout the airspeed range shown. Although faster airspeeds could be obtained at high C_T's with the K747 IMRB installed, the V_H is always less than the never exceed airspeed (V_{NE}).

CONTROL POSITIONS IN TRIMMED FORWARD FLIGHT

15. Control positions in trimmed (zero sideslip) forward flight were evaluated in conjunction with level flight performance tests at the conditions listed in table 1. Test results are presented in figures 24 through 27, appendix E. No significant control position change due to different blade types was noted.

ACOUSTIC CHARACTERISTICS

16. The acoustic signature of the AH-1S was measured by personnel of the Aeromechanics Laboratory for both sets of main rotor blades in tests conducted at Edwards AFB. The acoustic data were measured from the YO-3A as the AH-1S was flown in close formation at relative azimuths of approximately 100, 180, and 260 degrees from the recording YO-3A. Flight profiles included level flight and rates of descent to 1000 feet per minute. High-speed impulsive noise was determined to be considerably lower with the K747 IMRB. The acoustic test results and conclusions prepared by the Aeromechanics Laboratory are presented in appendix G. The internal cockpit noise at the pilot and copilot station was qualitatively judged to be less with the K747 IMRB than with the B540 MRB.

AIRCRAFT EQUIPMENT PERFORMANCE

17. During the evaluation of the K747 IMRB, various skin voids (separation of the blade skin from the nomex honeycomb core) were noticed on both blades. After 7.7 flight hours, two voids had grown in excess of allowable tolerances and a field repair was attempted. The void on the first blade was successfully repaired by KAC personnel but the attempt to repair the second blade resulted in damage to the main spar. This damage occurred because the repair instructions did not describe the precise location of the spar. Two equipment performance reports were submitted: one on the skin voids and the other on the maintenance repair instructions of the

FIGURE A
LEVEL FLIGHT PERFORMANCE COMPARISON
JAH-1S USA S/N 76-22573

GROSS WEIGHT (LB)	LONGITUDINAL CG LOCATION	PRESSURE ALTITUDE (FT)	OAT (°C)	ROTOR SPEED (RPM)	C_T	CONFIGURATION
10,000	FWD	10,000	-4.8	324	.006725	CLEAN

NOTES:
1. SPECIFIC RANGE BASED ON SPECIFICATION FUEL FLOW.
2. SHP VS V_T CURVE DERIVED FROM FIGURES 4 THROUGH 9. APPENDIX E.
3. ZERO SIDESLIP

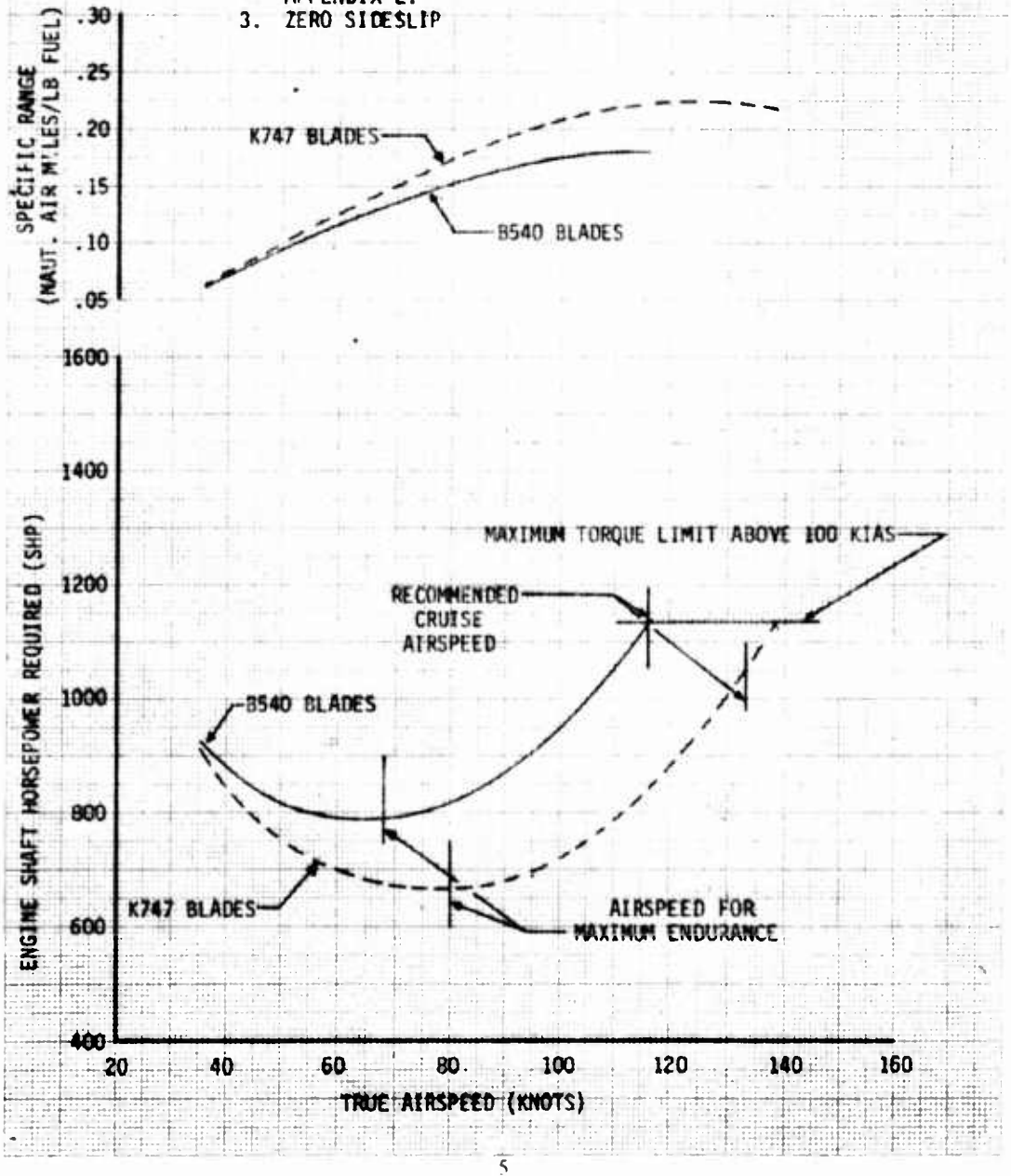

FIGURE B
LEVEL FLIGHT PERFORMANCE COMPARISON
JAH-1S USA S/N 76-22573

GROSS WEIGHT (LB)	LONGITUDINAL CG LOCATION	PRESSURE ALTITUDE (FT)	OAT (°C)	ROTOR SPEED (RPM)	C_T	CONFIGURATION
8700	FWD	SEA LEVEL	15.0	324	.004320	CLEAN

NOTES:
1. SPECIFIC RANGE BASED ON SPECIFICATION FUEL FLOW.
2. SHP VS V_T CURVE DERIVED FROM FIGURES 4 THROUGH 9, APPENDIX E.
3. ZERO SIDESLIP.

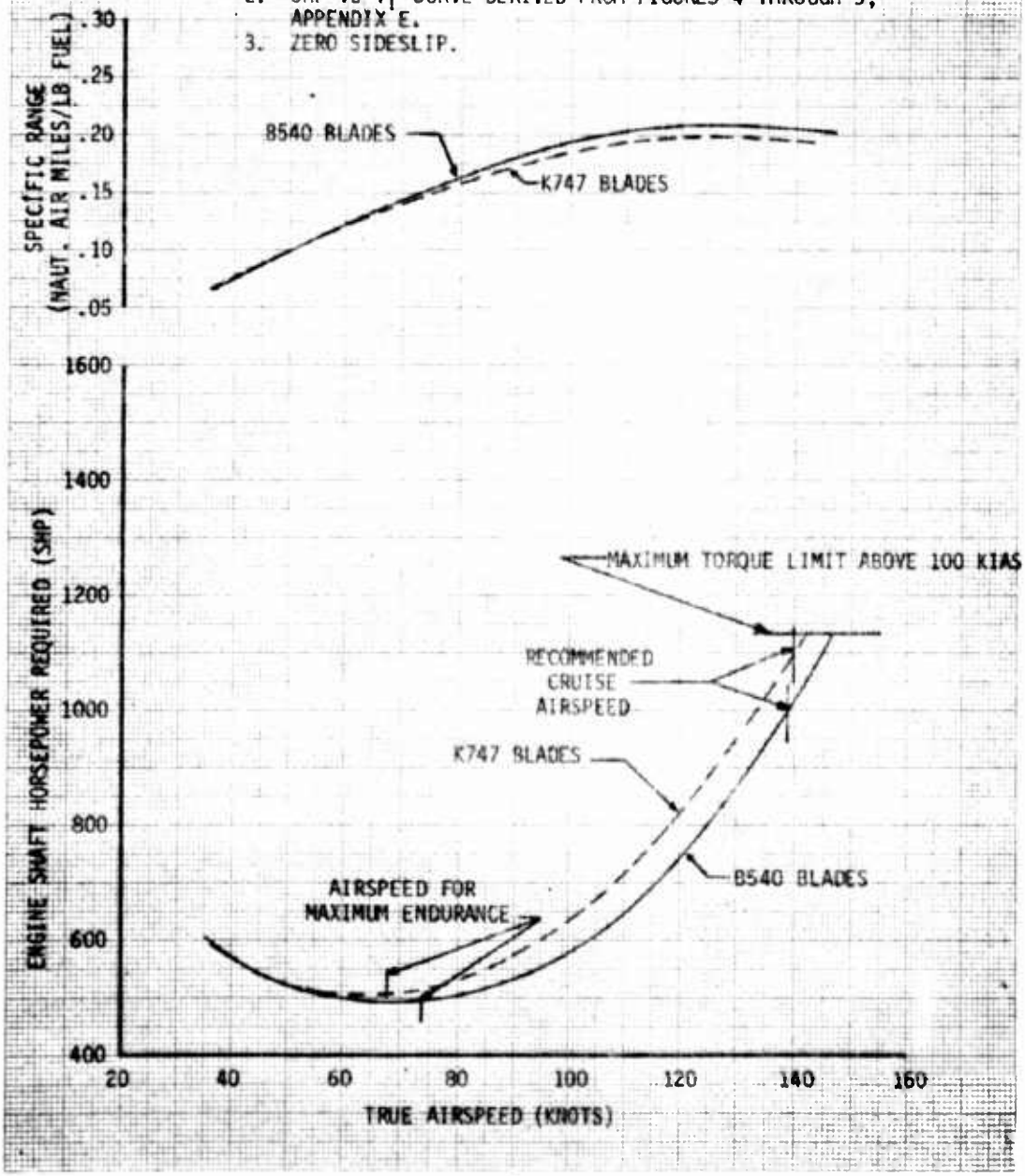

K747 IMRB (EPR 77-38-1 and 77-38-2, app G). In addition to the skin void, the internal insulation blanket located between tail boom stations 80.44 and 122.33 was found charred on the right side where the blanket was attached to the tail boom (EPR 77-38-3, app G).

18. A leaking mast seal led to an inspection of the mast bearing. This inspection revealed excessive radial play in the mast bearing and is a shortcoming. An equipment performance report concerning this shortcoming was submitted (EPR 77-38-4).

SUBSYSTEMS TESTS

Airspeed Calibration

19. The airspeed system was calibrated using both a trailing bomb pitot-static source and ground speed course. The ship's airspeed calibration is presented in figures 28 and 29, app E.

20. In level flight the ship's position error was nonlinear and varied from near zero at 47.5 and 92.0 knots indicated airspeed (KIAS) to +1.5 knots at 65 KIAS and to -10 knots at 150 KIAS. In a 1500 feet per minute rate of climb, the variation of position error with airspeed was slightly nonlinear and varied from -16 knots at 50 KIAS to -12 knots at 115 KIAS. In rates of descent of 1000 feet per minute or greater the position error varied from +10 knots at 30 KIAS to +4 knots at 105 KIAS. The excessive shift in airspeed position error from climbing to descending flight is unsatisfactory and is a shortcoming. The large deviation in airspeed position errors throughout the level flight airspeed envelope is a shortcoming previously noted (ref 8, app A). In stabilized level flight changes in collective position caused an immediate change in airspeed indication. The excessive shift in airspeed position error with power application is a shortcoming. The airspeed position error problems are unrelated to blade type. An equipment performance report concerning this shortcoming was submitted (EPR 77-38-5, app G).

CONCLUSIONS

GENERAL

21. The AH-1S (PROD) with the K747 IMRB demonstrated a 3.4 percent improvement in maximum OGE hover gross weight at Army hot day conditions when compared to the B540 MRB configuration. The AH-1S with the K747 IMRB required slightly more power in level flight for C_T's less than 0.0054 and significantly less power for C_T's more than 0.0054 when compared to the B540 MRB configuration. A C_T of 0.0054 corresponds to a gross weight of 8780 pounds at 324 rpm, 4000 feet H_p, 35°C or a gross weight of 10,000 pounds at 324 rpm, 2840 feet H_p, standard day. High-speed impulsive noise was determined by personnel of the Aeromechanics Laboratory to be considerably lower with the K747 IMRB. There were three shortcomings which were unrelated to the rotor blade type.

SHORTCOMINGS

22. The following shortcomings which were unrelated to blade type were identified:

a. The excessive radial play in the mast bearing (para 18).

b. The excessive shift in airspeed position error with power application (para 20).

c. The large deviation in airspeed position errors throughout the level flight airspeed envelope (para 20).

RECOMMENDATIONS

23. The shortcomings noted in paragraph 22 be corrected as soon as possible.

APPENDIX A. REFERENCES

1. Final Report, USAAEFA, Project No. 76-07, *Army Preliminary Evaluation, Improved Main Rotor Blade Installed on a YAH-1R Helicopter*, June 1977.

2. Final Report, USAAEFA, Project No. 76-08, *Airworthiness and Flight Characteristics Evaluation, Improved Main Rotor Blade Installed on a YAH-1R Helicopter*, November 1977.

3. Test Plan, USAAEFA, Project No. 77-38, *Production Validation Test - Government Kaman K747 Improved Main Rotor Blade*, August 1978.

4. Letter, DARCOM, DRDAV-EQI, 19 October 1978, subject: Airworthiness Release for Kaman K747 Improved Main Rotor Blades (IMRB) Production Validation Test (PVT-G) on AH-1S Helicopter.

5. Technical Manual, TM 55-1520-236-10, *Operator's Manual, Army Model AH-1S (PROD) Helicopter*, 29 April 1977.

6. Letter, Lycoming Division, 20 July 1978, subject: Calibration of T53-L-703 Engine LE131457.

7. Final Report, US Army Aviation Test Activity (USAAVNTA), Project No. 66-06, *Engineering Flight Test AH-1G Helicopter (HUEY COBRA), Phase D, Part 2, Performance*, April 1970.

8. Final Report, USAAEFA, Project No. 77-04, *Army Preliminary Evaluation, YAH-1S Helicopter with Modified Flat Plate Canopy Installed*, August 1977.

9. Engineering Design Handbook, Army Materiel Command, AMCP 706-204, *Helicopter Performance Testing*, August 1974.

10. Flight Test Manual, Naval Air Test Center, FTM No. 102, *Helicopter Performance Testing*, 28 June 1968.

11. Army Regulation AR 310-25, *Dictionary of United States Army Terms*, 15 September 1975.

12. Specification, Lycoming Division of AVCO Corporation, No. 104-43, "Model Specification T53-L-703 (LTCIK-4G) Turboshaft Engine," 1 May 1974.

APPENDIX B. DESCRIPTION

1. B540 MRB utilizes a symmetrical, constant chord airfoil section with a 2024 T_4 aluminum spar and nomex honeycomb core. The K747 IMRB has a multicell filament wound fiberglass spar, a nomex core afterbody and a Kevlar trailing edge spline, all enclosed by fiberglass skin. At the inboard end, cheekplates carry blade loads to an aluminum adapter which attaches the blade to the AH-1 rotor hub using the standard hub pin. The K747 IMRB has the same radius and essentially an equivalent solidity as the standard B540 MRB (0.0625 as compared with 0.0651 for the B540) although the blade planform is changed. The blade linear twist is increased from -10 degrees to -12 degrees and a nonsymmetrical airfoil shape is employed. The blade weight and stiffness distribution for the K747 were designed to match the dynamic characteristics of the B540.

2. The K747 IMRB airfoil shape is based on a family of airfoils developed by the Boeing Vertol Company. Planform dimensions are shown in figure 1. The outer 15 percent of the K747 IMRB is tapered in thickness and planform with a tip chord of 0.83 foot. The airfoil design varies from blade tip to blade root as follows:

r/R (Blade Radius Station)	Airfoil Design
From Tip to 0.85	8% thick Boeing Vertol VR-8
From 0.85 to 0.67	Linear Transition to 12% thick VR-7
From 0.67 to 0.25	12% thick Boeing Vertol VR-7
From 0.25 to 0.18	Gradual buildup to 25% by cheekplates

The current AH-1S hub with hub pin is located at r/R = 0.15.
There is an attachment adapter fitting and drag brace between the pin and the end of the blade.

Principal Dimensions

3. The principal dimensions and general data concerning the AH-1S (PROD) helicopter (photos 1 through 4) are as follows:

Overall Dimensions

Length, rotor turning	53 ft, 1 in.
Width, rotor turning	44 ft
Height, tail rotor vertical	13 ft, 9 in.
Length, rotor removed	44 ft, 7 in.

Main Rotor	K747 IMRB	B540 MRB
Diameter[1]	44 ft	44 ft
Disc area	1520.5 ft^2	1520.5 ft^2
Solidity	0.0625	0.0651
Number of blades	2	2
Blade chord	See figure 1	2.25 ft, constant
Blade twist	-0.556 deg/ft	-0.455 deg/ft
Airfoil	See paragraph 2	9.33 percent thickness special symmetrical section

[1] Blade tie-down fixture is not included in the diameter.

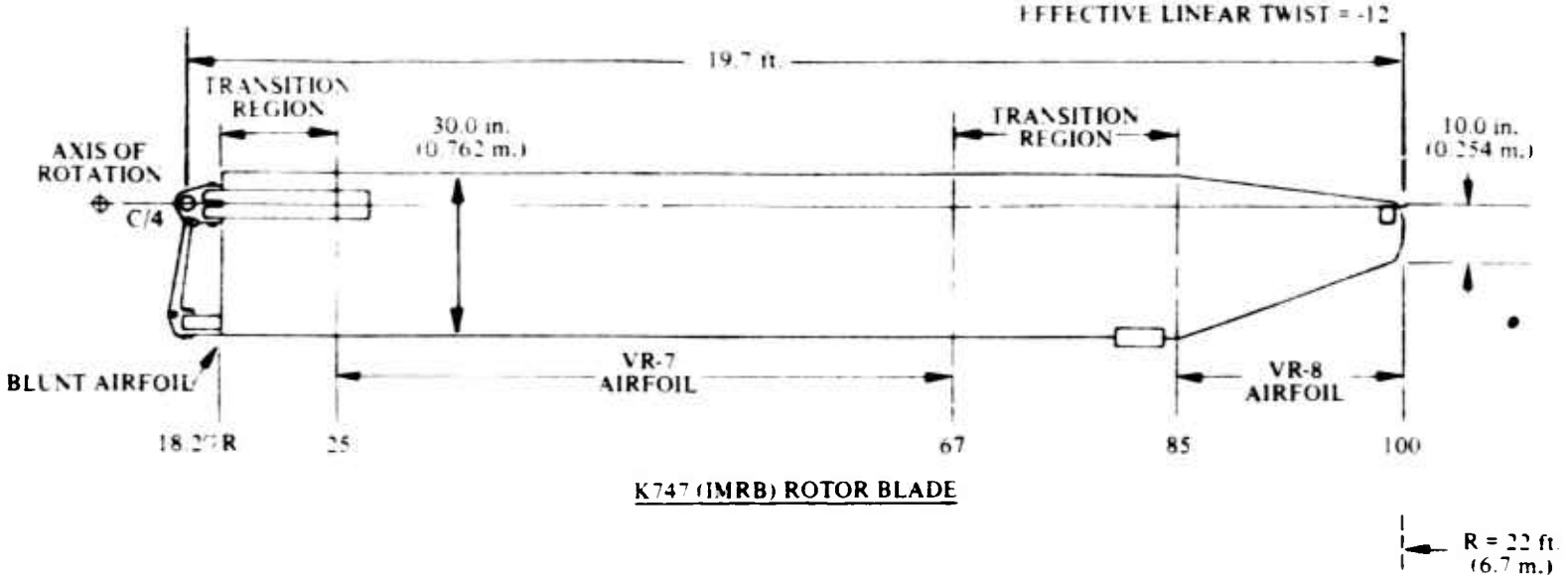

K747 (IMRB) ROTOR BLADE

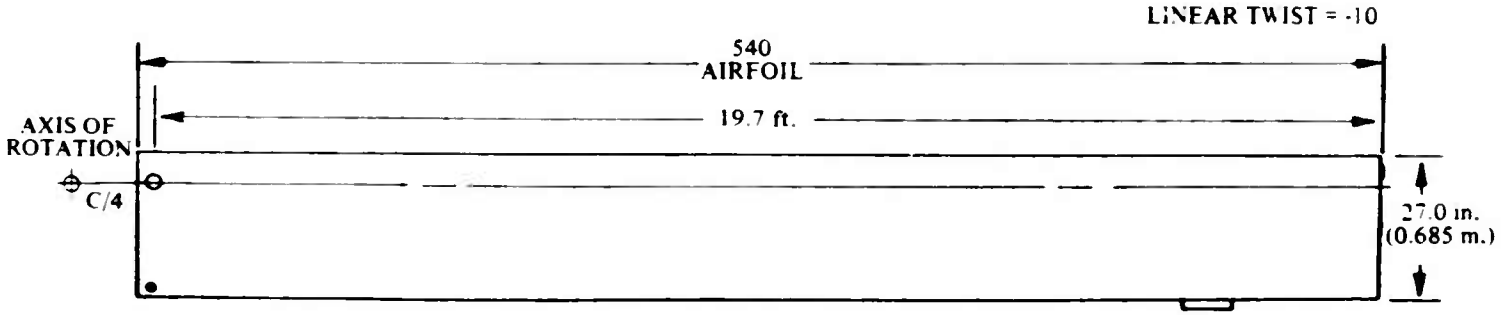

540 ROTOR BLADE

Figure 1. Comparison of K747 (a) and B540 (b) Planforms.

Photo 1 AH-1S Front View

Photo 2. AH-1S Left Side View

Photo 3. AH-1S Right Side View

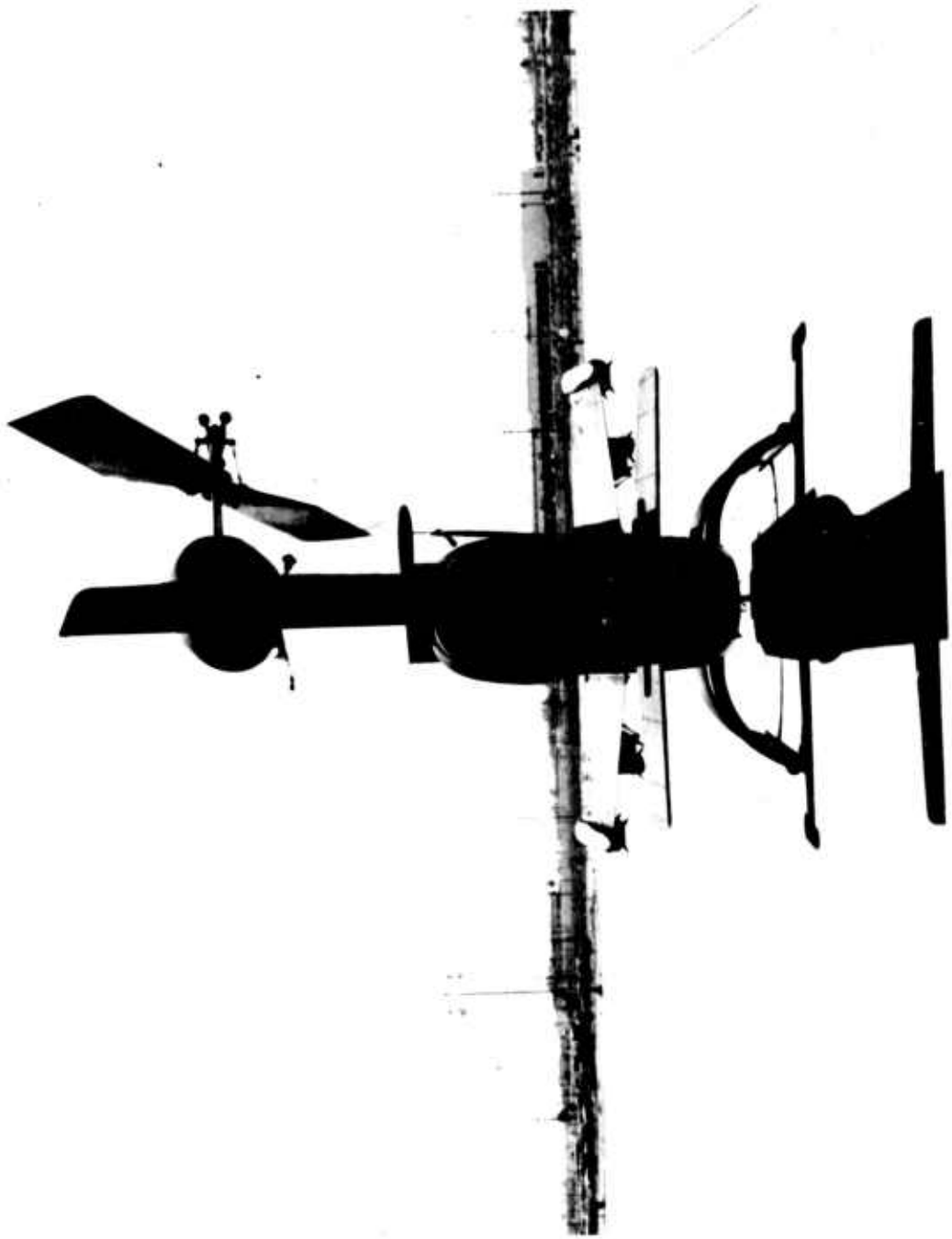

Photo 4. AH-1S Aft View

Tail Rotor

Diameter	8 ft, 6 in.
Disc area	56.75 ft^2
Solidity	0.1436
Number of blades	2
Blade chord, constant	11.5 in.
Blade twist	0.0 deg/ft
Airfoil	NACA 0018 at the blade root changing linearly to a special cambered section at 8.27 percent of the tip

Fuselage

Length, rotor removed	44 ft, 7 in.
Height:	
To tip of tail fin	10 ft, 8 in.
Ground to top of mast	12 ft, 3 in.
Ground to top of transmission fairing	10 ft, 2 in.
Width:	
Fuselage only	3 ft
Wing span	10 ft, 9 in.
Skid gear tread	7 ft.
Elevator:	
Span	6 ft, 11 in.
Airfoil	Inverted Clark Y
Vertical Fin:	
Area	18.5 ft^2
Airfoil	Special cambered
Height	5 ft, 6 in.
Wing:	
Span	10 ft, 9 in.
Incidence	17.0 deg
Airfoil (root)	NACA 0030
Airfoil (tip)	NACA 0024
Airfoil	Inverted Clark Y

APPENDIX C. INSTRUMENTATION

1. The test instrumentation system was designed, calibrated, installed, and maintained by USAAEFA. Digital and analog data were obtained from calibrated instrumentation and were recorded on magnetic tape and/or displayed in the cockpit. The digital instrumentation system consisted of various transducers, signal conditioning units, a ten-bit PCM encoder, and the Ampex AR 700 tape recorder. The digital and analog data were also telemetered to a ground station for in-flight monitoring. Time correlation was accomplished with a pilot/engineer event switch and on-board recorded and displayed Inter-Range Instrumentation Group (IRIG) B time. Various specialized test indicators displayed data to the pilot and engineer continuously during the flight. A boom with the following sensors was mounted on the nose of the aircraft: swiveling pitot-static head, sideslip vane, angle-of-attack vane, and total-temperature sensor. Boom airspeed system calibration is shown in figure 1. The engine torquemeter calibration is shown in figure 2.

2. Calibrated cockpit monitored parameters and special equipment are listed below.

Pilot Station

Airspeed (boom)
Airspeed (ship's system)
Altitude (boom)
Altitude (ship's system)
Rate of climb (boom)
Rate of climb (ship's system)
Rotor speed
Engine torque
Measured gas temperature
Gas generator speed
Angle of sideslip
Outside air temperature (ship's system)
Event switch
Tether cable angle indicator

Copilot/Engineer Station

Event switch
Airspeed (boom)
Altitude (boom)
Rotor speed
Engine torque
Measured gas temperature
Gas generator speed (ship's system)
Outside air temperature
Fuel used (totalizer)
Instrumentation control
Time of day
Record counter
Cable tension

FIGURE 1
BOOM AIRSPEED CALIBRATION
AH-1S USA S/N 76-22573

AVG GROSS WEIGHT (LB)	AVG CG LOCATION LONG (FS)	AVG CG LOCATION LAT (BL)	AVG DENSITY ALTITUDE (FT)	AVG OAT (°C)	AVG ROTOR SPEED (RPM)	TRIM FLIGHT CONDITION
8340	195.2(FWD)	0.1(RT)	3520	21.0	324	LEVEL FLT

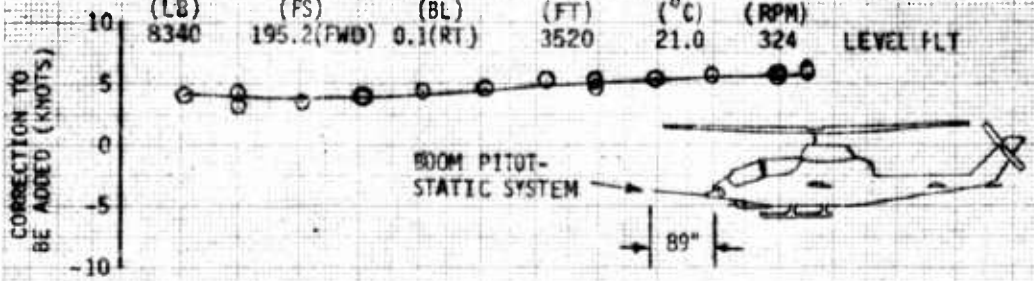

NOTES:
1. CLEAN CONFIGURATION.
2. K747 BLADES S/N A2016 AND A2025.
3. GROUND SPEED COURSE UTILIZED.
4. DATA NOT FOR HANDBOOK USE.

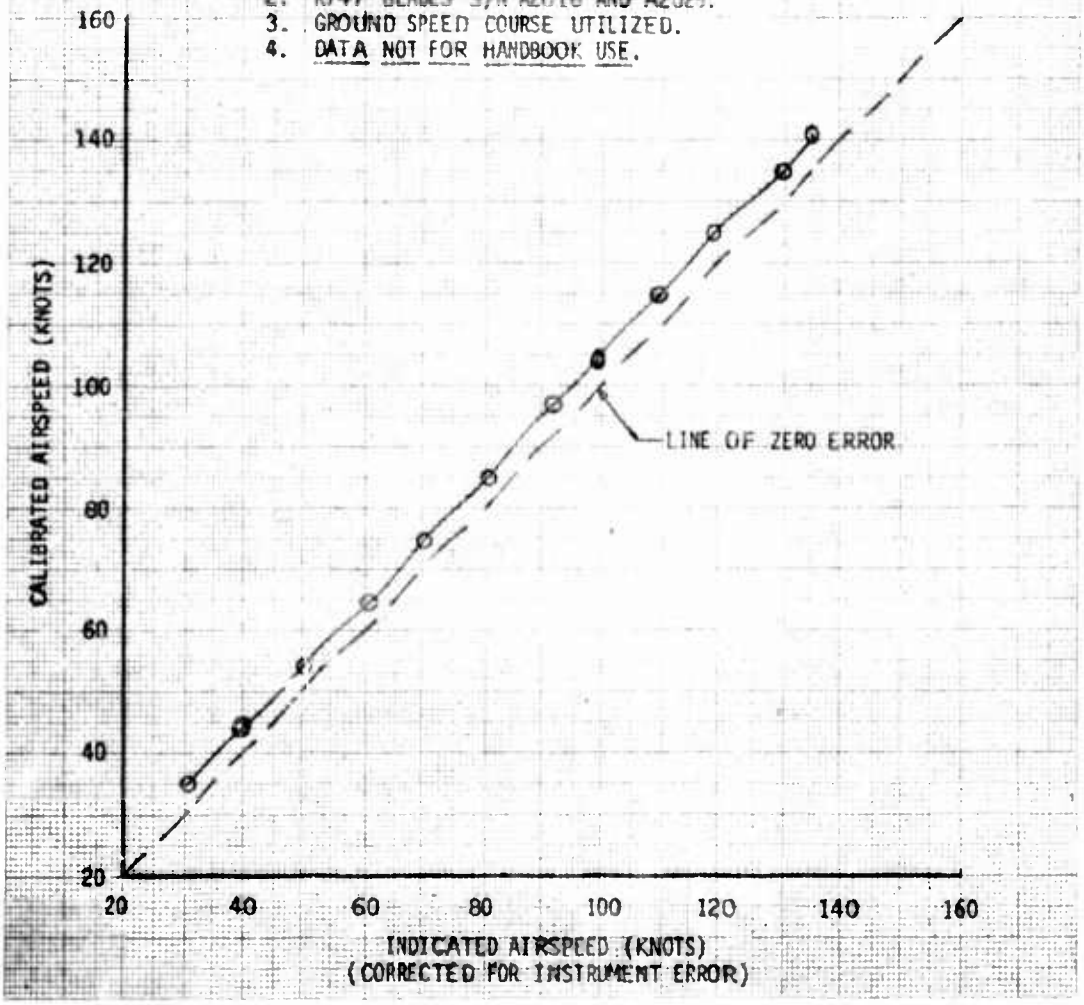

FIGURE 2
ENGINE TORQUEMETER CALIBRATION
JAH-1S USA S/N 76-22573
LYCOMING ENGINE MODEL T53-L-703 SN LE13145Z

NOTES: 1. TORQUEMETER CALIBRATION DATA PROVIDED BY LYCOMING BASED ON TEST CONDUCTED 13 JULY 1978.
2. N_p = 6604 RPM

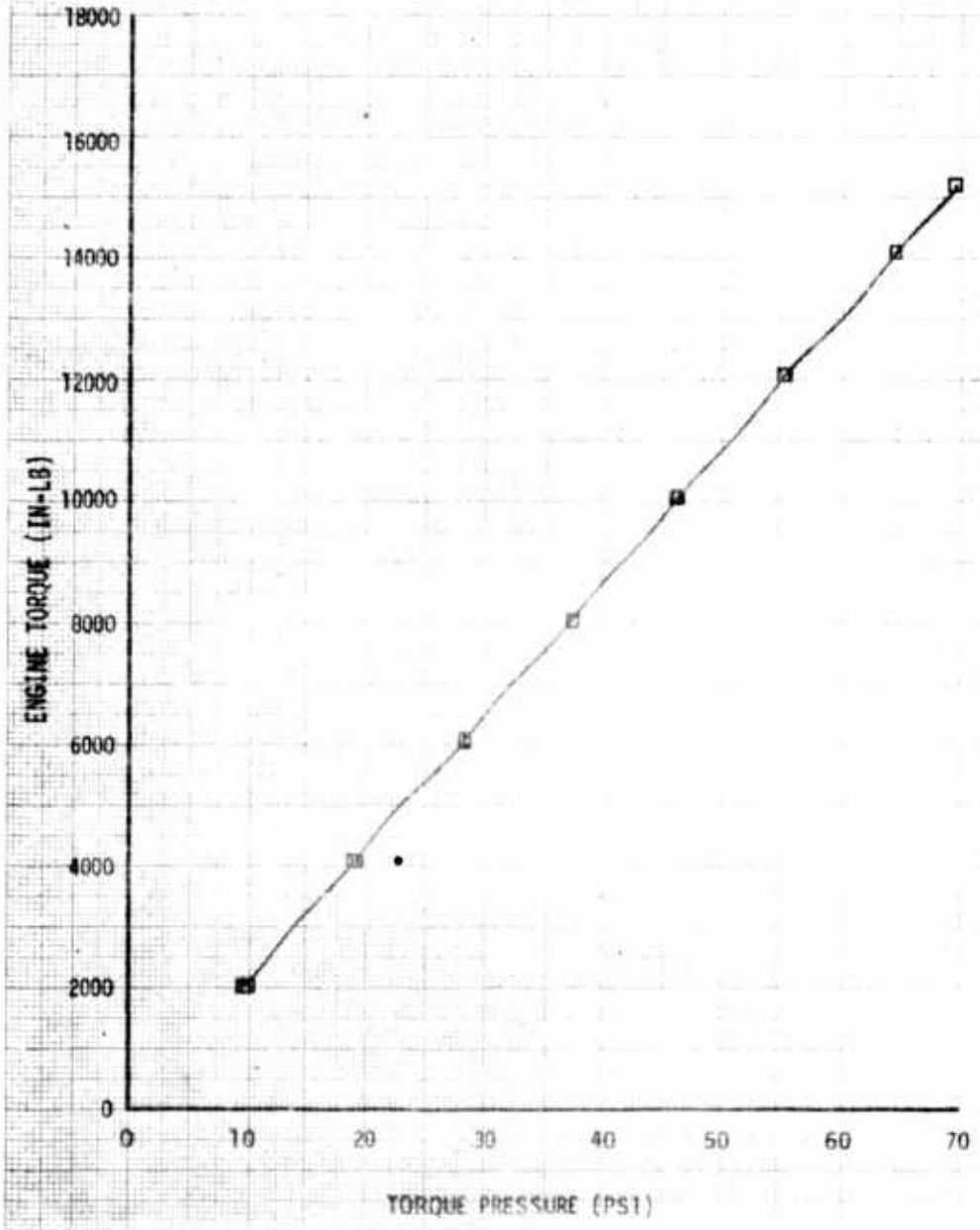

3. Parameters recorded on magnetic tape were as follows:

PCM Parameters

Time code
Flight number
Pilot/engineer event
Rotor speed
Fuel used
Run number
Airspeed (ship's system)
Airspeed (boom)
Altitude (ship's system)
Altitude (boom)
Control position:
- Longitudinal
- Lateral
- Directional
- Collective

Angle of sideslip
Angle of attack
Gas generator speed
Engine speed (N_2)

4. The acoustic tests conducted by the Areomechanics Laboratory, US Army Research and Technology Laboratories, AVRADCOM required that a tone generator be installed. This device was attached to the swashplate and produced a tone when one blade was at the 90 degree position (0 degrees being along the tail boom). The tone was transmitted over the aircraft's FM radio to the instrumentation tape on the NASA Ames Research Center YO-3A.

APPENDIX D. TEST TECHNIQUES AND DATA ANALYSIS METHODS

General

1. Conventional test techniques were used in the tests. Detailed descriptions of all test techniques are contained in references 9 and 10, appendix A, except where referred to in the following paragraphs. Definitions of deficiencies and shortcomings are as stipulated in Army Regulation 310-25 (ref 11).

DATA ANALYSIS METHODS

Nondimensional Coefficients

2. The nondimensional coefficients listed below were used to generalize the hover and level flight performance test data obtained during this evaluation.

a. Coefficient of power (C_p):

$$C_p = \frac{SHP \times 550}{\rho A (\Omega R)^3} \qquad (1)$$

b. Coefficient of thrust (C_T):

$$C_T = \frac{GW + PCAB}{\rho A (\Omega R)^2} \qquad \text{(Hover)} \qquad (2)$$

$$C_T = \frac{GW}{\rho A (\Omega R)^2} \qquad \text{(Level Flight)} \qquad (3)$$

c. Advance ratio (μ):

$$\mu = \frac{1.6878\ V_T}{\Omega R} \qquad (4)$$

d. Advancing blade tip mach number (M_{tip}):

$$M_{tip} = \frac{\Omega R + 1.6878\ V_T}{a} \qquad (5)$$

Where:

SHP = Engine output shaft horsepower
550 = Conversion factor (ft-lb/sec/shp)
ρ = Air density (slug/ft^3) = δ/θ

A = Main rotor disc area (ft^2)
Ω = Main rotor angular velocity (radian/sec)
R = Main rotor radius (ft)
GW = Aircraft gross weight (lb)
PCAB = Cable tension (lb) (used for tethered hover only)
V_T = True airspeed (kt)
a = Speed of sound (ft/sec) - $1116.45\sqrt{\theta}$
1.6878 = Conversion factor (ft/sec/kt)

$$\delta = \frac{p_a}{14.696}$$

$$\theta = \frac{273.15 + T_a}{288.15}$$

p_a = Static pressure (lb/in^2)
T_a = Ambient temperature (°C)

True airspeed (V_T) was calculated using calibrated airspeed (V_{CAL}) and density ratio (σ) as follows:

$$V_T = V_{CAL}/\sqrt{\sigma} \tag{6}$$

Where:

$$\sigma = \rho/.0023769$$

3. The constants used in calculating aircraft performance from nondimensional values are as follows:

A = 1520.530845
R = 22 feet
Ω = 33.93
ΩR = 746.44
$(\Omega R)^2$ = 557176.28
$(\Omega R)^3 = 4.159000067 \times 10^8$

Shaft Horsepower Required

4. Engine output shaft torque was determined from the engine manufacturer's differential torque pressure system. The relationship of measured differential torque pressure (psi) to engine output shaft torque (in.-lb) is illustrated in figure 2, appendix C. The output shp was determined from the engine output shaft torque and rotational speed by the following equation:

$$SHP = 20.38362 \times N_R \times Q \times 1.586663 \times 10^{-5} \tag{7}$$

Where:

N_R = Rotor shaft rotational speed (rpm)
Q = Engine output shaft torque (in.-lb)
20.38362 - Gear ratio of transmission
1.586663×10^{-5} = Conversion factor (shp/rpm/in.-lb)

Hover

5. OGE hover performance was obtained by tethered and free flight hover techniques. All hover tests were conducted in winds of less than 3 knots. Atmospheric pressure, temperature, and wind velocity were recorded from a ground weather station. Free flight hover tests consisted of stabilizing the helicopter at a desired height with reference to a premeasured weighted cord hung from the landing gear skid. Tethered hover consisited of applying power until specified torque was obtained. Data were recorded when the cable angle indicated 0, ±3 degrees, laterally and longitudinally. All hover data were reduced to nondimensional parameters of C_P and C_T (equations 1 and 2, respectively).

Level Flight Performance and Specific Range

6. Level flight performance was determined by using equations 1, 2, and 3. Each speed power was flown at a predetermined constant C_T by maintaining a constant referred gross weight (W/δ) and referred rotor speed ($N/\sqrt{\theta}$). A constant W/δ was maintained by increasing altitude (decreasing ambient pressure ratio (δ)) as the aircraft gross weight decreased with fuel burnoff. Rotor speed was also varied to maintain a constant $N/\sqrt{\theta}$ as the ambient air temperature varied.

7. Test-day power level flight was corrected to standard-day conditions using equation 8.

$$SHP_s = SHP_t \times \rho_s/\rho_t \tag{8}$$

Where:

$_t$ = Test day
$_s$ = Standard day

8. Specific range was calculated using level flight performance curves and the specification installed engine fuel flow characteristics.

$$NAMPP = V_T/W_f \tag{9}$$

Where:

NAMPP = Nautical air miles per pound of fuel
V_T = True airspeed (kt)
W_f = Fuel flow (lb/hr)

Engine Performance Characteristics

9. The AH-1S (PROD) was equipped with a calibrated T53-L-703 engine, S/N LE13145Z. Data for engine torque, fuel flow, measured gas temperature, and gas producer speed were obtained from a special engine test cell calibration (ref 6, app A.). Referred engine characteristics data obtained during hover testing, level flight testing, and the test cell calibration are presented in figures 1 through 3. The T53-L-703 specification engine power available and fuel flow data were estimated using a computer program documented in Lycoming program file number LS19.04.32.00 dated 1 May 1974 (ref 12, app A). These data are presented in figures 4 through 7 and have been adjusted for engine inlet temperature and inlet pressure characteristics obtained from figure 113 of USAAVNTA Final Report No. 66-06 (ref 7, app A).

10. The referred terms of the engine parameters were used to compare the test engine with the model specification engine. Data on shp, measured gas temperature (T_7), fuel flow, and gas producer speed (N_1) were referred as follows:

a. Referred SHP (RSHP):

$$RSHP = SHP/(\delta_1 \times \theta_1^{.587}) \tag{10}$$

b. Referred measured gas temperature (RMGT)

$$RMGT = T_7/\theta_1^{1.022} \tag{11}$$

c. Referred fuel flow (RW_f)

$$RW_f = W_f/(\delta_1 \times \theta_1^{.712}) \tag{12}$$

d. Referred gas producer speed (RN_1)

$$RN_1 = N_1/\sqrt{\theta_1} \tag{13}$$

Where:

$$\delta_1 = \frac{P_{T_1}}{14.697}$$

$$\theta_1 = \frac{T_1}{288.15}$$

W_f = Engine fuel flow (lb/hr)

P_{T_1} = Engine inlet total pressure (psi)

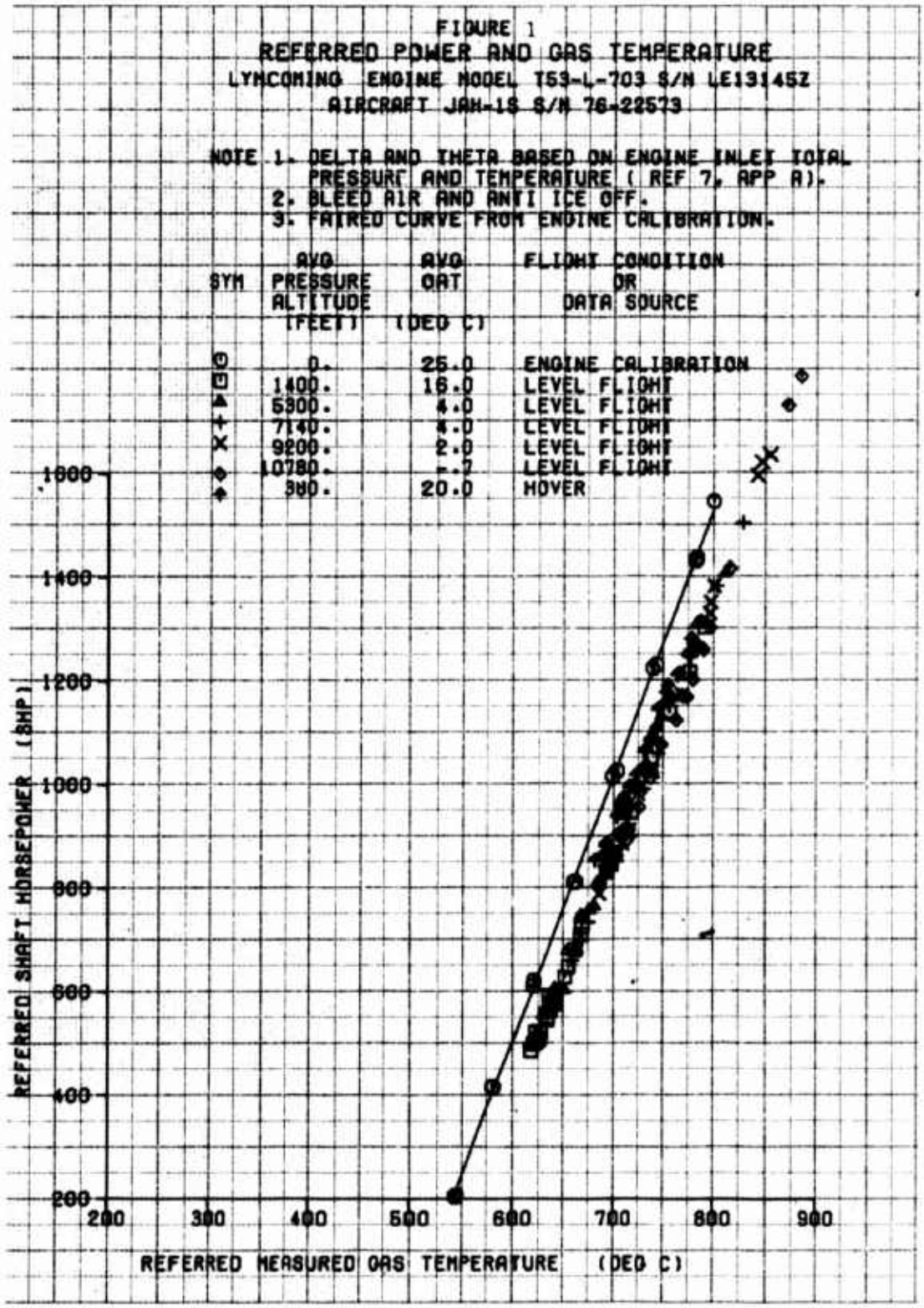
FIDURE 1
REFERRED POWER AND GAS TEMPERATURE
LYNCOMING ENGINE MODEL T53-L-703 S/N LE13145Z
AIRCRAFT JAH-1S S/N 76-22573
NOTE 1. DELTA AND THETA BASED ON ENGINE INLET TOTAL PRESSURE AND TEMPERATURE (REF 7, APP A).
2. BLEED AIR AND ANTI ICE OFF.
3. FAIRED CURVE FROM ENGINE CALIBRATION.
SYM | AVG PRESSURE ALTITUDE (FEET) | AVG OAT (DEG C) | FLIGHT CONDITION OR DATA SOURCE
0 | 0. | 25.0 | ENGINE CALIBRATION
1400. | 16.0 | LEVEL FLIGHT
5300. | 4.0 | LEVEL FLIGHT
7140. | 4.0 | LEVEL FLIGHT
9200. | 2.0 | LEVEL FLIGHT
10780. | -.7 | LEVEL FLIGHT
380. | 20.0 | HOVER
1600
1400
1200
1000
800
600
400
200
REFERRED SHAFT HORSEPOWER (SHP)
200
300
400
500
600
700
800
900
REFERRED MEASURED GAS TEMPERATURE (DEG C)

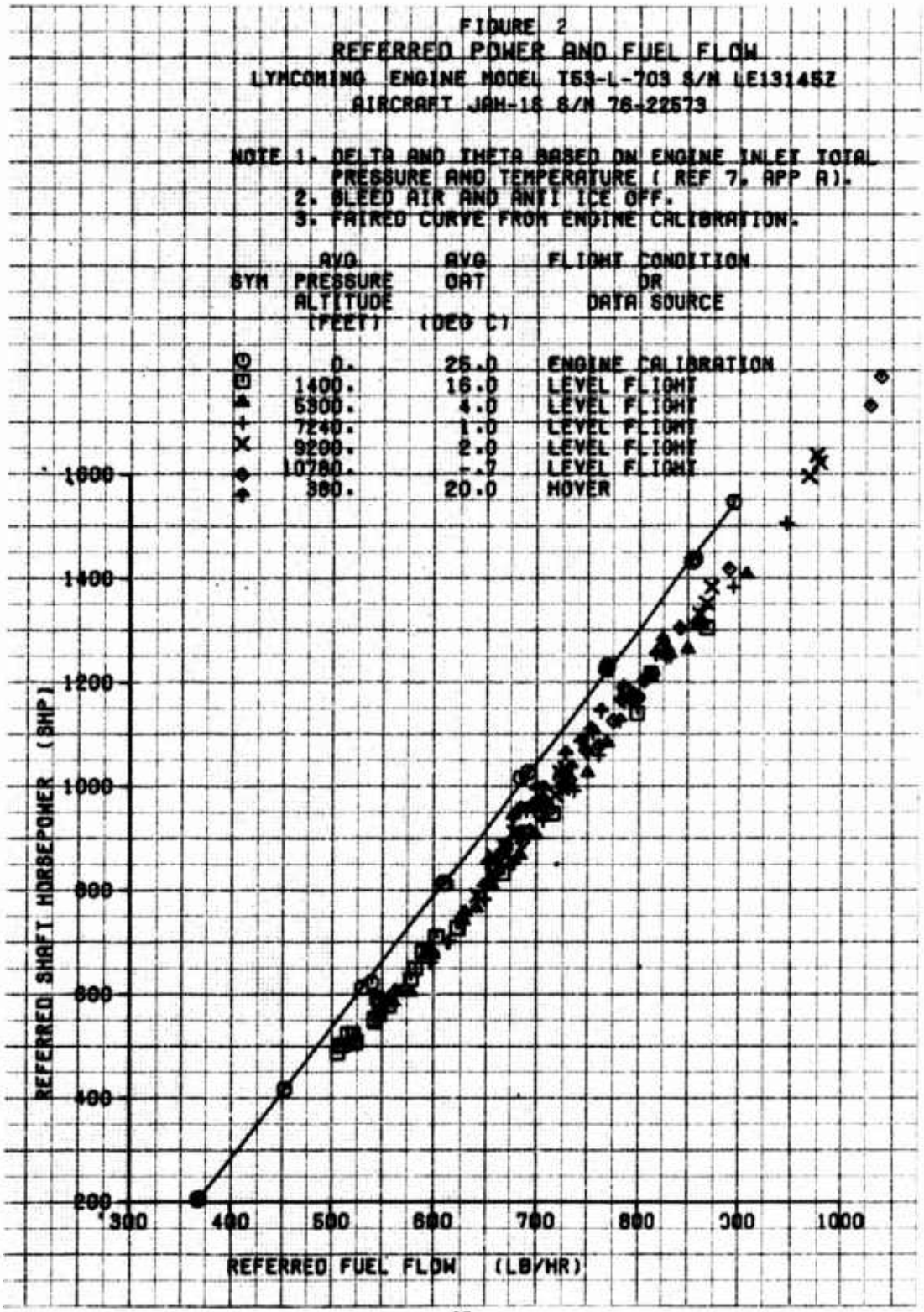
FIGURE 2
REFERRED POWER AND FUEL FLOW
LYCOMING ENGINE MODEL T53-L-703 S/N LE13145Z
AIRCRAFT JAH-16 S/N 76-22573
NOTE 1. DELTA AND THETA BASED ON ENGINE INLET TOTAL PRESSURE AND TEMPERATURE (REF 7, APP A).
2. BLEED AIR AND ANTI ICE OFF.
3. FAIRED CURVE FROM ENGINE CALIBRATION.
SYM
AVG PRESSURE ALTITUDE (FEET)
AVG OAT (DEG C)
FLIGHT CONDITION OR DATA SOURCE
0. 25.0 ENGINE CALIBRATION
1400. 16.0 LEVEL FLIGHT
5300. 4.0 LEVEL FLIGHT
7240. 1.0 LEVEL FLIGHT
9200. 2.0 LEVEL FLIGHT
10780. -.7 LEVEL FLIGHT
380. 20.0 HOVER
1600
1400
1200
1000
800
600
400
200
REFERRED SHAFT HORSEPOWER (SHP)
300
400
500
600
700
800
900
1000
REFERRED FUEL FLOW (LB/HR)

FIGURE 3

REFERRED POWER AND GAS PRODUCER SPEED

LYNCOMING ENGINE MODEL T53-L-703 S/N LE13145Z

AIRCRAFT JAH-1S S/N 76-22573

NOTE 1. DELTA AND THETA BASED ON ENGINE INLET TOTAL PRESSURE AND TEMPERATURE (REF 7, APP A).
2. BLEED AIR AND ANTI ICE OFF.
3. FAIRED CURVE FROM ENGINE CALIBRATION.

SYM	AVG PRESSURE ALTITUDE (FEET)	AVG OAT (DEG C)	FLIGHT CONDITION OR DATA SOURCE
⊙	0.	25.0	ENGINE CALIBRATION
□	1400.	16.0	LEVEL FLIGHT
▲	5300.	4.0	LEVEL FLIGHT
+	7240.	1.0	LEVEL FLIGHT
×	9200.	2.0	LEVEL FLIGHT
◆	10780.	-.7	LEVEL FLIGHT
◆	380.	20.0	HOVER

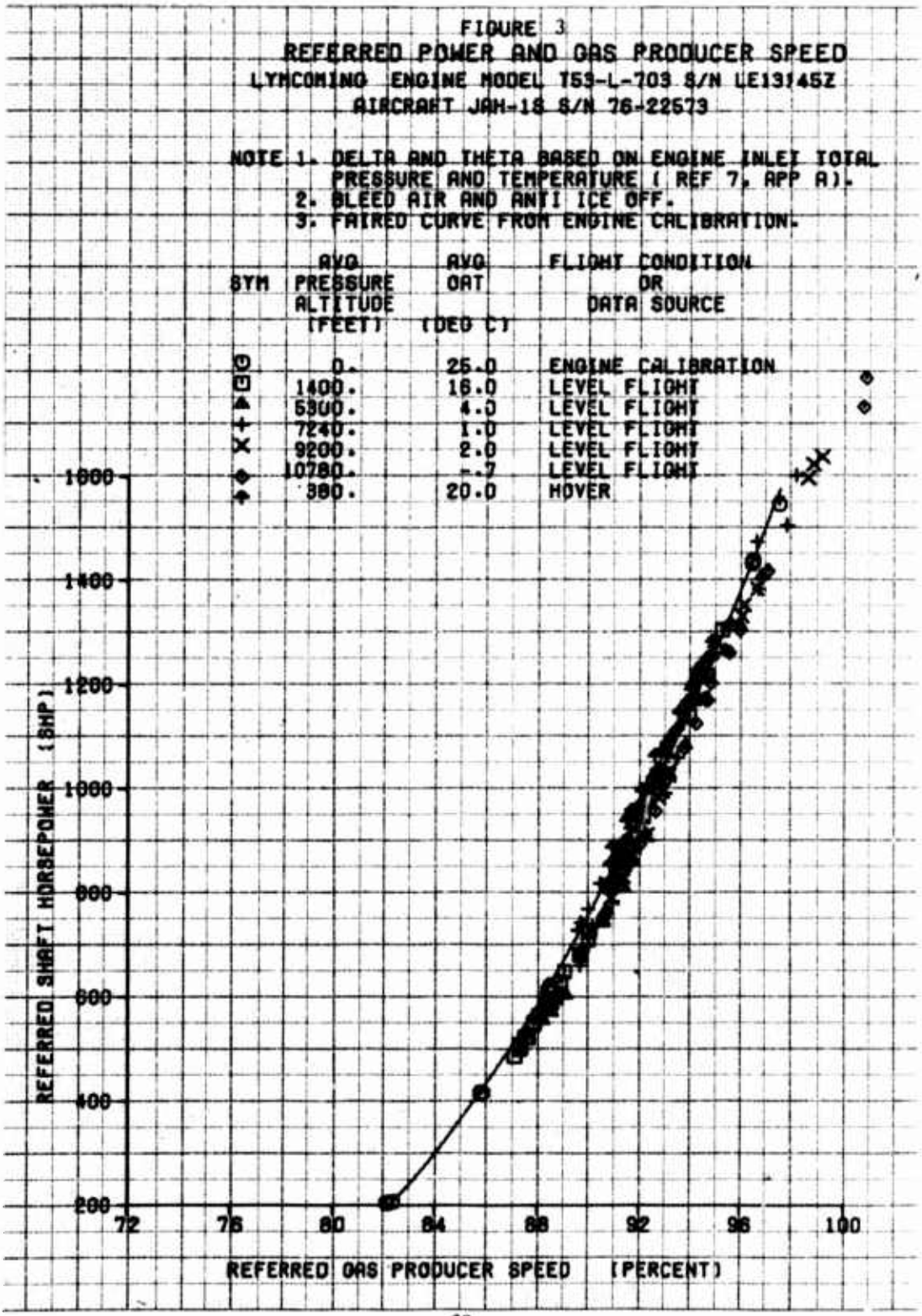

FIGURE 4

INTERMEDIATE (30 MINUTE LIMIT) POWER AVAILABLE

JAH-1S USA S/N 76-22573 T53-L-703 ENGINE

6600 OUTPUT SHAFT (324 ROTOR) RPM ZERO KNOTS TRUE AIRSPEED

NOTE: BASED ON LYCOMING T53-L-703 CARD DECK FILE NO. 19.04.32.00. CORRECTED FOR THE FOLLOWING INSTALLATION CONDITIONS:

1. ENGINE INLET TEMPERATURE RISE = 3°C.
2. ENGINE INLET PRESSURE RATIO = .985.
3. CUSTOMER BLEED AIR = 0.6%.
4. ENGINE ANTI-ICE OFF.
5. EXHAUST DUCT PRESSURE LOSS = ZERO.
6. HORSEPOWER EXTRACTION = ZERO.

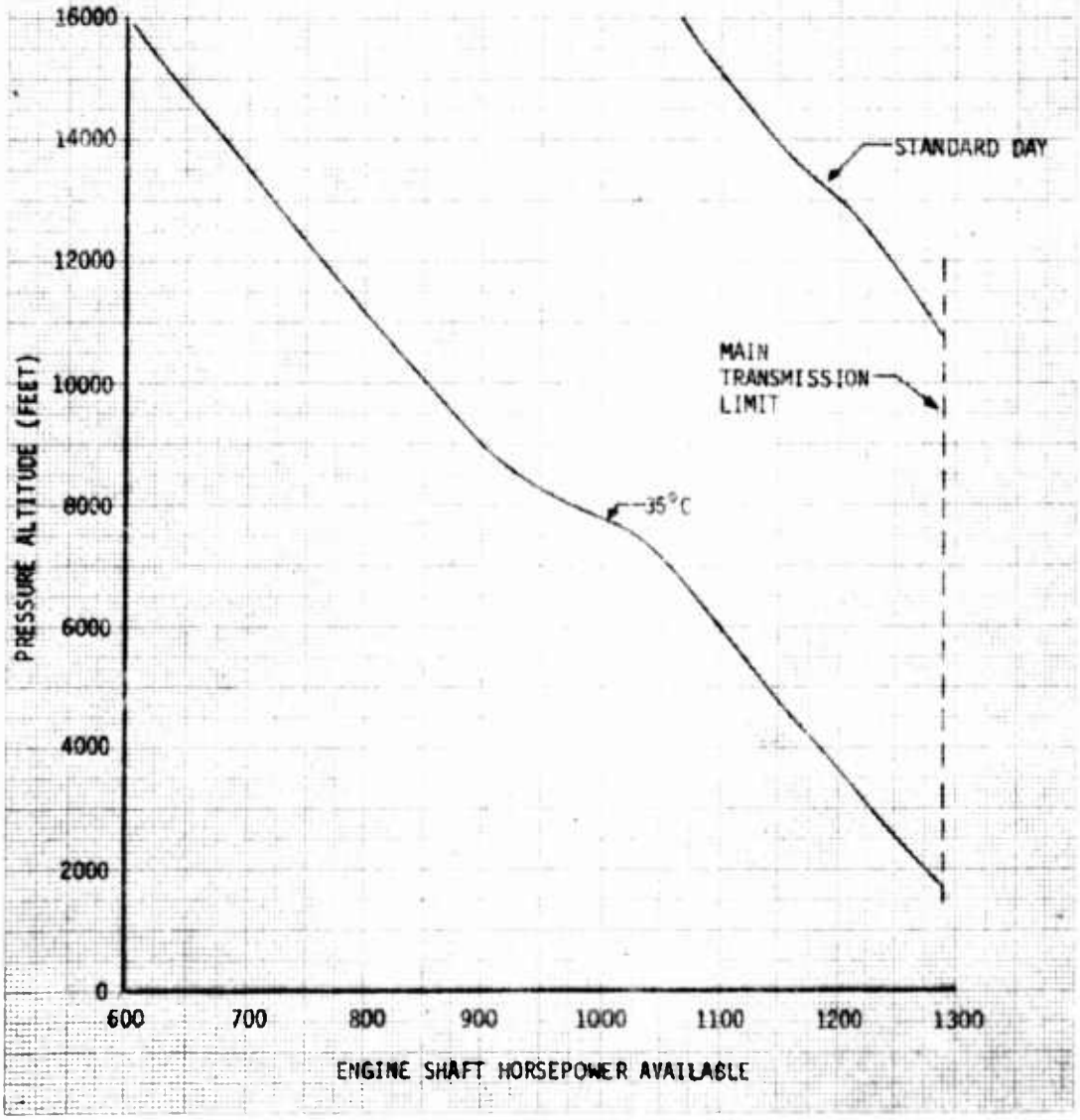

FIGURE 5
SPECIFICATION SHAFT HORSEPOWER AVAILABLE
JAH-1S USA S/N 76-22573 T53-L-703 ENGINE
6600 OUTPUT SHAFT RPM

NOTE: BASED ON LYCOMING T53-L-703 CARD DECK FILE NO. 19.04.32.00, CORRECTED FOR THE FOLLOWING INSTALLATION CONDITIONS:
1. ENGINE INLET TEMPERATURE RISE AND PRESSURE RATIO OBTAINED FROM REFERENCE 7, APPENDIX A.
2. CUSTOMER BLEED AIR = 0.6%.
3. ENGINE ANTI-ICE OFF.
4. EXHAUST DUCT PRESSURE LOSS = ZERO.
5. HORSEPOWER EXTRACTION = ZERO.

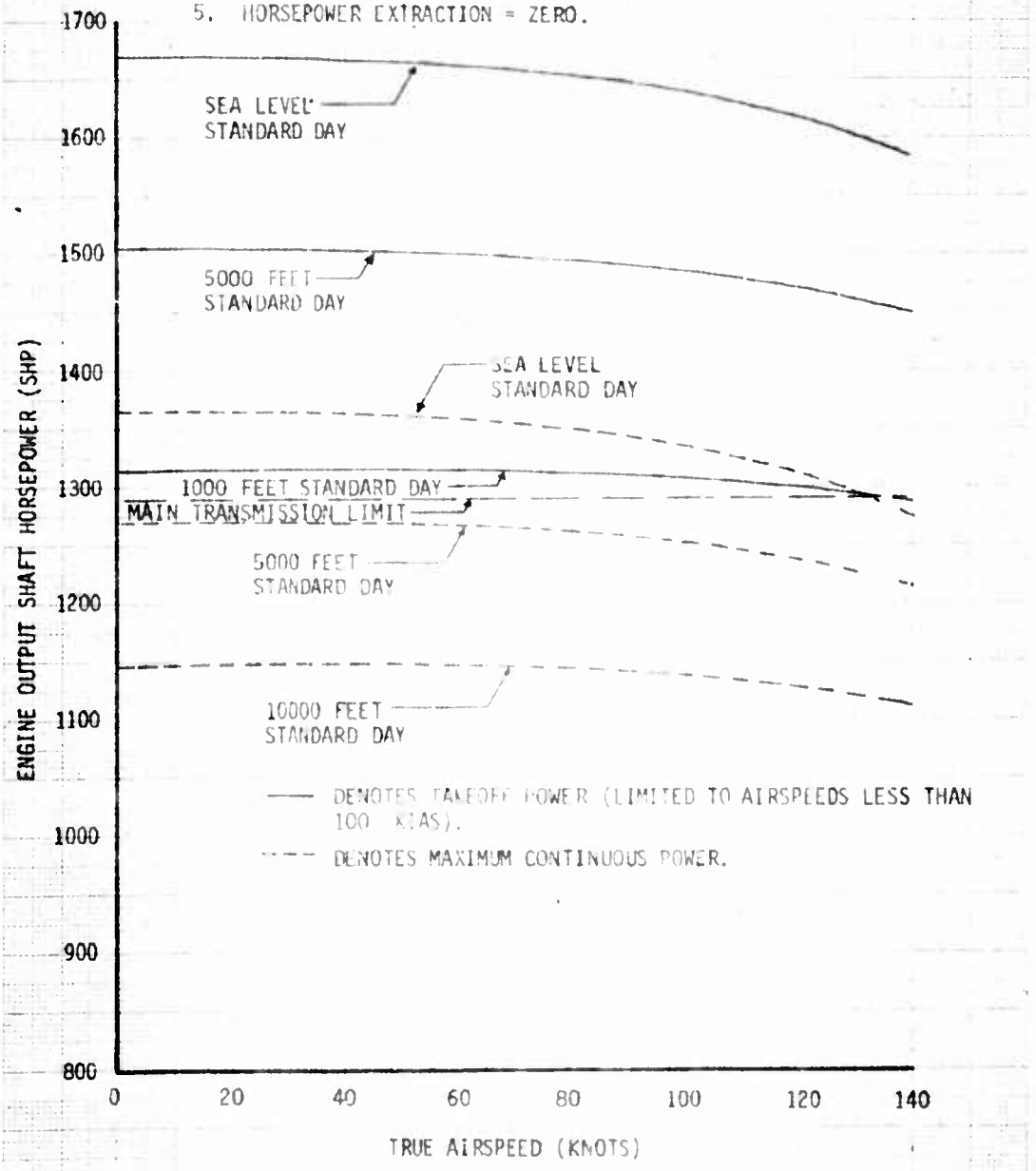

FIGURE 6
SPECIFICATION FUEL FLOW
JAH-1S USA S/N 76-22573 T53-L-703 ENGINE
6600 OUTPUT SHAFT RPM
ZERO KNOTS TRUE AIRSPEED

NOTE: BASED ON LYCOMING T53-L-703 CARD DECK FILE NO. 19.04.32.00, CORRECTED FOR THE FOLLOWING INSTALLATION CONDITIONS:
1. ENGINE INLET TEMPERATURE RISE = 3°C
2. ENGINE INLET PRESSURE RATIO = .985
3. CUSTOMER BLEED AIR = 0.6%
4. ENGINE ANTI-ICE OFF
5. EXHAUST DUCT PRESSURE LOSS = ZERO
6. HORSEPOWER EXTRACTION = ZERO

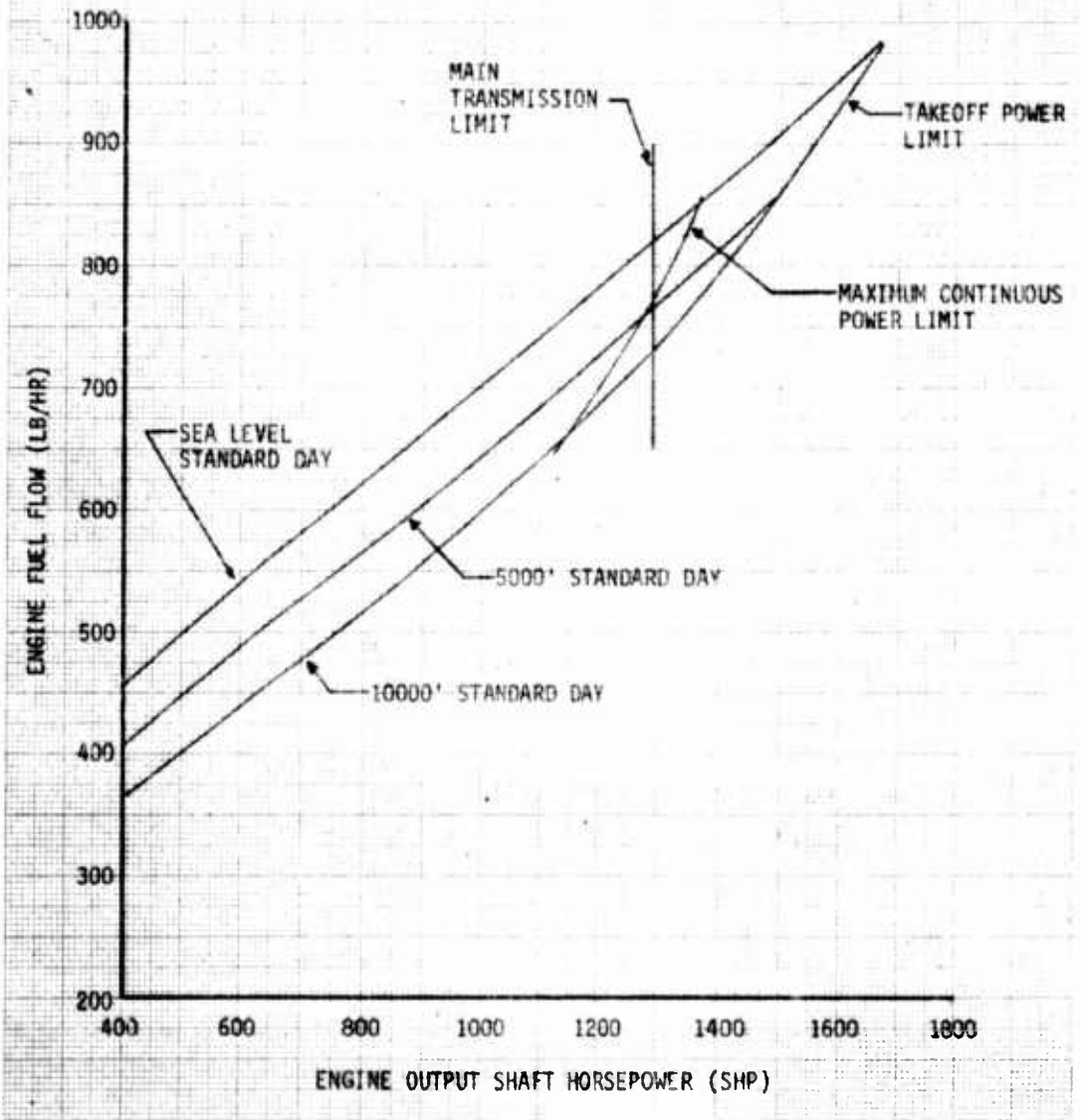

FIGURE 7
SPECIFICATION FUEL FLOW
JAH-1S USA S/N 76-22573 T53-L-703 ENGINE
6600 OUTPUT SHAFT RPM

NOTE: BASED ON LYCOMING T53-L-703 CARD DECK FILE NO. 19.04.32.00, CORRECTED FOR THE FOLLOWING INSTALLATION CONDITIONS:
1. ENGINE INLET TEMPERATURE RISE AND PRESSURE RATIO OBTAINED FROM REFERENCE 7, APPENDIX A.
2. CUSTOMER BLEED AIR = 0.6%
3. ENGINE ANTI-ICE OFF
4. EXHAUST DUCT PRESSURE LOSS = ZERO
5. HORSEPOWER EXTRACTION = ZERO

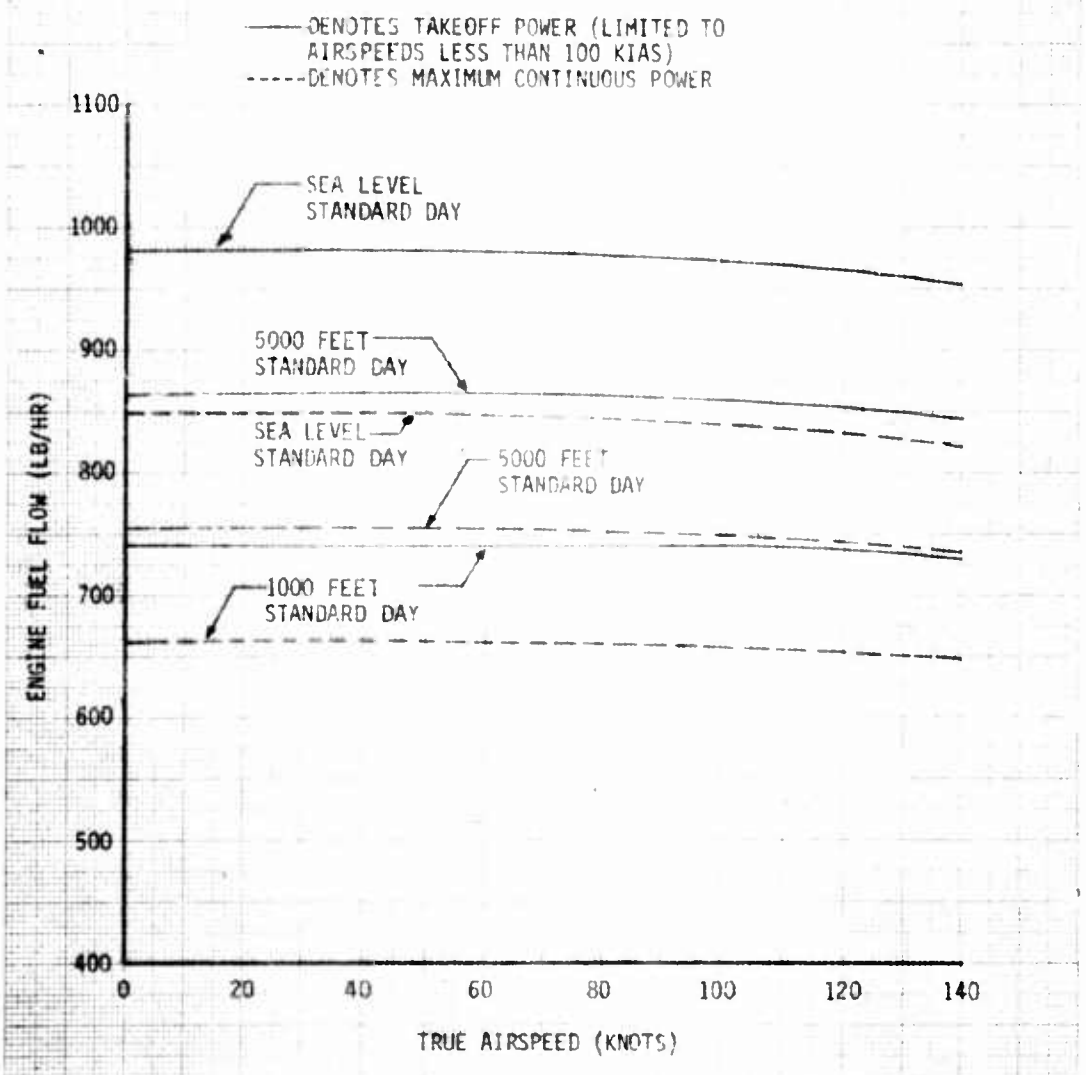

T_1 = Engine inlet total temperature (°K)

N_1 = Gas producer speed referenced to 25,150 rpm (100 percent)

Pitot-Static Calibration

11. The boom and ship's standard pitot-static system were calibrated on a 3 mile measured course. The start and stop times were recorded by ground station for each run, with reciprocal runs at each speed to average the effect of wind (true airspeed was the average airspeed of the two runs based on elapsed time and known distance.) Additionally, the ship's pitot-static system was calibrated in climbs and descents using a trailing bomb pitot-static source.

Rigging Check

12. A flight control rigging check performed in accordance with procedures outlined in TM 55-1520-236-20 demonstrated the cyclic, collective pitch and directional controls were within prescribed limits. The swashplate angles which were measured with respect to aircraft axes, and tail rotor blade pitch angles are listed in table 1.

Weight and Balance

13. The aircraft weight, longitudinal center-of-gravity (cg) location and lateral cg location were determined prior to testing, and checked periodically throughout the tests. A fuel cell calibration was also performed prior to testing. All weighings were accomplished with instrumentation installed, without external stores, chin turret weapons, crewmembers, or ballast.

14. The fuel loading for each test flight was determined prior to engine start and following engine shutdown by using a calibrated external sight gage to determine fuel volume and by measuring the fuel specific gravity. Fuel used in flight was recorded by a fuel-used system and verified with the pre- and postflight sight gage readings.

Table 1. Rigging Check

SWASHPLATE ANGLES		
Cyclic Control Position[1]	Lateral Angle	Longitudinal Angle
Neutral	1.5 deg L down	1 deg fwd up
Full Forward	5 deg R down	10 deg fwd down
Full AFT	5 deg L down	12.5 deg fwd up
Full Right	7 deg R down	4.5 deg fwd up
Full Left	7.5 deg L down	3.5 deg fwd down

TAIL ROTOR BLADE PITCH ANGLES	
Pedal Position	Blade Angle
Full Left	19.9 deg
Full Right	-11.0 deg

[1] Collective control full down.

APPENDIX E. TEST DATA

INDEX

FIGURE 1
SUMMARY HOVER PERFORMANCE
OUT-OF-GROUND EFFECT
JAH-1S USA S/N 76-22573
LYCOMING ENGINE MODEL T-53-L-703 S/N LE 131457
INTERMEDIATE RATED POWER
SKID HEIGHT = 100 FEET

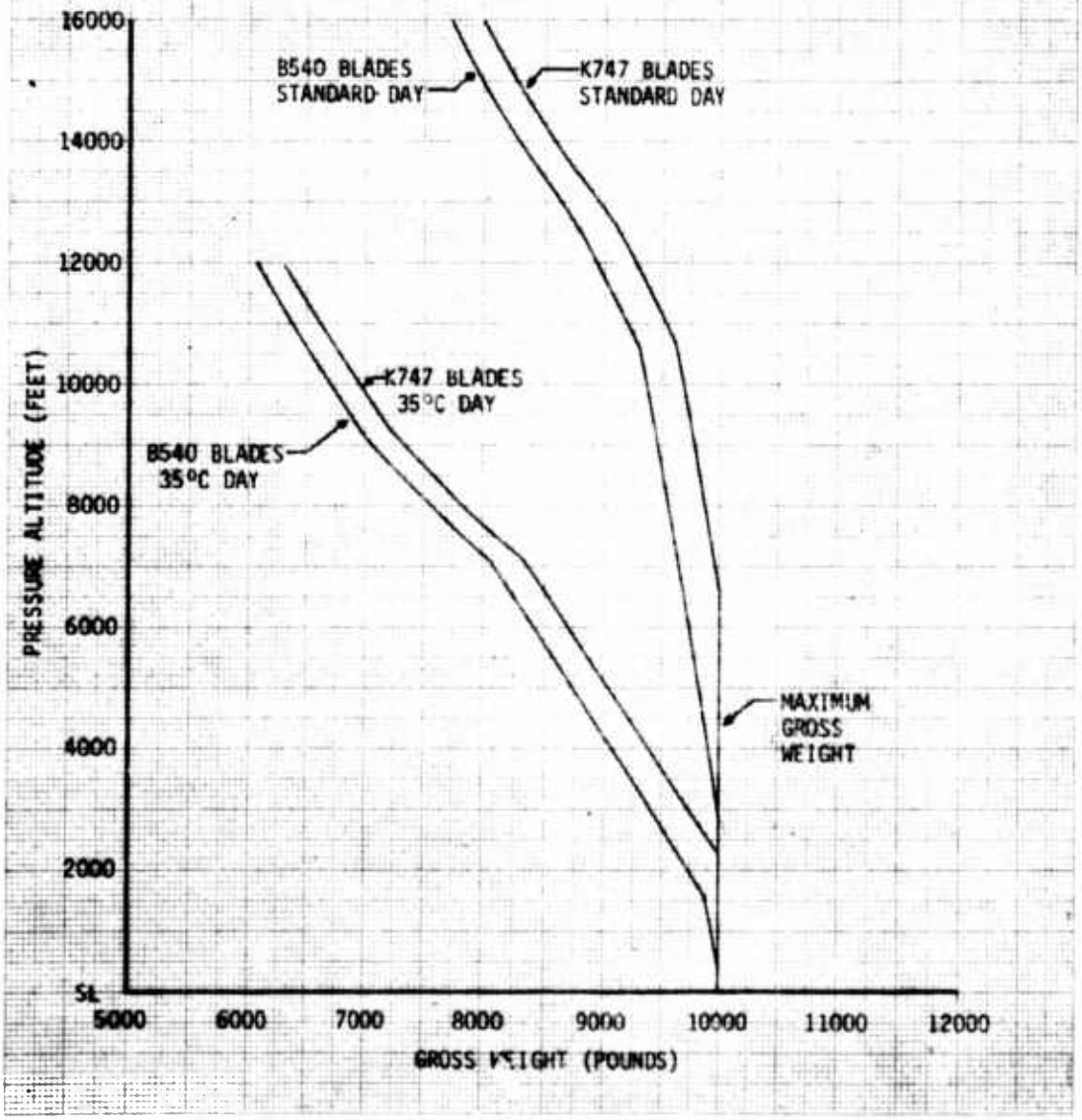

FIGURE 2
OUT-OF-GROUND EFFECT NONDIMENSIONAL HOVERING PERFORMANCE
JAH-1S USA SN 76-22873 8640 BLADES NO. AWR 00021, 50107
LYCOMING ENGINE MODEL T53-L-703 SN LE131452
SKID HEIGHT = 100 FEET

SYM	AVERAGE REFERRED ROTOR SPEED (RPM)	AVERAGE DENSITY ALTITUDE (FEET)	AVERAGE OAT (DEGREES C)
⊡	293	5600	19.5
⊙	296	1100	21.0
▽	303	3260	2.0
◇	311	5640	20.0
△	311	1040	20.5
◇	321	1080	21.0
▷	321	5600	20.5
⊙	322	3260	2.0
⊙	332	3260	2.0

POWER COEFFICIENT, $C_p \times 10^5 = \frac{550 \times SHP}{\rho A(\Omega R)^3} \times 10^5$

THRUST COEFFICIENT, $C_T \times 10^4 = \frac{GW \pm FCAB}{\rho A(\Omega R)^2} \times 10^4$

NOTE:
1. VERTICAL HEIGHT FROM BOTTOM OF SKIDS TO CENTER OF ROTOR HUB = 11.9 FEET
2. WINDS LESS THAN 3 KNOTS
3. TETHERED HOVER TECHNIQUE
4. SHADED SYMBOLS DENOTE FREE FLIGHT HOVER
5. CLEAN CONFIGURATION
6. FAIRED CURVE OBTAINED FROM USAAEFA PROJECT NO. 76-08

FIGURE 3
OUT-OF-GROUND EFFECT NONDIMENSIONAL HOVERING PERFORMANCE
JAH-1S USA SN 76-22573 K747 BLADES NO. A2018, 2025
LYCOMING ENGINE MODEL T53-L-703 SN LE13145Z
SKID HEIGHT = 100 FEET

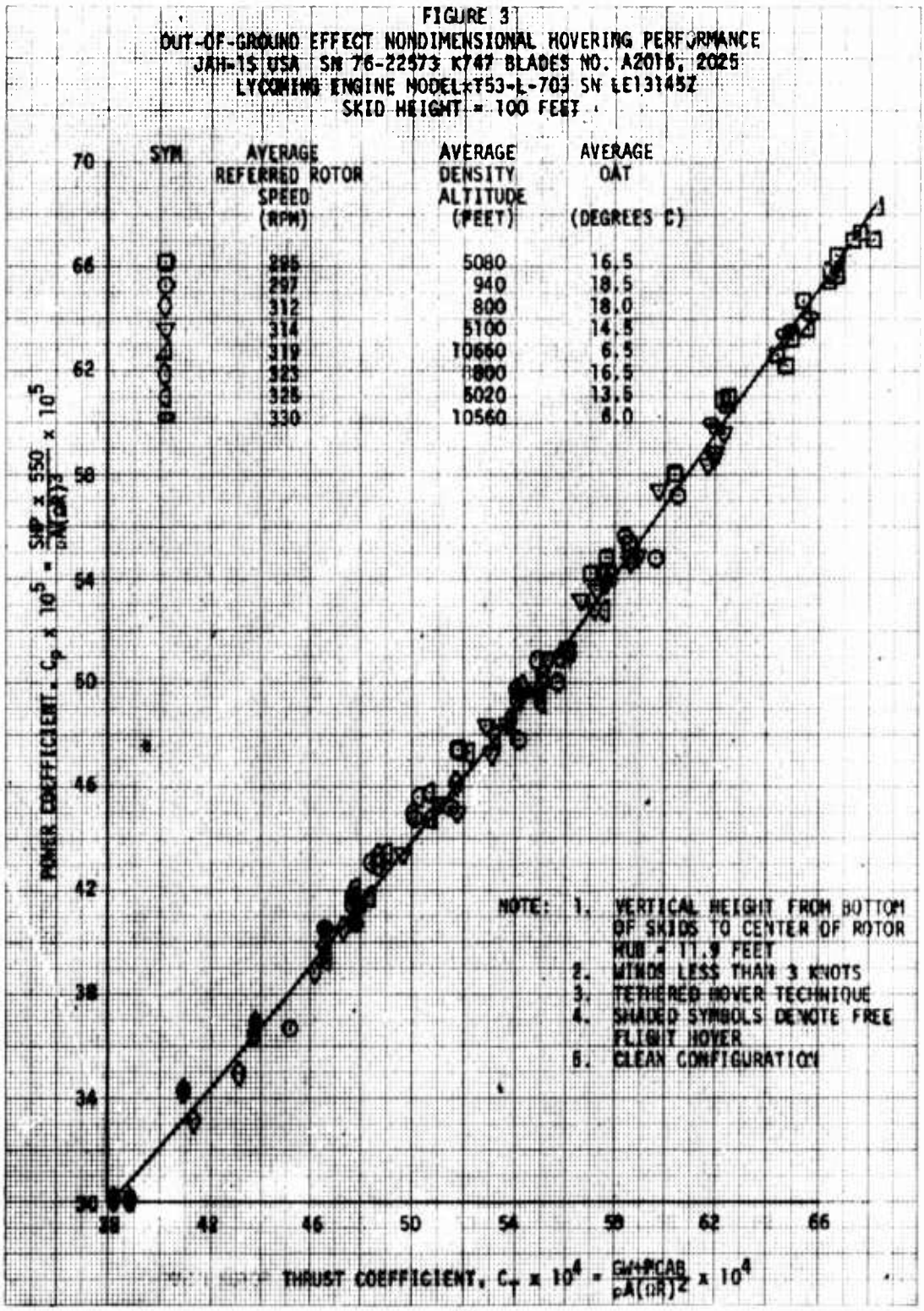

FIGURE 4
NONDIMENSIONAL LEVEL FLIGHT PERFORMANCE
AH-1S USA S/N 76-22573

NOTES:
1. B540 BLADES
2. REFERRED ROTOR SPEED = 324 RPM
3. AVG LONGITUDINAL CG = (FS) 194.0 (FWD)
4. CLEAN CONFIGURATION
5. CURVES DERIVED FROM FIGURES 10 THROUGH 14
6. ZERO SIDESLIP

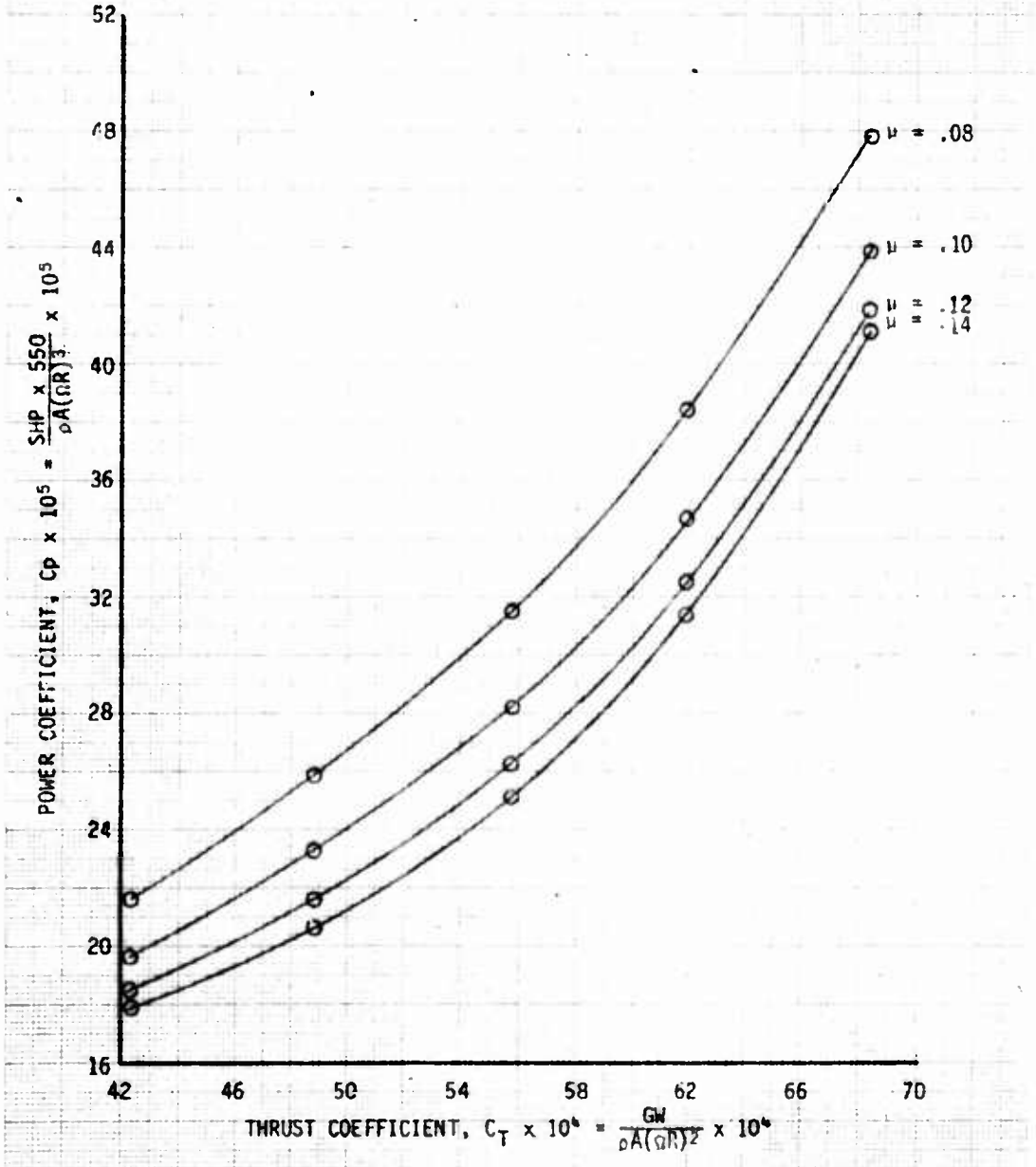

FIGURE 5
NONDIMENSIONAL LEVEL FLIGHT PERFORMANCE
AH-1S USA S/N 76-22573

NOTES:
1. 8540 BLADES
2. REFERRED ROTOR SPEED = 324 RPM
3. AVG LONGITUDINAL CG = (FS) 194.0 (FWD)
4. CLEAN CONFIGURATION
5. CURVES DERIVED FROM FIGS 10 THROUGH 14
6. ZERO SIDESLIP

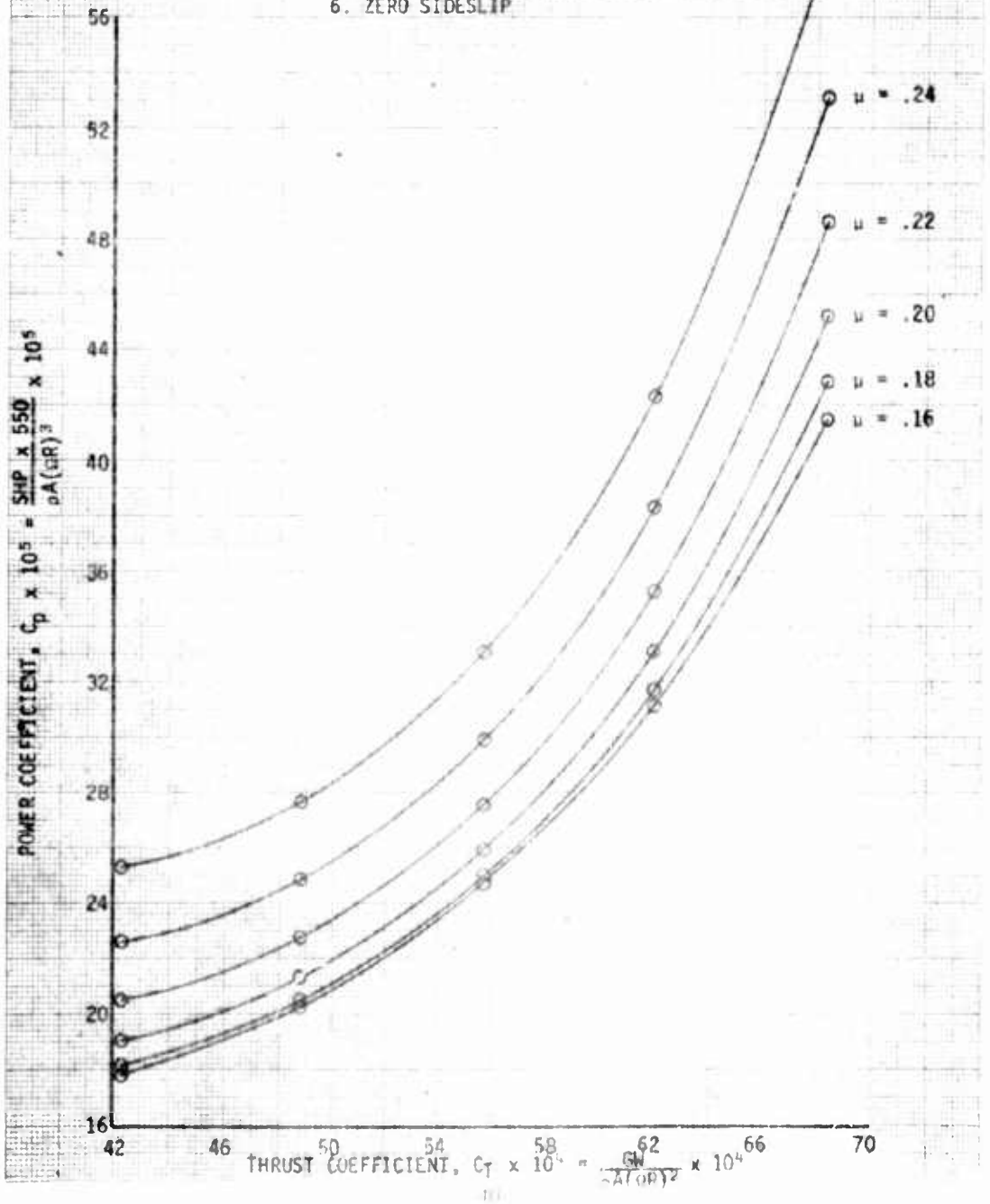

FIGURE 6
NONDIMENSIONAL LEVEL FLIGHT PERFORMANCE
AH-1S USA S/N 76-22573

NOTES:
1. B540 BLADES
2. REFERRED ROTOR SPEED = 324 RPM
3. AVG LONGITUDINAL CG = (FS) 194.0 (FWD)
4. CLEAN CONFIGURATION
5. CURVES DERIVED FROM FIGS 10 THROUGH 14
6. ZERO SIDESLIP

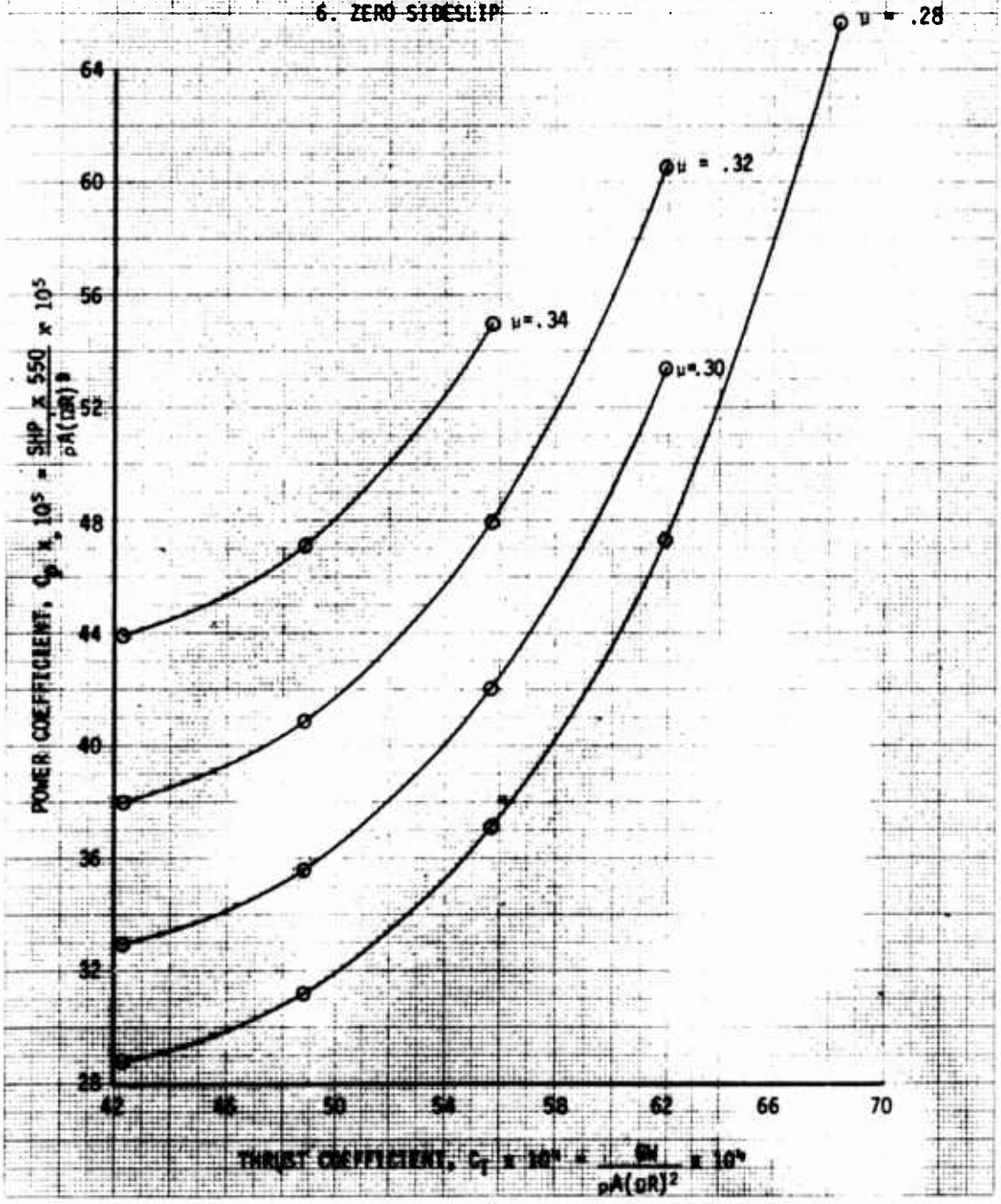

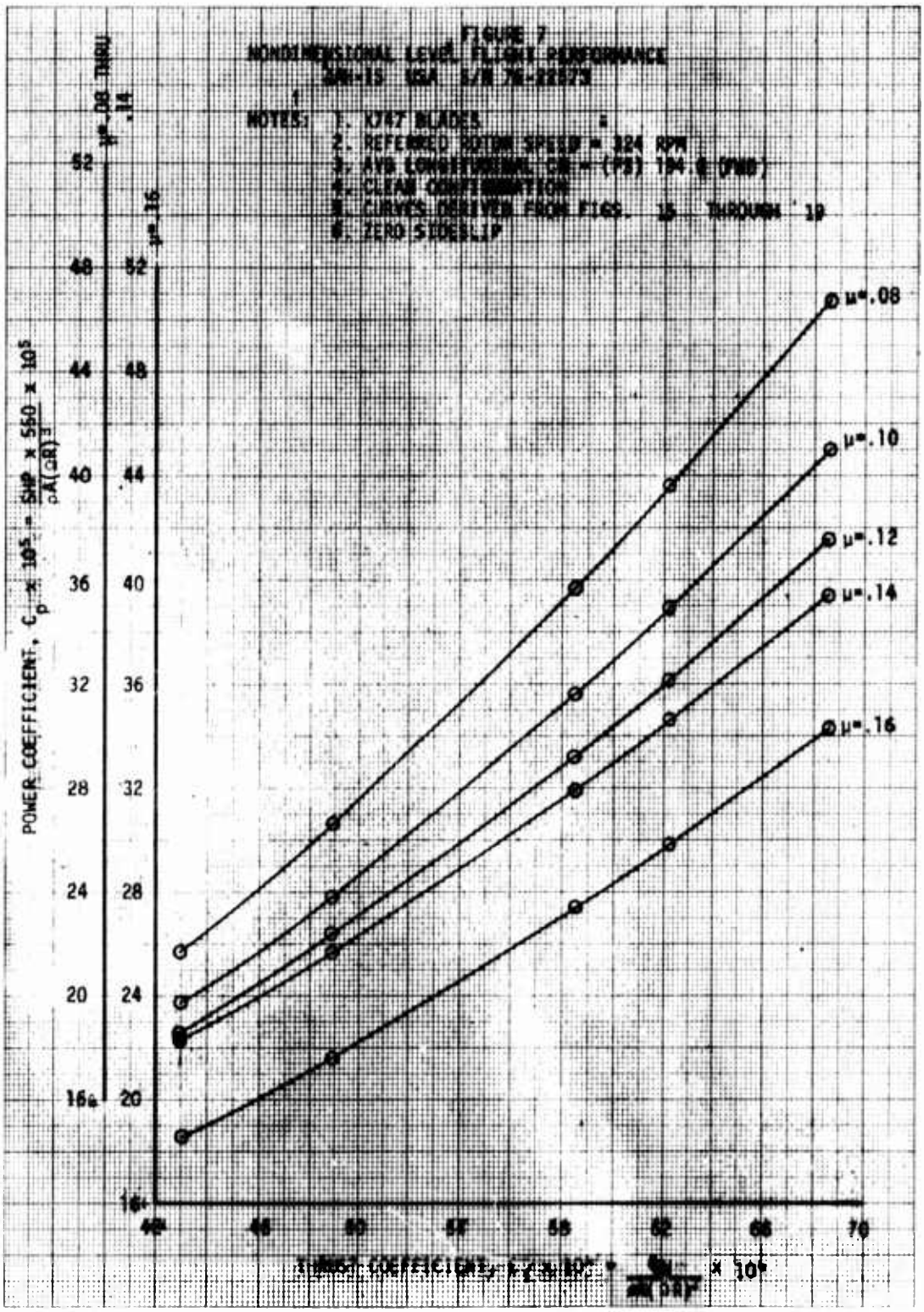
FIGURE 7
NONDIMENSIONAL LEVEL FLIGHT PERFORMANCE
SIKORSKY S-61R (CH-3E) S/N 76-22575
NOTES:
1. X747 BLADES
2. REFERRED ROTOR SPEED = 324 RPM
3. AVG LONGITUDINAL CG = (FS) 194.6 (FWD)
4. CLEAN CONFIGURATION
5. CURVES DERIVED FROM FIGS. 15 THROUGH 19
6. ZERO SIDESLIP
μ=.08
μ=.10
μ=.12
μ=.14
μ=.16
POWER COEFFICIENT, $C_p \times 10^5 = \frac{SHP \times 550 \times 10^5}{\rho A(\Omega R)^3}$
TORQUE COEFFICIENT, $C_Q \times 10^5 = \frac{Q \times 10^5}{\rho A R(\Omega R)^2}$

FIGURE 8
NONDIMENSIONAL LEVEL FLIGHT PERFORMANCE
JAH-1S USA S/N 76-22573

NOTES:
1. K747 BLADES
2. REFERRED ROTOR SPEED = 324 RPM
3. AVG LONGITUDINAL CG = (FS) 194.2 (FWD)
4. CLEAN CONFIGURATION
5. CURVES DERIVED FROM FIGS. 15 THROUGH 19
6. ZERO SIDESLIP

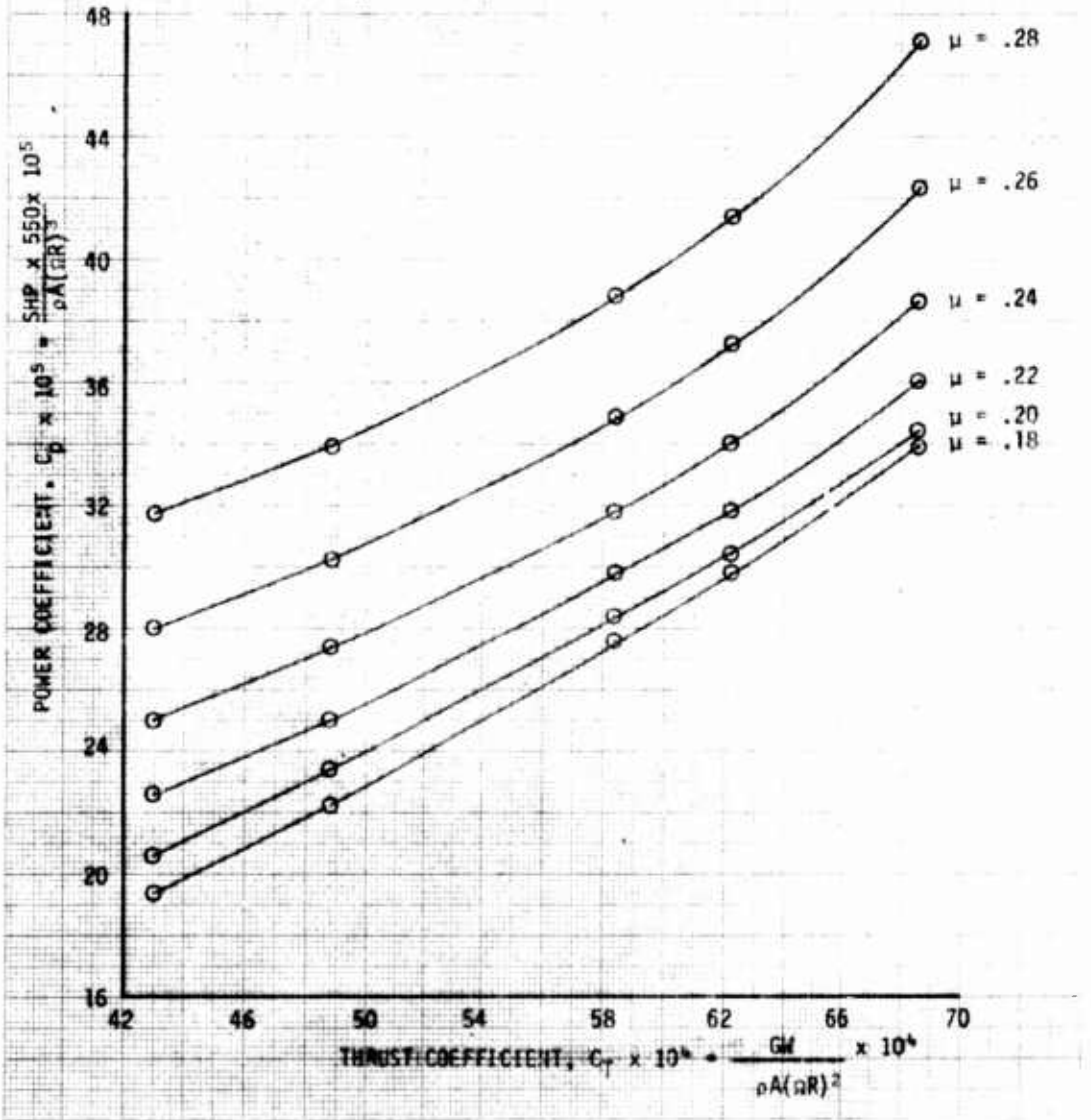

FIGURE 9
NONDIMENSIONAL LEVEL FLIGHT PERFORMANCE
JAH-1S USA S/N 76-22573

NOTES:
1. K747 BLADES
2. REFERRED ROTOR SPEED = 324 RPM
3. AVG LONGITUDINAL CG = (FS) 194.2 (FWD)
4. CLEAN CONFIGURATION
5. CURVES DERIVED FROM FIGURES 15 THROUGH 19
6. ZERO SIDESLIP

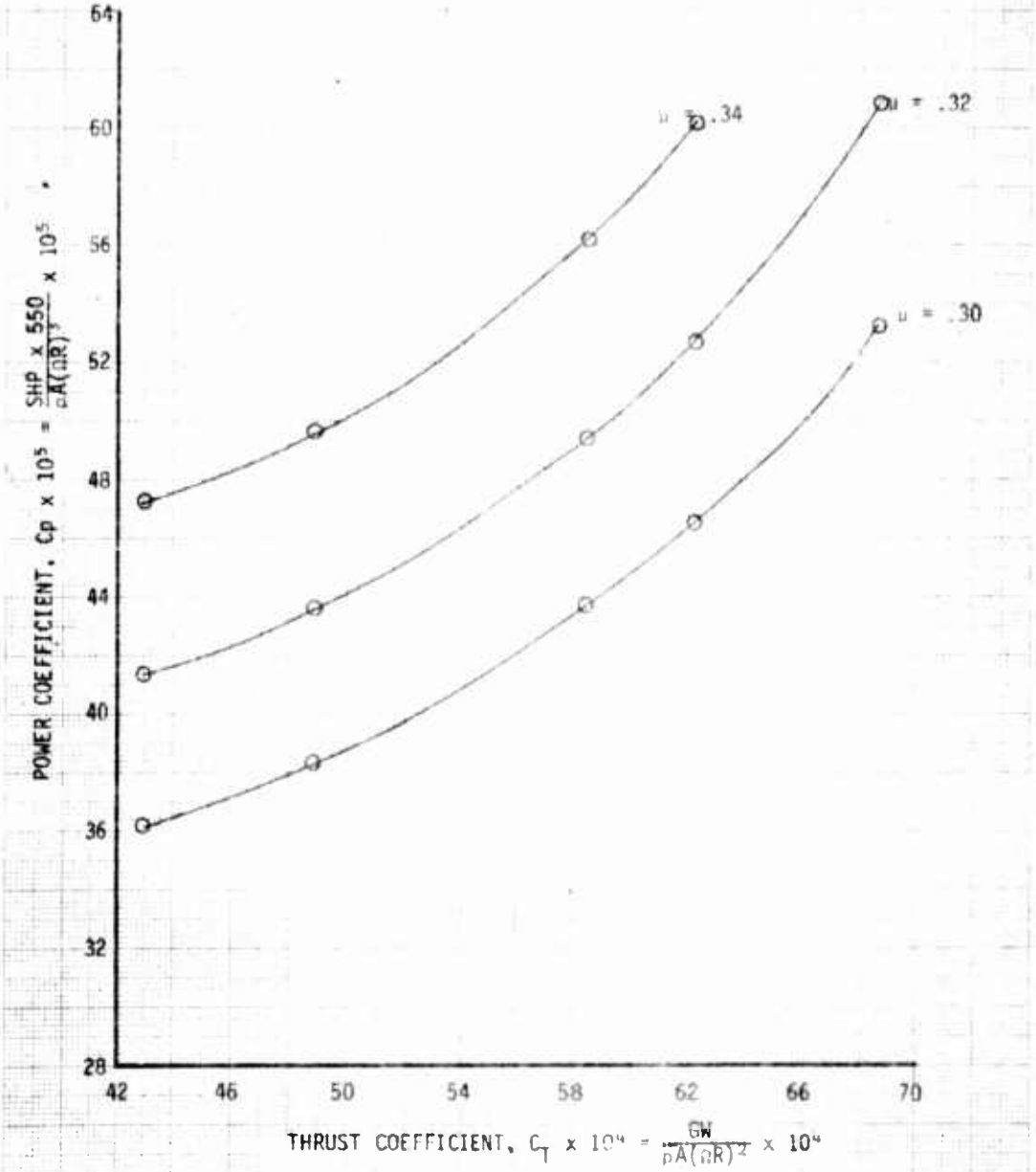

FIGURE 10
LEVEL FLIGHT PERFORMANCE
JAH-1S S/N 76-22573
LYCOMING ENGINE MODEL T53-L-703 S/N 13145Z
B540 BLADES S/N 00021 AND S/N 50107

AVG GROSS WEIGHT (LB)	AVG LONGITUDINAL CG (FS)	AVG LATERAL CG (BL)	AVG DENSITY ALT (FT)	AVG OAT (DEG. C)	AVG ROTOR SPEED (RPM)	AVG C_T	CONFIGURATION
8140	194.0(FWD)	0.1(RT)	1300	14.5	323.0	0.004226	CLEAN

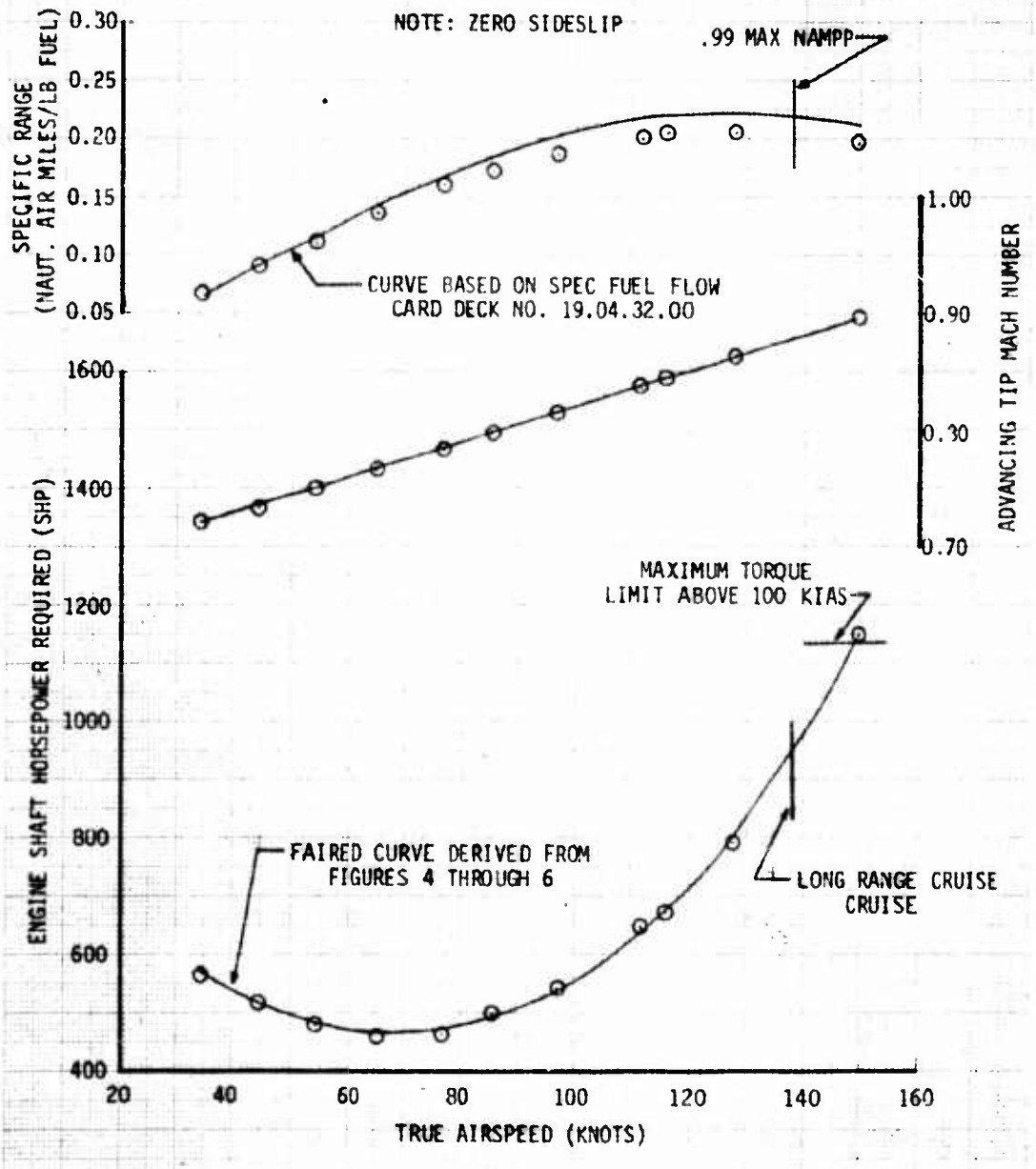

FIGURE 11
LEVEL FLIGHT PERFORMANCE
JAH-1S S/N 76-22573
LYCOMING ENGINE MODEL T53-L-703 S/N 13145Z
B540 BLADES S/N 00021 AND S/N 50107

AVG GROSS WEIGHT (LB)	AVG LONGITUDINAL CG (FS)	AVG LATERAL CG (BL)	AVG DENSITY ALT (FT)	AVG OAT (DEG. C)	AVG ROTOR SPEED (RPM)	AVG C_T	CONFIGURATION
8160	194.0(FWD)	0.1(RT)	5200	7.5	319.0	0.004881	CLEAN

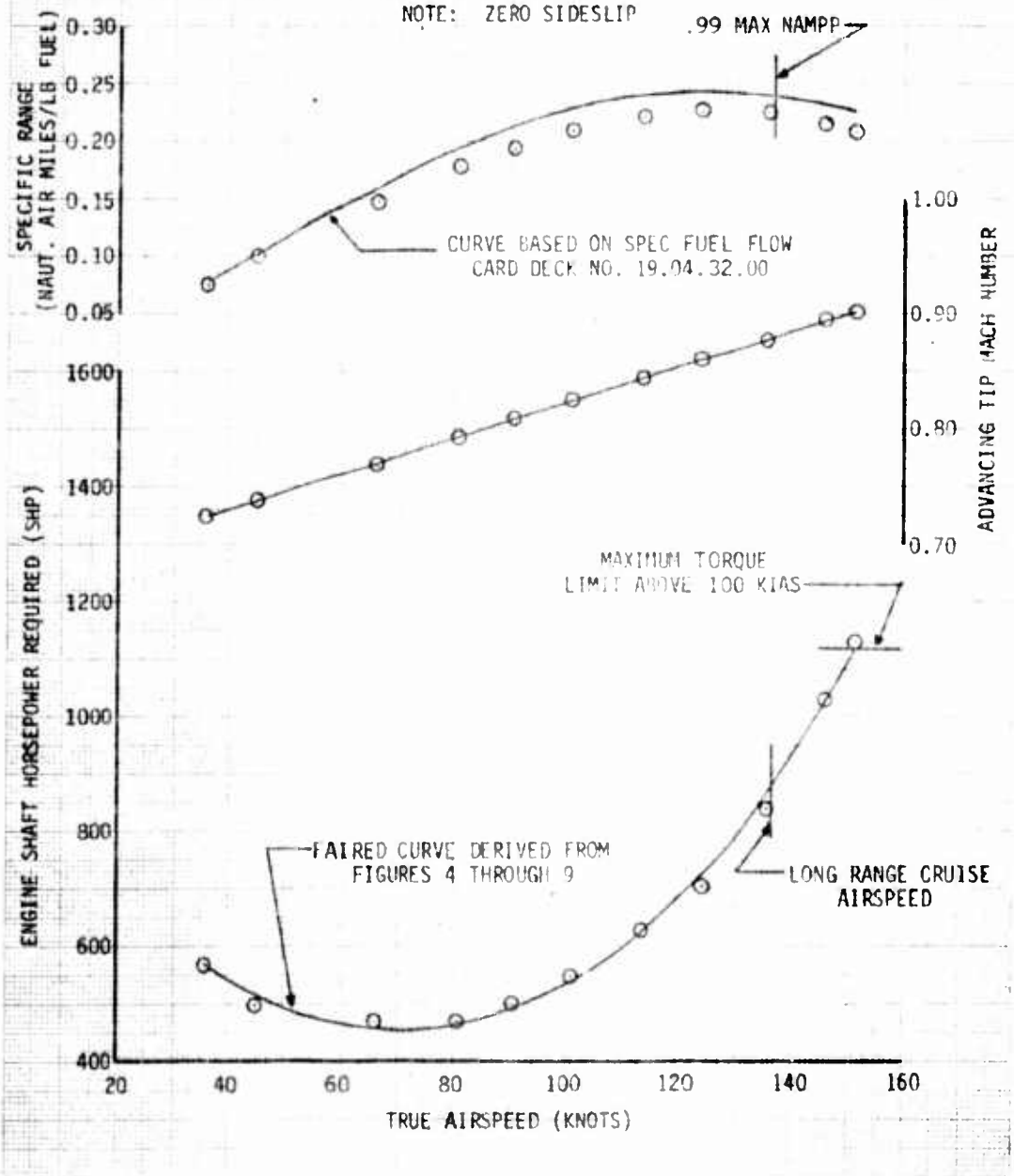

FIGURE 12
LEVEL FLIGHT PERFORMANCE
JAH-1S S/N 76-22573
LYCOMING ENGINE MODEL T53-L-703 S/N 13145Z
8450 BLADES S/N 00021 AND S/N 50107

AVG GROSS WEIGHT (LB)	AVG LONGITUDINAL CG (FS)	AVG LATERAL CG (BL)	AVG DENSITY ALT (FT)	AVG OAT (DEG. C)	AVG ROTOR SPEED (RPM)	AVG C_T	CONFIGURATION
8600	194.5(FWD)	0.1(RT)	7400	3.5	317.0	0.005572	CLEAN

NOTE: ZERO SIDESLIP

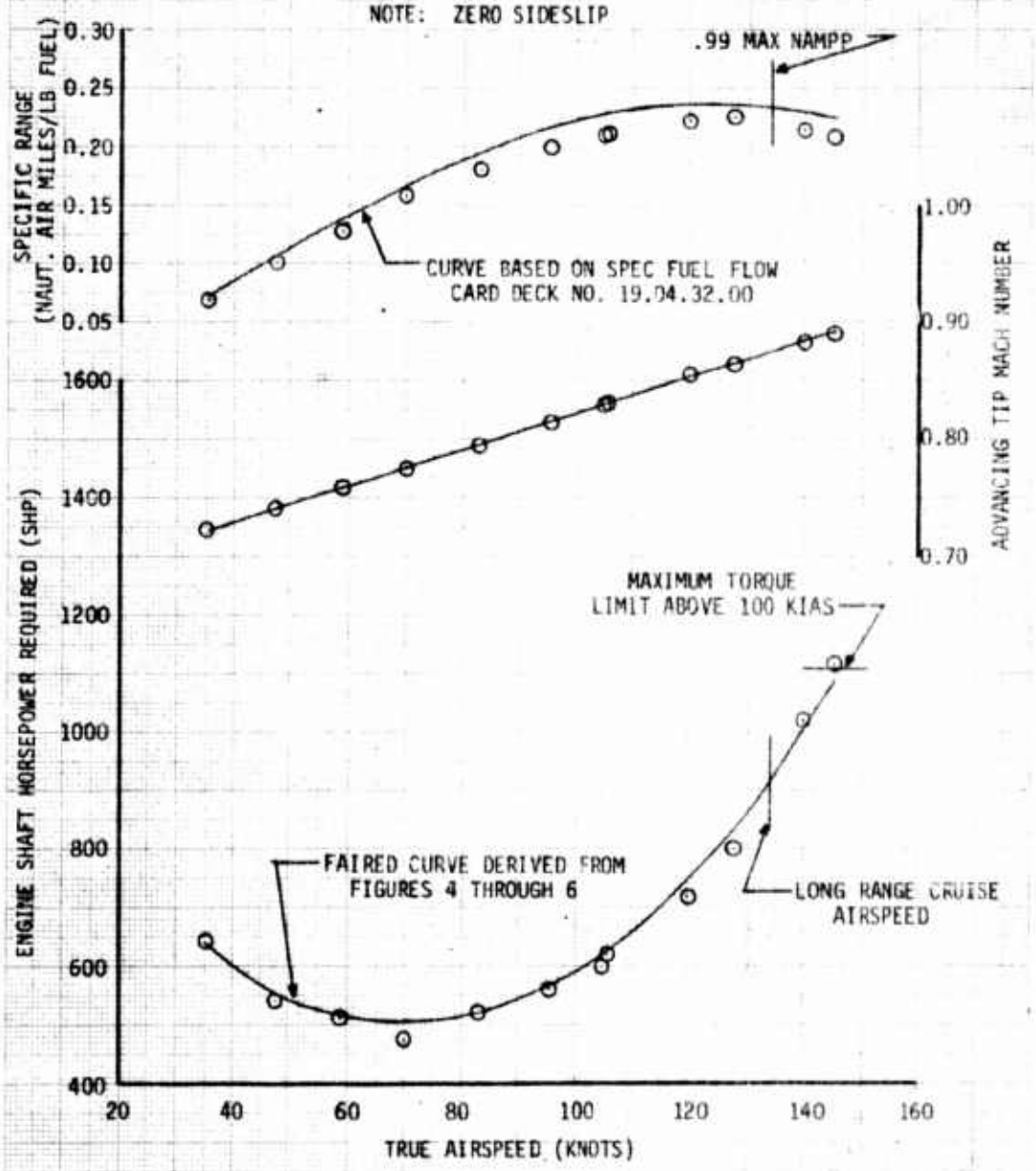

FIGURE 13
LEVEL FLIGHT PERFORMANCE
JAH-1S S/N 76-22573
LYCOMING ENGINE MODEL T53-L-703 S/N 13145Z
B540 BLADES S/N 00021 AND S/N 50107

AVG GROSS WEIGHT (LB)	AVG CG LOCATION LONG (FS)	AVG CG LOCATION LAT (BL)	AVG DENSITY ALT (FT)	AVG OAT (DEG.C)	AVG ROTOR SPEED (RPM)	AVG C_T	CONFIGURATION
8760	194.4 (FWD)	0.1 (RT)	10220	2.0	317.0	0.006196	CLEAN

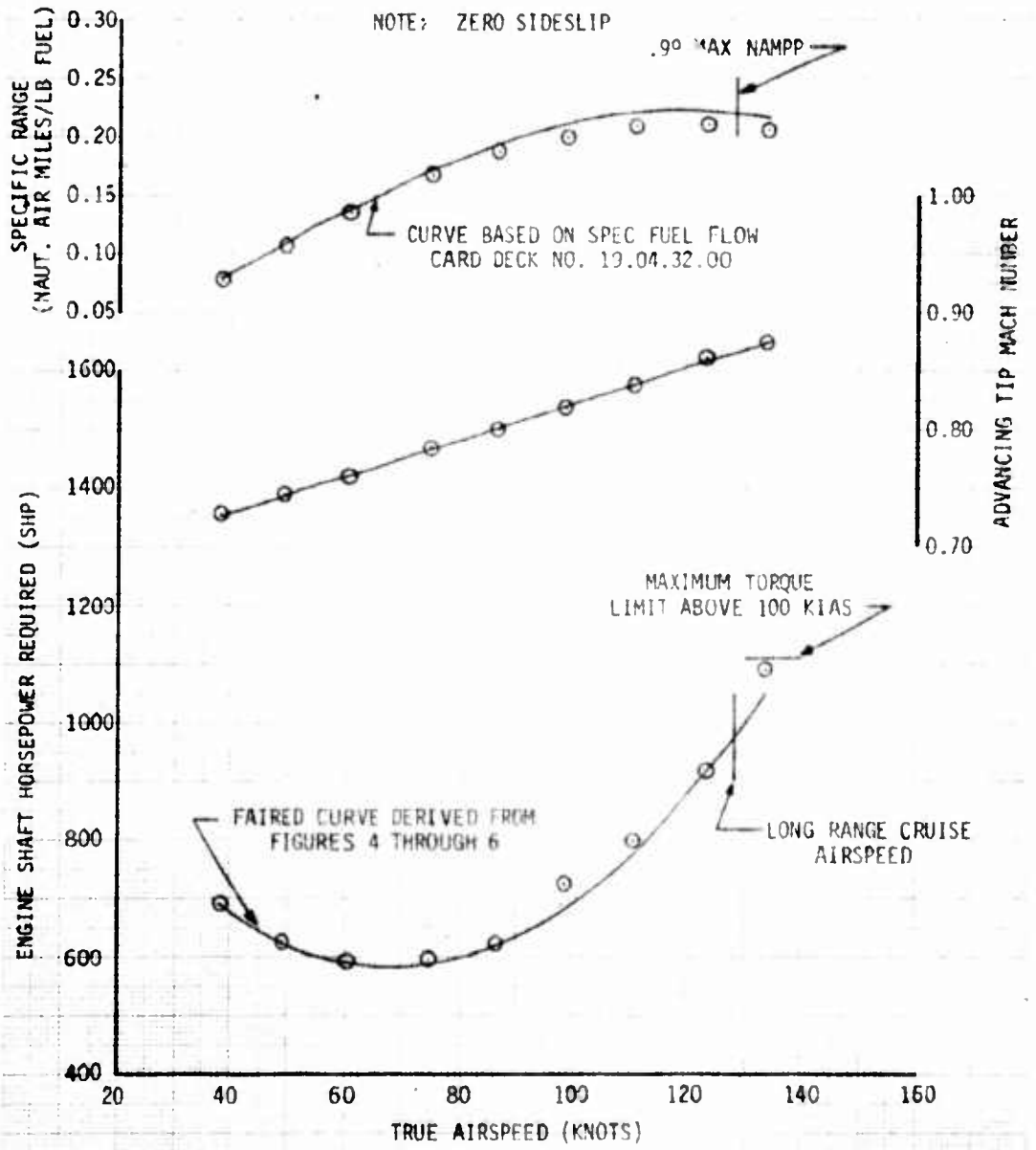

FIGURE 14
LEVEL FLIGHT PERFORMANCE
JAH-1S S/N 76-22573
LYCOMING ENGINE MODEL T53-L-703 S/N 131452
B540 BLADES S/N 00021 AND S/N 50107

AVG GROSS WEIGHT (LB)	AVG CG LOCATION LONG (FS)	LAT (BL)	AVG DENSITY ALT (FT)	AVG OAT (DEG.C)	AVG ROTOR SPEED (RPM)	AVG C_T	CONFIGURATION
9100	194.7 (FWD)	0.1 (RT)	11700	-1.0	315.0	0.006832	CLEAN

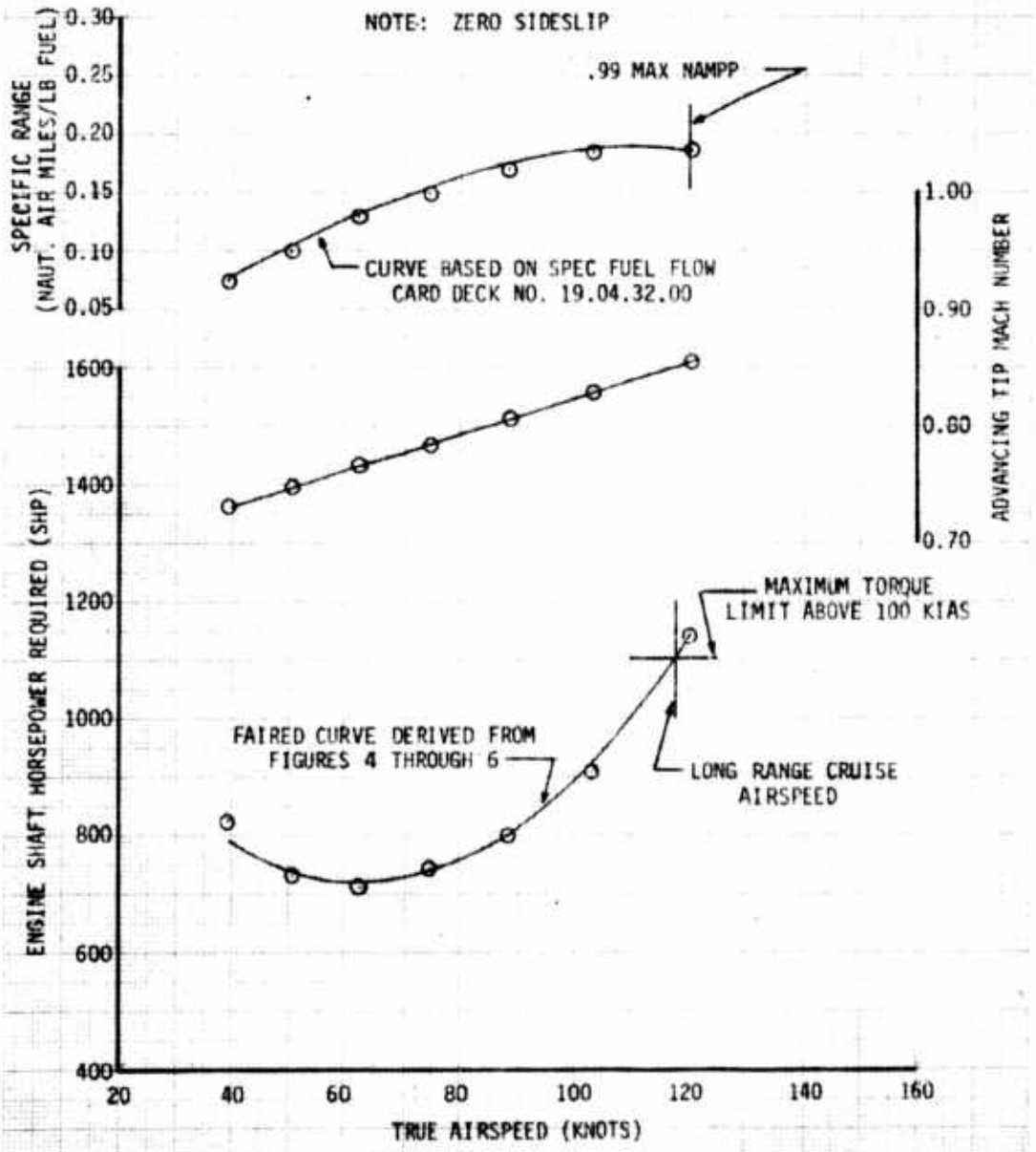

FIGURE 15
LEVEL FLIGHT PERFORMANCE
JAH-1S S/N 76-22573
LYCOMING ENGINE MODEL T53-L-703 S/N 13145Z
K747 BLADES S/N 2016 AND S/N 2025

AVG GROSS WEIGHT (LB)	AVG CG LOCATION LONG (FS)	LAT (BL)	AVG DENSITY ALT (FT)	AVG OAT (DEG. C)	AVG ROTOR SPEED (RPM)	AVG C_T	CONFIGURATION
8120	193.9 (FWD)	0.1 (RT)	2180	16.5	324.0	0.004300	CLEAN

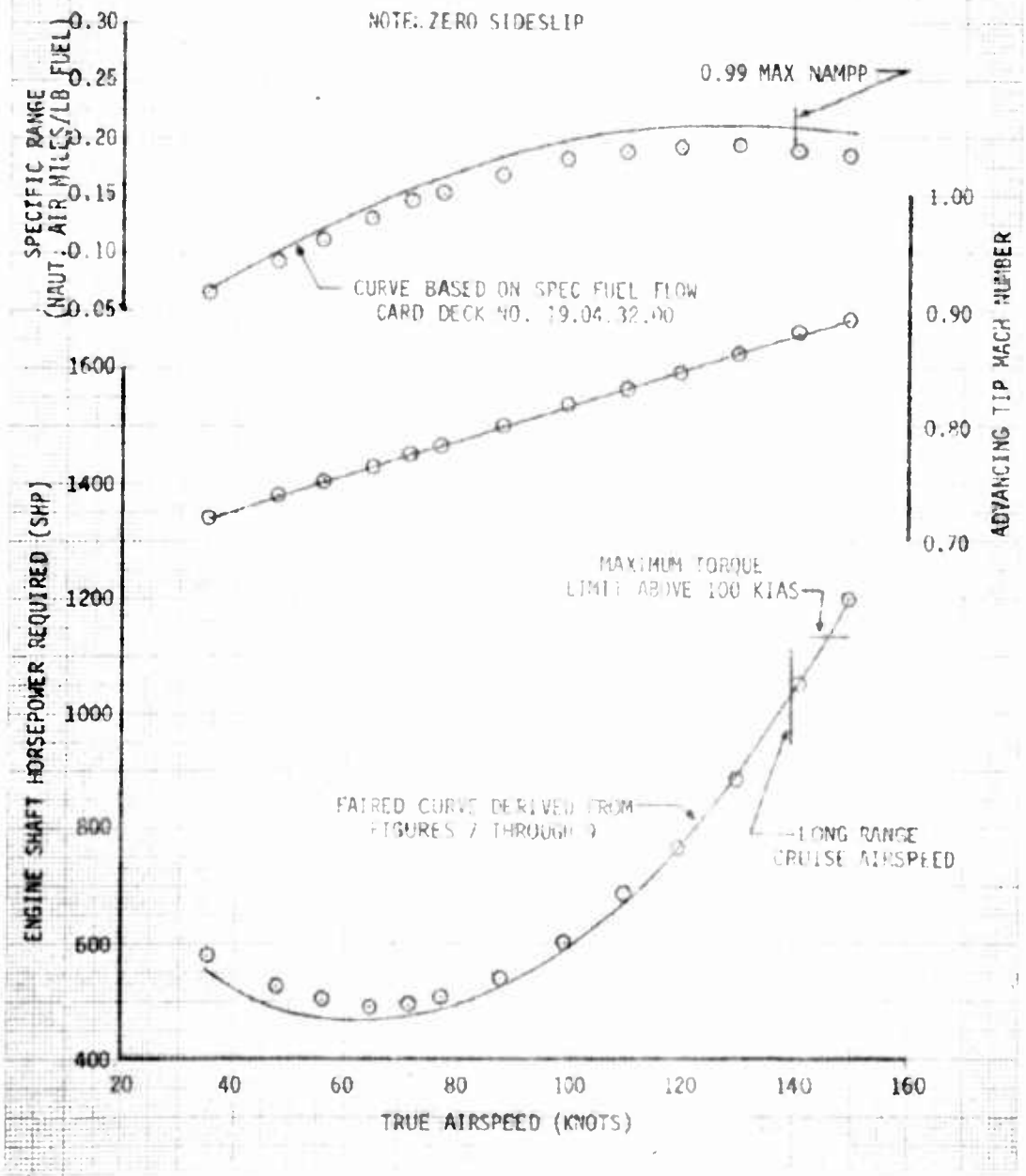

FIGURE 16
LEVEL FLIGHT PERFORMANCE
JAH-1S S/N 76-22573
LYCOMING ENGINE MODEL T53-L-703 S/N 13145Z
K747 BLADES S/N 2016 AND S/N 2025

AVG GROSS WEIGHT (LB)	AVG CG LOCATION LONG (FS)	LAT (BL)	AVG DENSITY ALT (FT)	AVG OAT (DEG.C)	AVG ROTOR SPEED (RPM)	AVG C_T	CONFIGURATION
7980	193.7 (FWD)	0.1 (RT)	5160	0.0	315.0	0.004889	CLEAN

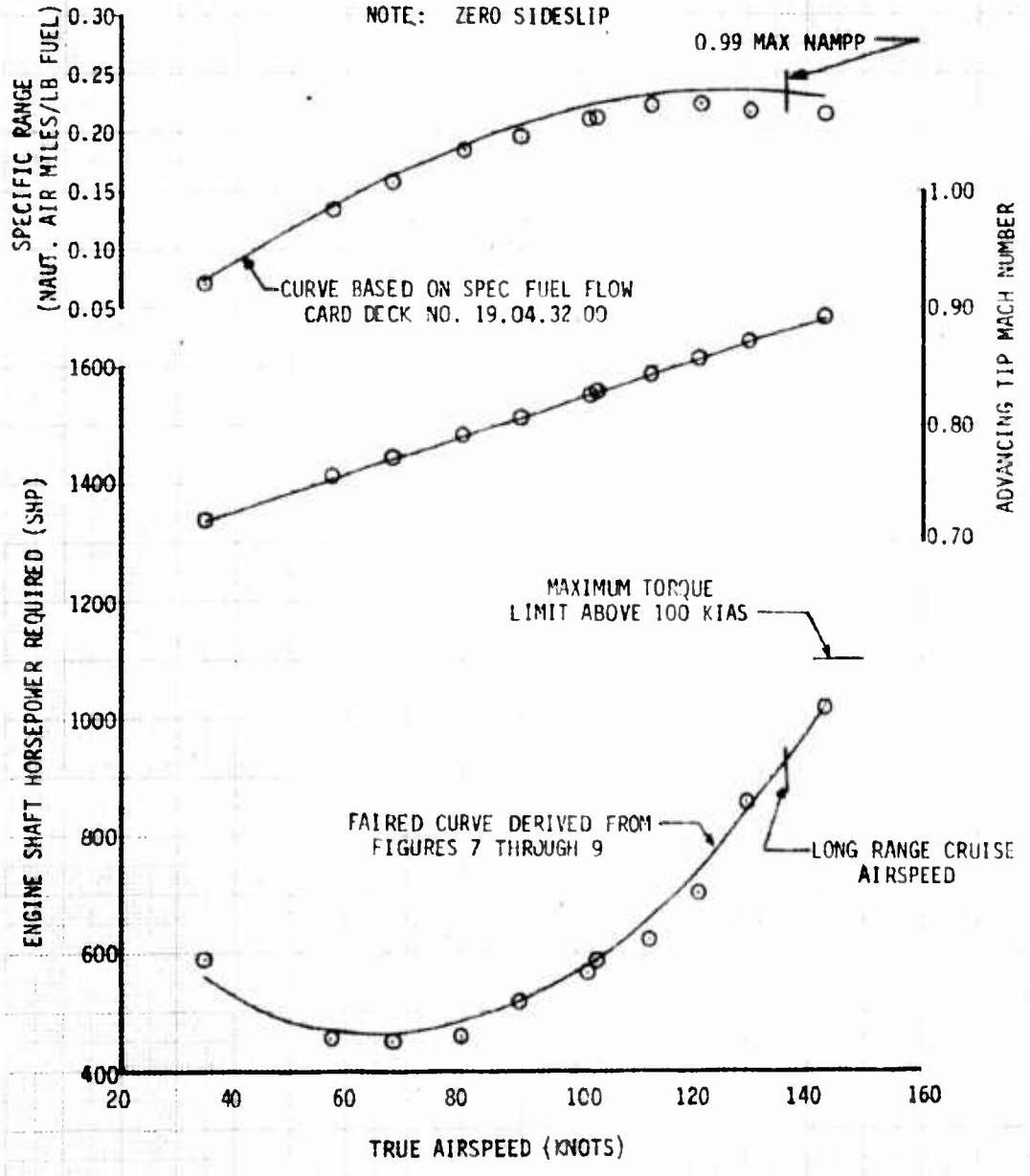

FIGURE 17
LEVEL FLIGHT PERFORMANCE
JAH-1S S/N 76-22673
LYCOMING ENGINE MODEL T53-L-703 S/N 13145Z
K747 BLADES S/N 2016 AND 2025

AVG GROSS WEIGHT (LB)	AVG CG LOCATION LONG (FS)	AVG CG LOCATION LAT (BL)	AVG DENSITY ALT (FT)	AVG OAT (DEG.C)	AVG ROTOR SPEED (RPM)	AVG C_T	CONFIGURATION
8940	194.0 (FWD)	0.1 (RT)	7100	-2.5	314.0	0.005849	CLEAN

NOTE: 1. ZERO SIDESLIP
2. FUEL FLOW DATA NOT AVAILABLE

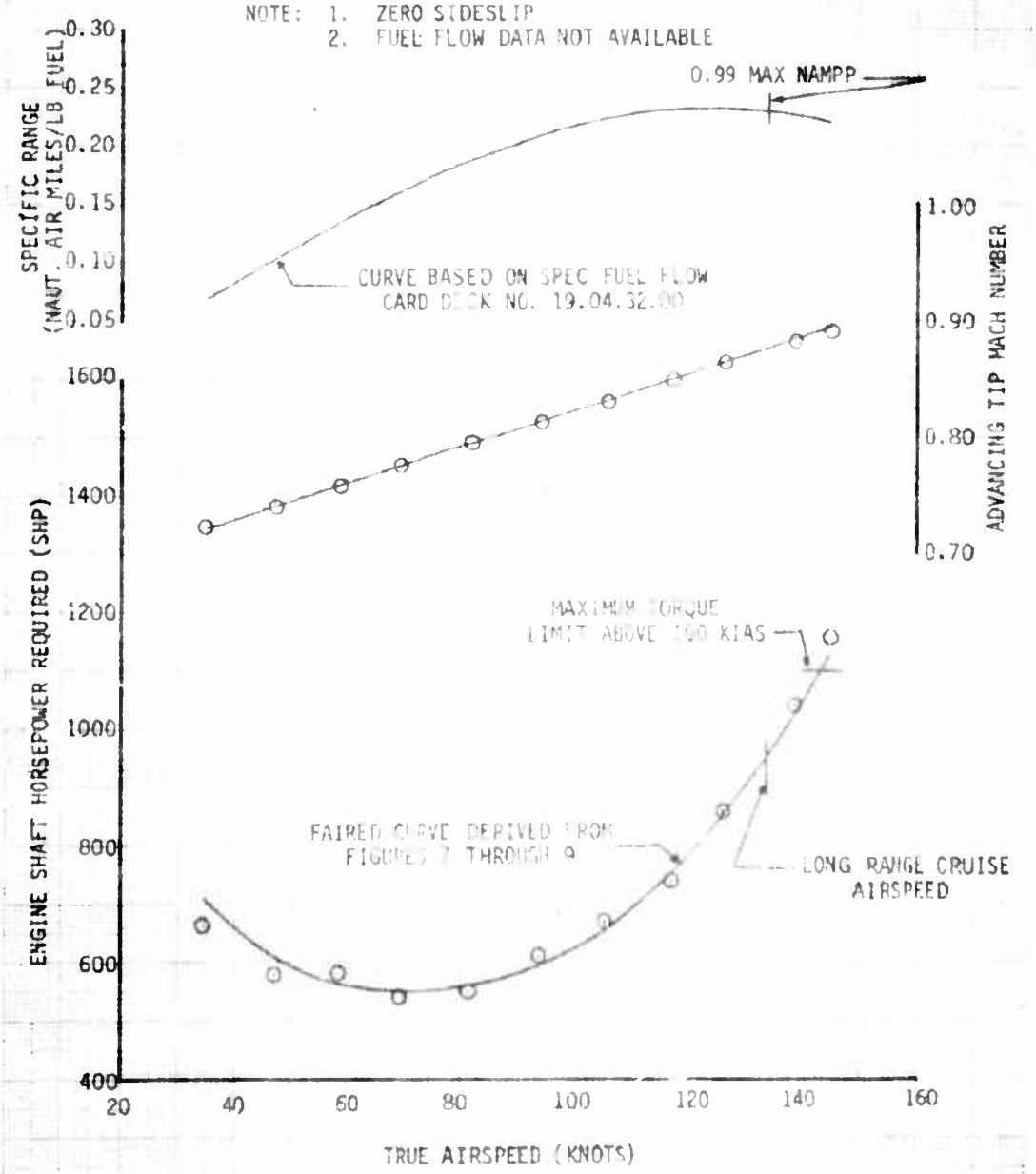

FIGURE 18
LEVEL FLIGHT PERFORMANCE
JAH-1S S/N 76-22573
LYCOMING ENGINE MODEL T53-L-703 S/N 13145Z
K747 BLADES S/N 2016 AND S/N 2025

AVG GROSS WEIGHT (LB)	AVG CG LOCATION LONG (FS)	LAT (BL)	AVG DENSITY ALT (FT)	AVG OAT (DEG.C)	AVG ROTOR SPEED (RPM)	AVG C_T	CONFIGURATION
8960	194.8 (FWD)	0.1 (RT)	9600	2.5	317.0	0.006216	CLEAN

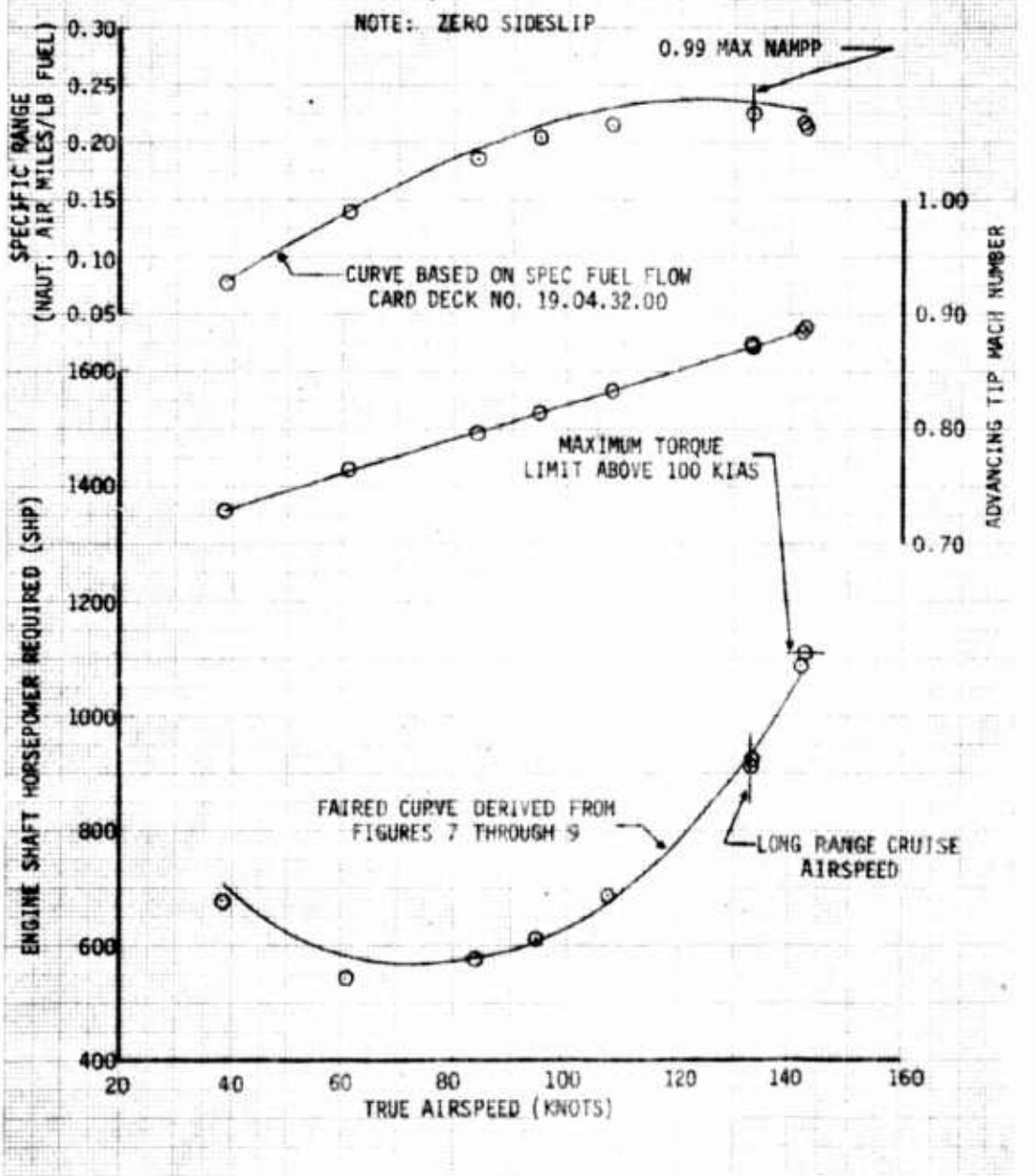

FIGURE 19
LEVEL FLIGHT PERFORMANCE
JAH-1S S/N 76-22573
LYCOMING ENGINE MODEL T53-L-703 S/N 13145Z
K747 BLADES S/N 2016 AND S/N 2025

AVG GROSS WEIGHT (LB)	AVG CG LOCATION LONG (FS)	AVG CG LOCATION LAT (BL)	AVG DENSITY ALT (FT)	AVG OAT (DEG.C)	AVG ROTOR SPEED (RPM)	AVG C_T	CONFIGURATION
9300	194.8 (FWD)	0.1 (RT)	11340	1.0	316.0	0.006859	CLEAN

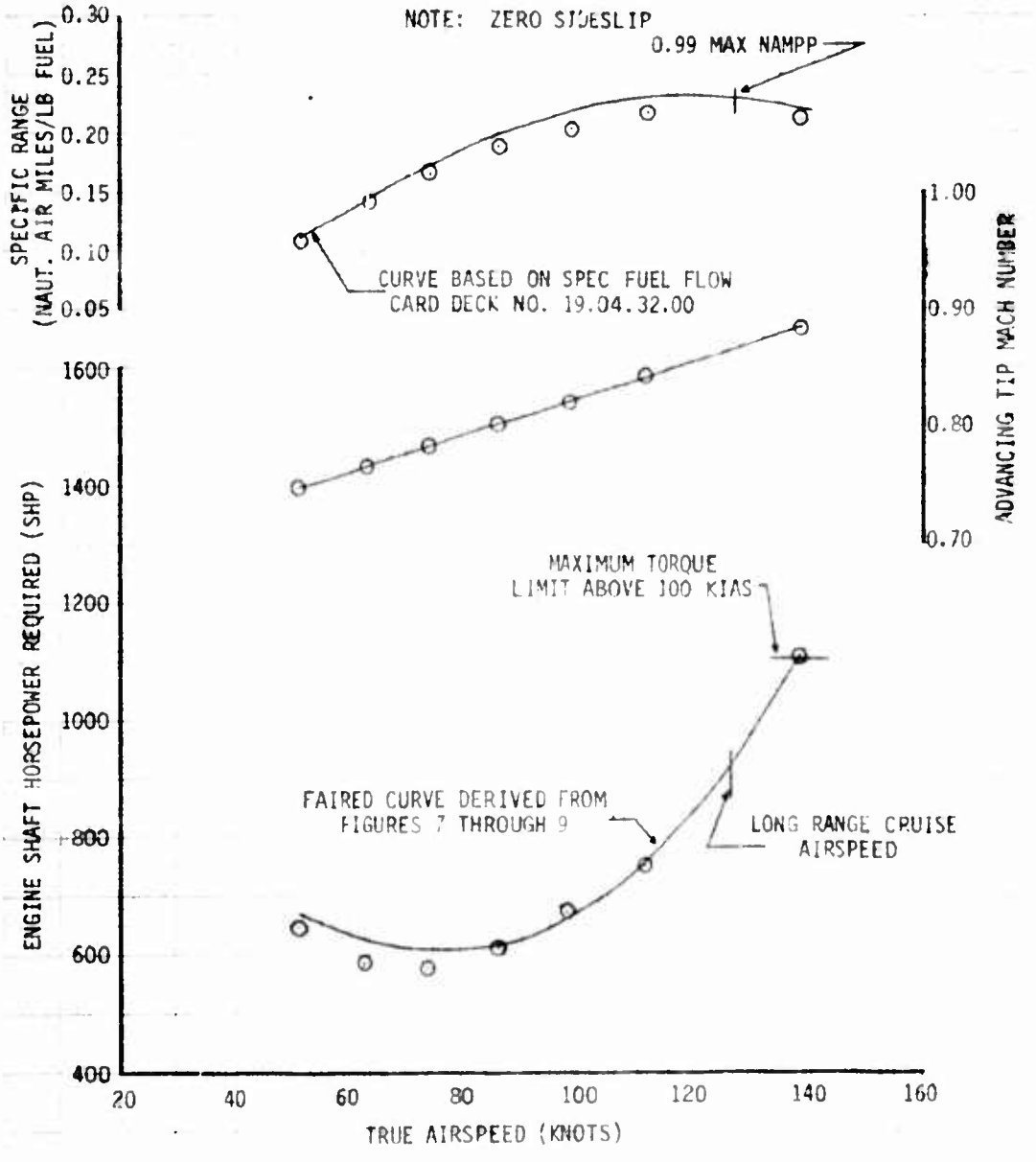

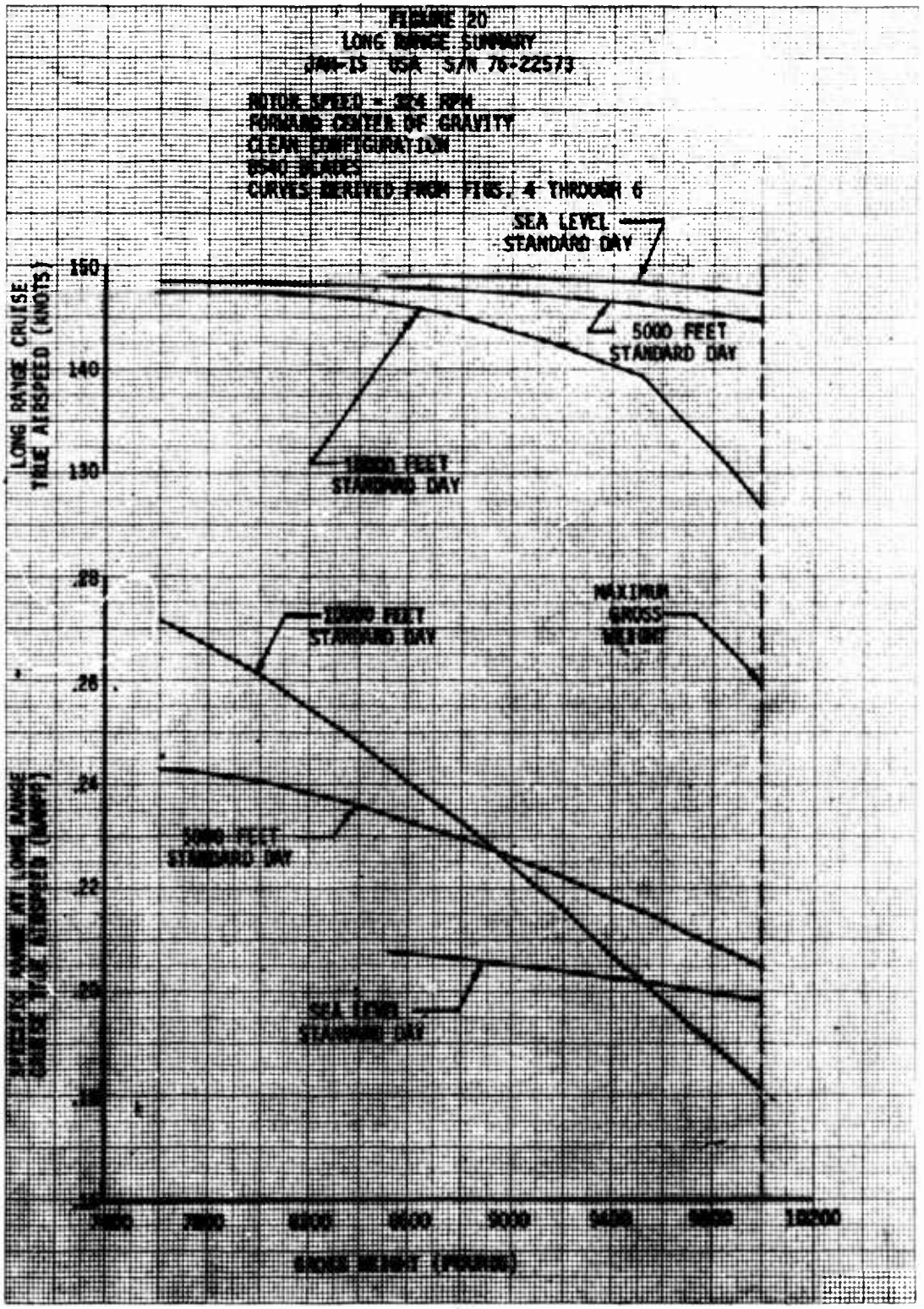
FIGURE 20
LONG RANGE SUMMARY
JAM-IS USA S/N 76-22573
MOTOR SPEED = 324 RPM
FORWARD CENTER OF GRAVITY
CLEAN CONFIGURATION
ISAU BASIS
CURVES DERIVED FROM FIGS. 4 THROUGH 6
SEA LEVEL STANDARD DAY
5000 FEET STANDARD DAY
10000 FEET STANDARD DAY
MAXIMUM GROSS WEIGHT
LONG RANGE CRUISE TRUE AIRSPEED (KNOTS)
150
140
130
.28
.26
.24
.22
10200

FIGURE 21
LONG RANGE CRUISE SUMMARY
JAH-1S USA S/N 76-22573

ROTOR SPEED = 324 RPM
FORWARD CENTER OF GRAVITY
CLEAN CONFIGURATION
K747 BLADES
CURVES DERIVED FROM FIGS. 7 THROUGH 9

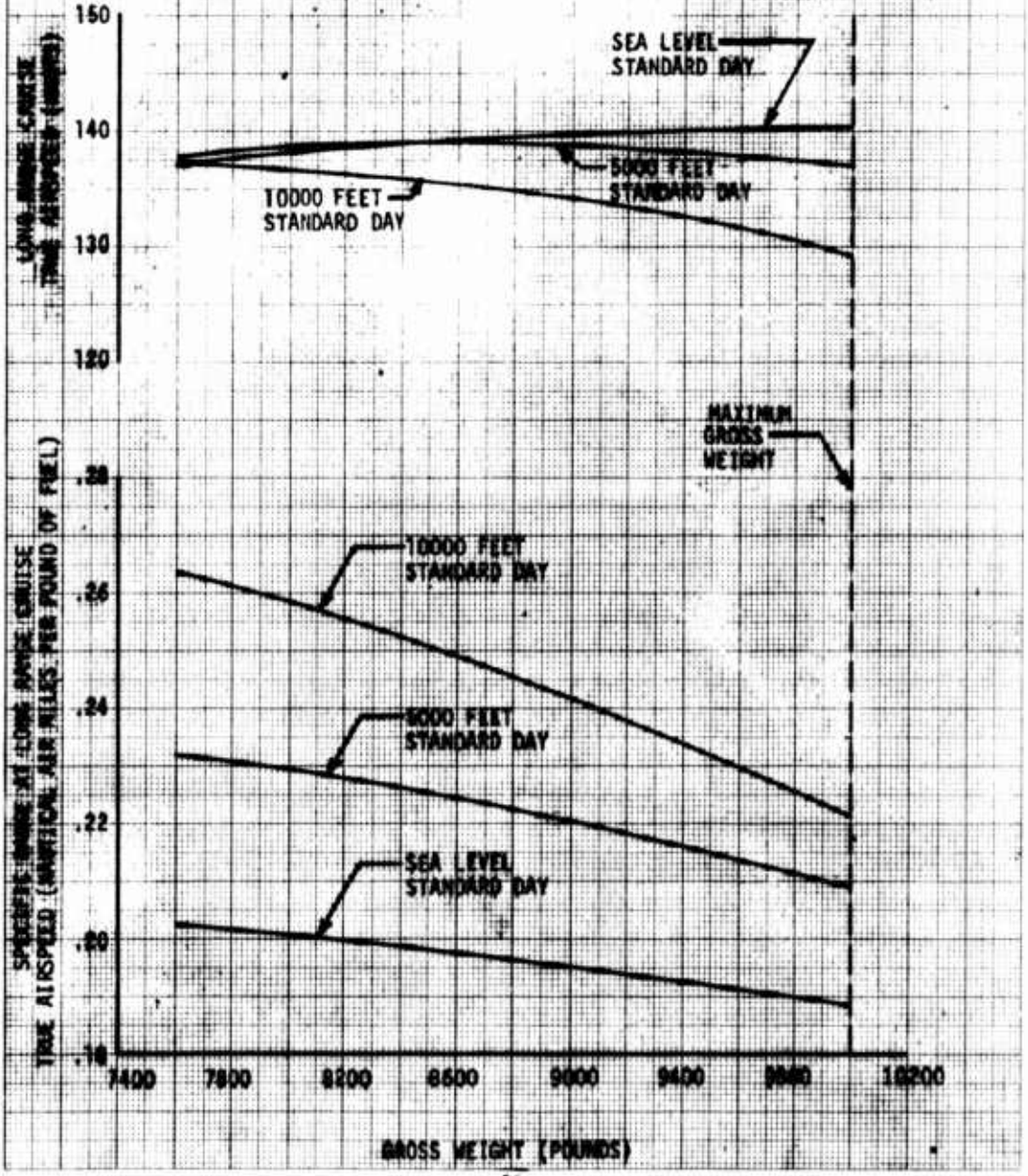

FIGURE 22
MAXIMUM ENDURANCE
JAH-1S USA S/N 76-22573

ROTOR SPEED - 324 RPM
FORWARD CENTER OF GRAVITY
CLEAN CONFIGURATION
K747 BLADES
CURVES DERIVED FROM FIGS. 4 THROUGH 6

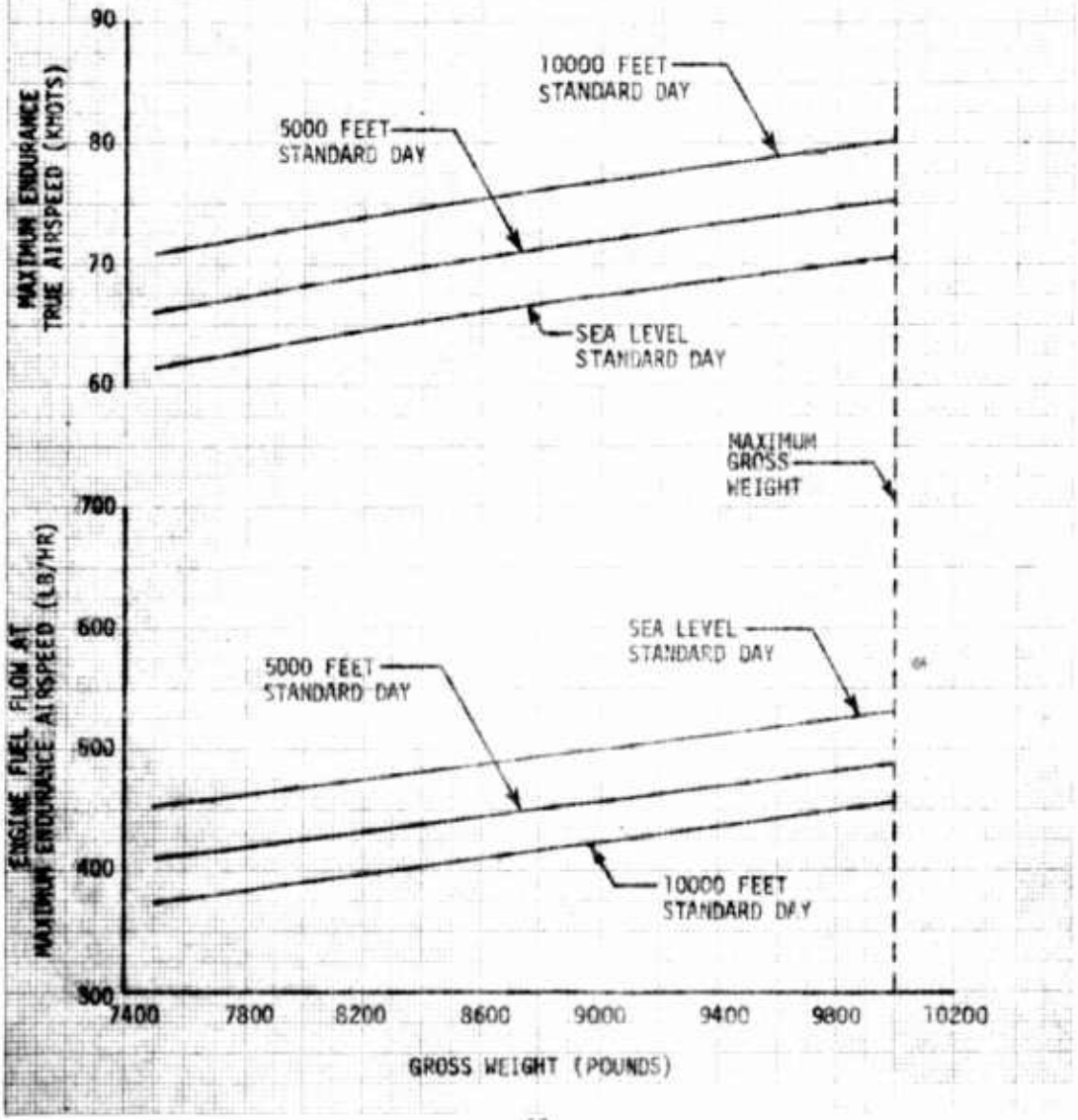

FIGURE 23
MAXIMUM ENDURANCE
JAH-1S USA S/N 76-22573

ROTOR SPEED = 324 RPM
FORWARD CENTER OF GRAVITY
CLEAN CONFIGURATION
B540 BLADES
CURVES DERIVED FROM FIGURES 4 THROUGH 6

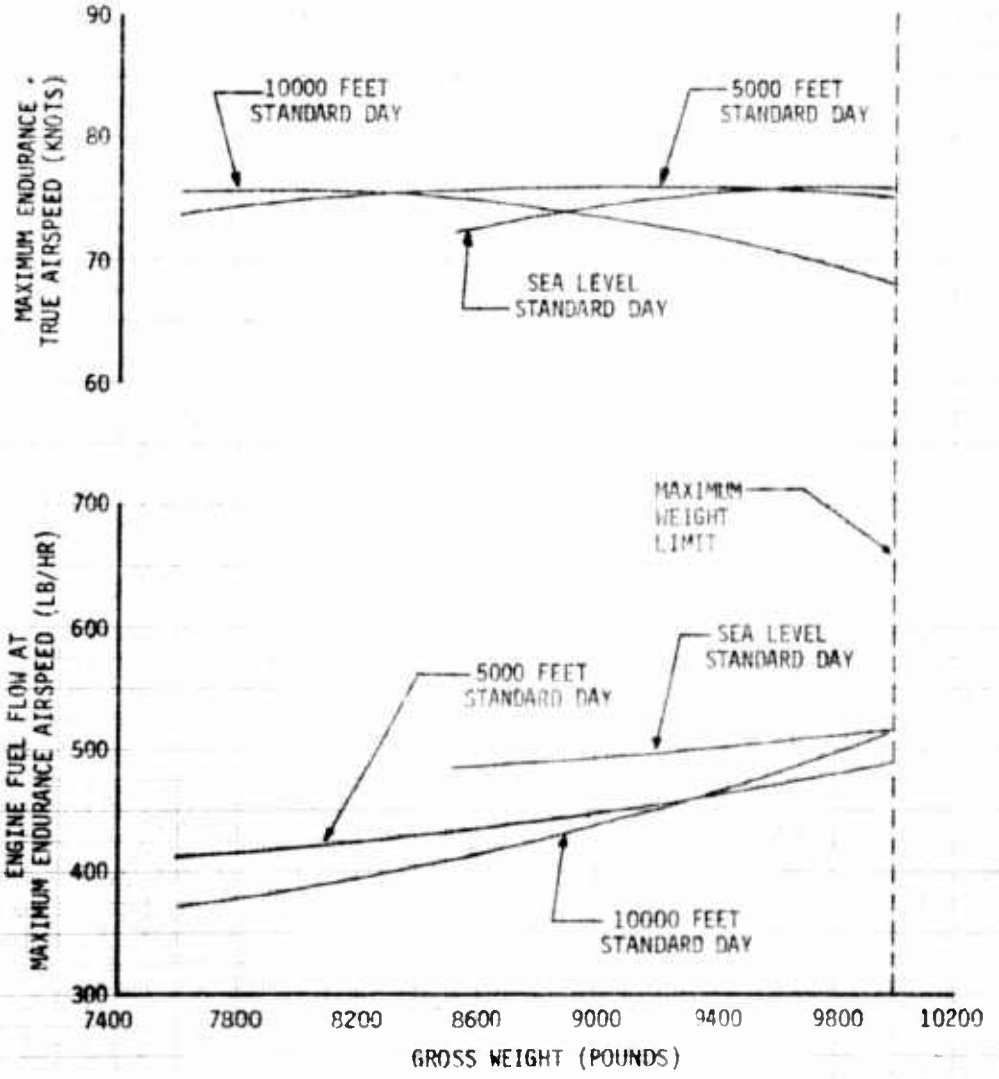

FIGURE 24

CONTROL POSITION IN TRIMMED FORWARD FLIGHT

JAH-1S USA S/N 76-22573

AVG GROSS WEIGHT (LB)	AVG CG LOCATION LONG (FS)	AVG CG LOCATION LAT (BL)	AVG DENSITY ALTITUDE (FT)	AVG OAT (°C)	AVG ROTOR SPEED (RPM)	AVG THRUST COEFF.	TRUE FLIGHT CONDITION	CONFIGURATION
8140	194.0 (FWD)	0.1 (RT)	1280	14.5	323	0.004226	LEVEL	CLEAN [illegible] BLADES

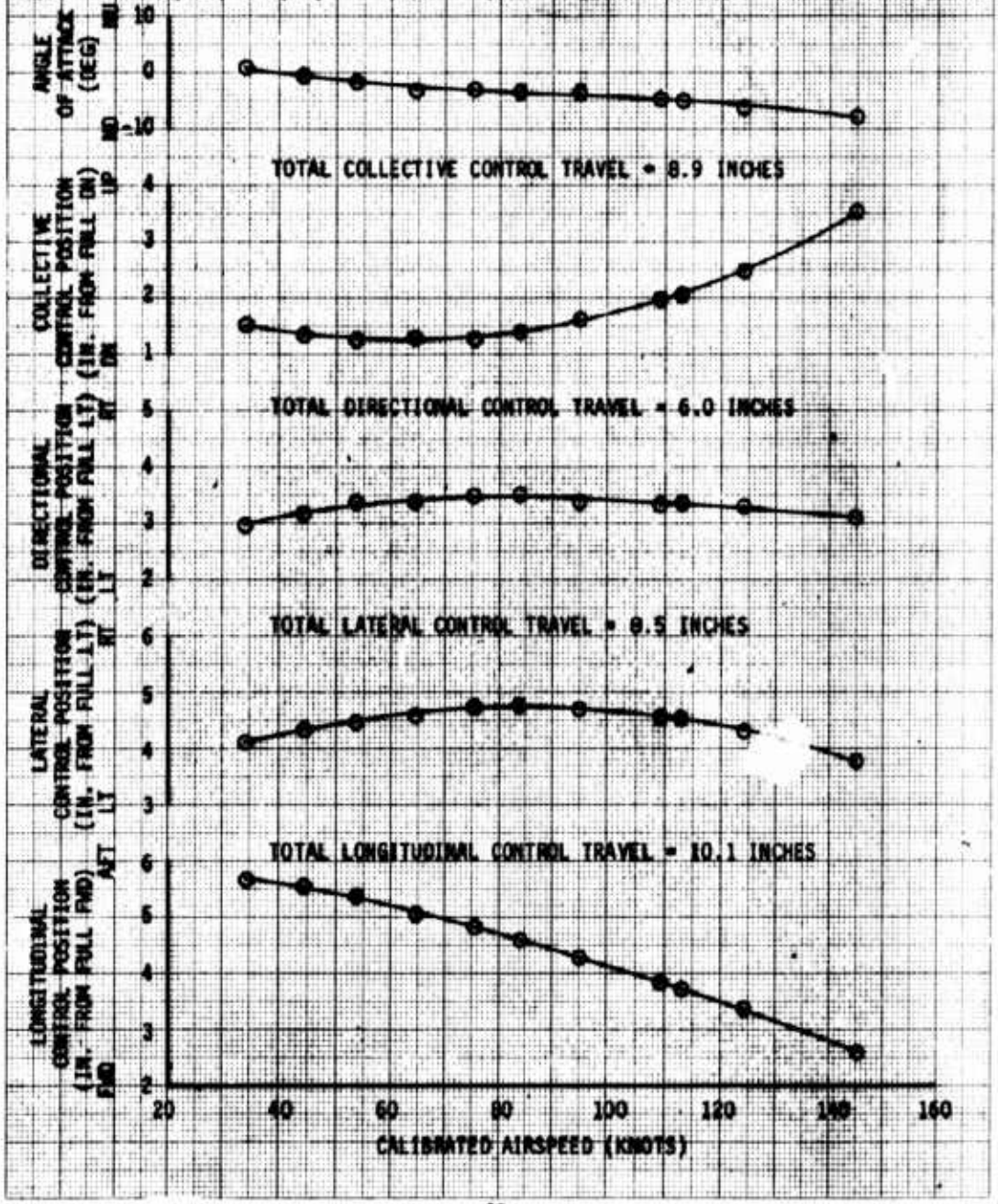

FIGURE 25
CONTROL POSITIONS IN TRIMMED FORWARD FLIGHT
JAH-1S USAF S/N 75-22573

AVG GROSS WEIGHT (LB)	AVG CG LOCATION LONG (FS)	AVG CG LOCATION LAT (BL)	AVG DENSITY ALTITUDE (FT)	AVG OAT (°C)	AVG ROTOR SPEED (RPM)	AVG THRUST COEFF.	TRIM FLIGHT CONDITION	CONFIGURATION
9100	194.7(FWD)	0.1(RT)	11680	-1.4	315	0.006833	LEVEL	CLEAN 8540 BLADES

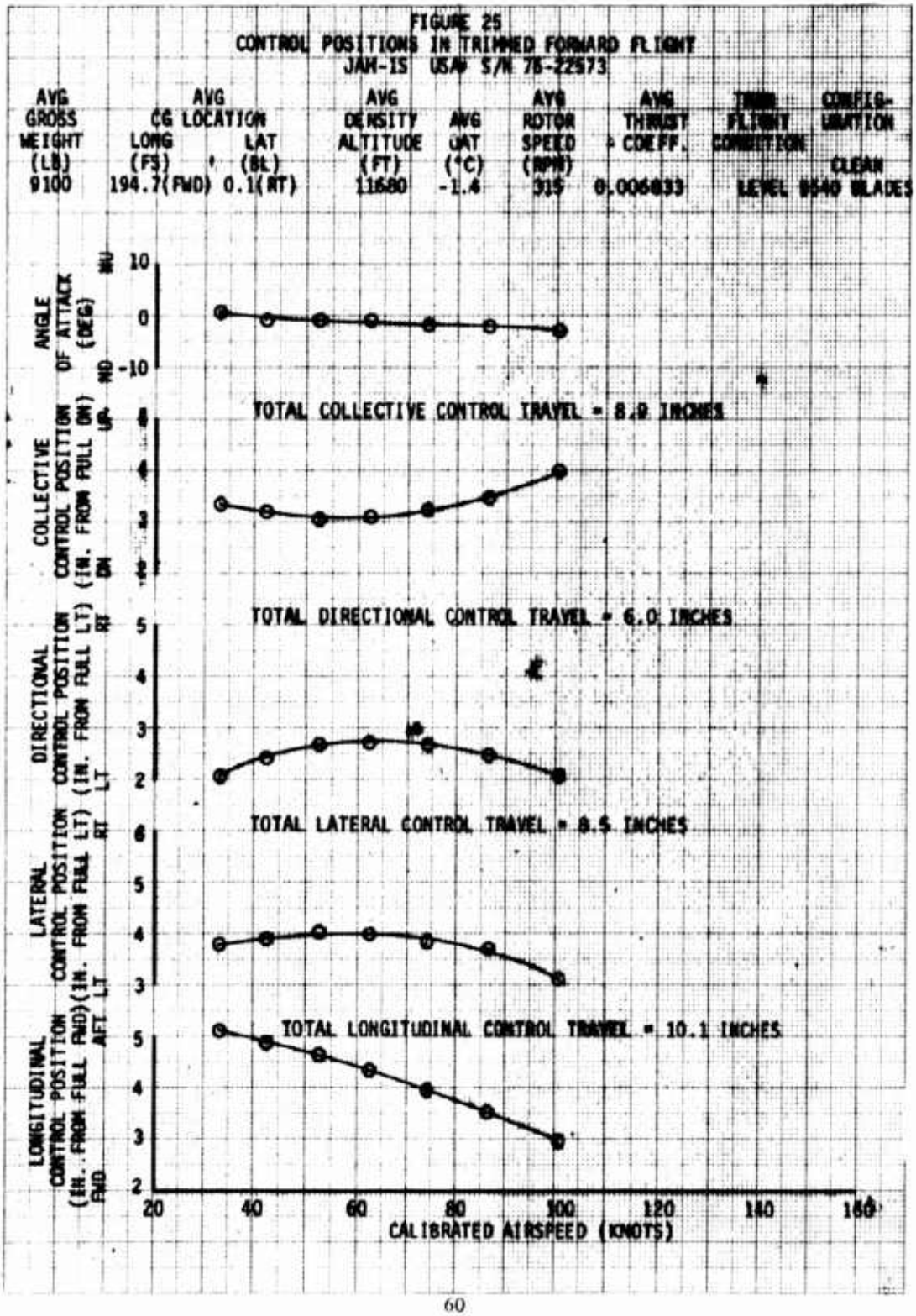

FIGURE 26
CONTROL POSITIONS IN TRIMMED FORWARD FLIGHT
JAH-1S USA S/N 76-22573

AVG GROSS WEIGHT (LB)	AVG CG LOCATION LONG (FS)	AVG CG LOCATION LAT (BL)	AVG DENSITY ALTITUDE (FT)	AVG OAT (°C)	AVG ROTOR SPEED (RPM)	AVG THRUST COEFF.	TRIM FLIGHT CONDITION	CONFIGURATION
8120	193.9 (FWD)	0.1 (RT)	2200	16.5	324	0.004581	LEVEL	CLEAN 4247 BLADES

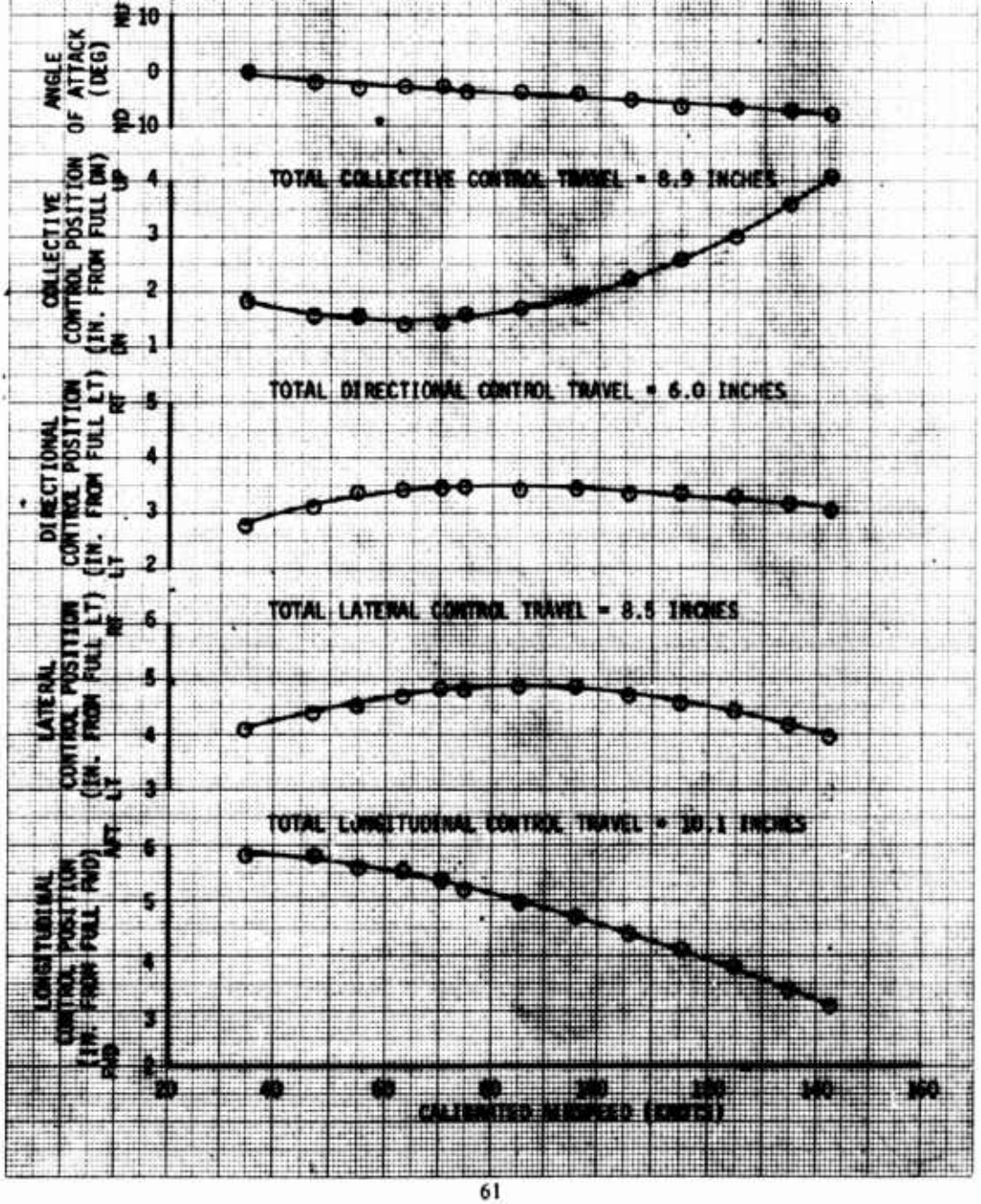

FIGURE 27
CONTROL POSITIONS IN TRIMMED FORWARD FLIGHT
JAH-1S USA S/N 76-22571

AVG GROSS WEIGHT (LB)	AVG CG LOCATION LONG (FS)	AVG CG LOCATION LAT (BL)	AVG DENSITY ALTITUDE (FT)	AVG OAT (°C)	AVG ROTOR SPEED (RPM)	AVG THRUST COEFF.	TRIM FLIGHT CONDITION	CONFIGURATION
9300	194.8(FWD)	0.1(RT)	[illegible]	1.0	316	0.[illegible]	LEVEL	CLEAN #347 BLADES

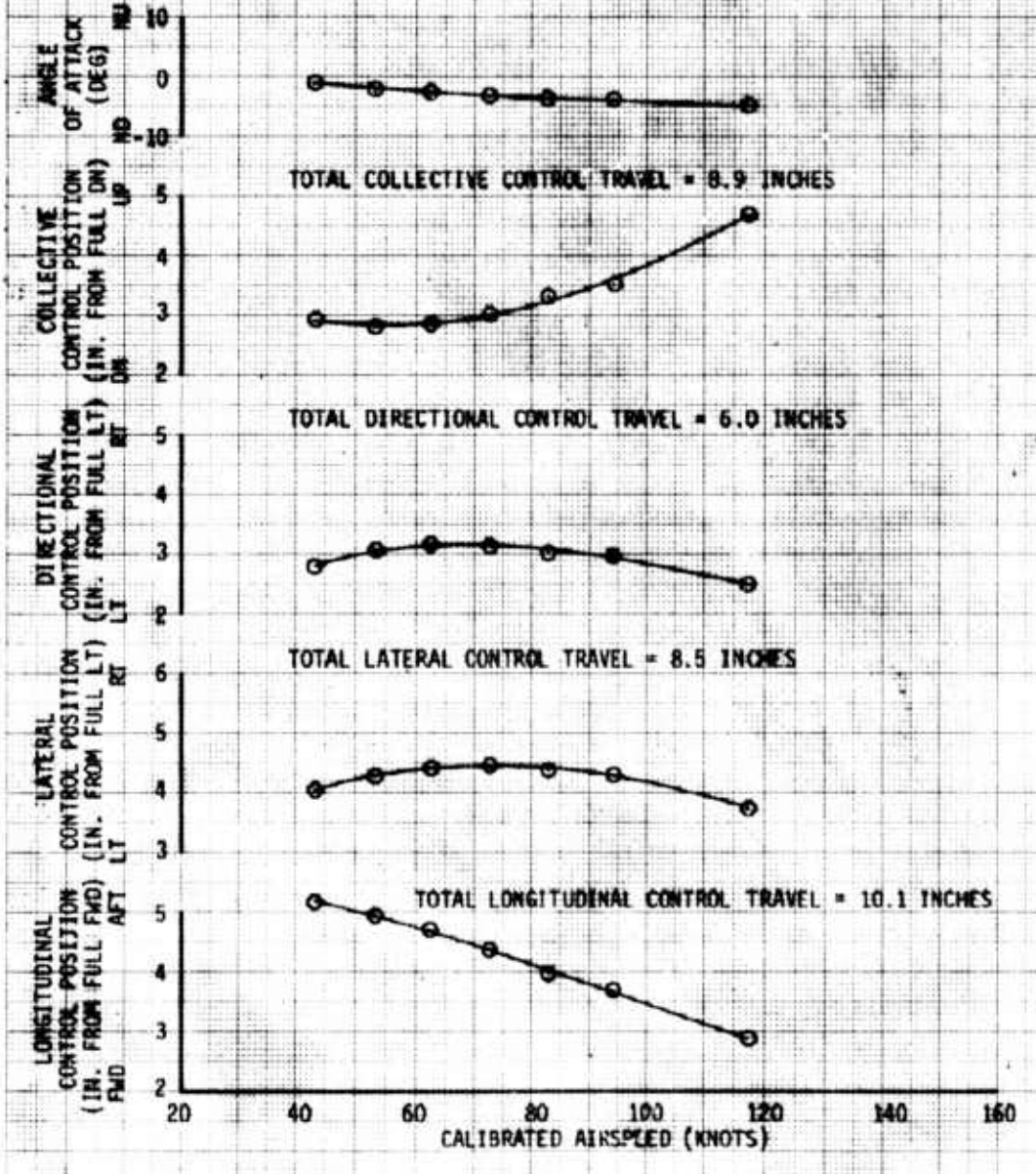

FIGURE 28
SHIP'S AIRSPEED CALIBRATION
AH-1S USA S/N 76-22573

AVG GROSS WEIGHT (LB)	AVG CG LOCATION LONG (FS)	AVG CG LOCATION LAT (BL)	AVG DENSITY ALTITUDE (FT)	AVG OAT (^{o}C)	AVG ROTOR SPEED (RPM)	TRIM FLIGHT CONDITION
8340	195.2(FWD)	0.1(RT)	3520	21.0	324	LEVEL FLT

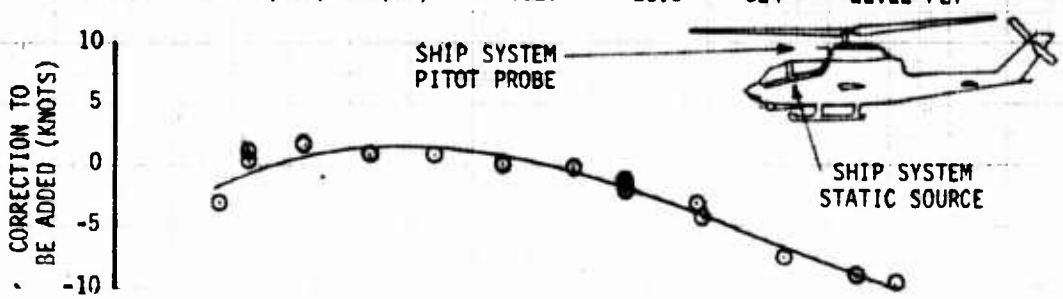

NOTES:
1. CLEAN CONFIGURATION
2. K747 BLADES S/N A2016 AND A2025
3. GROUND SPEED COURSE UTILIZED

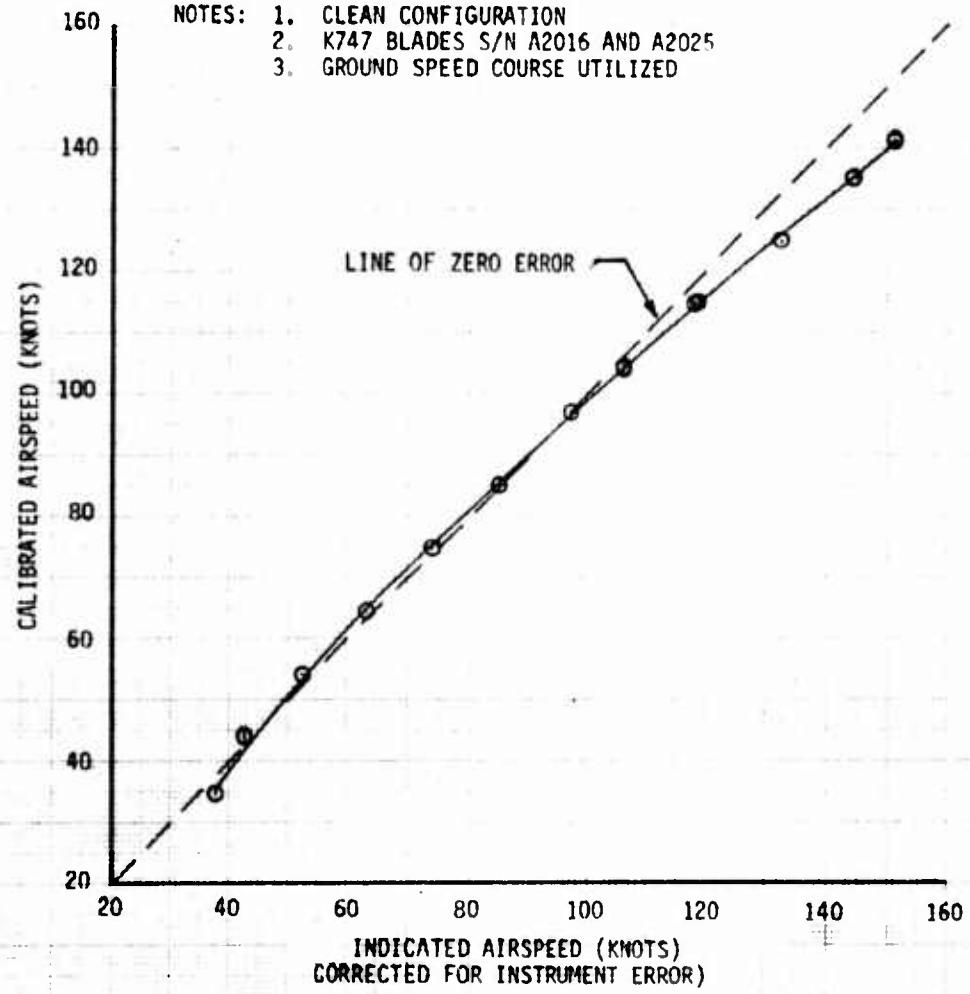

FIGURE 29
SHIP'S AIRSPEED CALIBRATION
AH-1S USA S/N 76-22573

AVG GROSS WEIGHT (LB)	AVG CG LOCATION LONG (FS)	LAT (BL)	AVG DENSITY ALTITUDE (FT)	AVG OAT (°C)	AVG ROTOR SPEED (RPM)	CONFIGURATION
7900	196.5(MID)	0.1 RT	5000	10.0	324	CLEAN (B540 BLADES)

NOTES: 1. TRAILING BOMB METHOD UTILIZED
2. ▽ 1500 FEET PER MINUTE RATE OF CLIMB
3. ○ 1000 FEET PER MINUTE RATE OF CLIMB
4. ◇ 500 FEET PER MINUTE RATE OF CLIMB
5. □ 500 FEET PER MINUTE RATE OF DESCENT
6. ▭ 1000 FEET PER MINUTE RATE OF DESCENT
7. △ 1500 FEET PER MINUTE RATE OF DESCENT
8. ○ 1750 FEET PER MINUTE RATE OF DESCENT

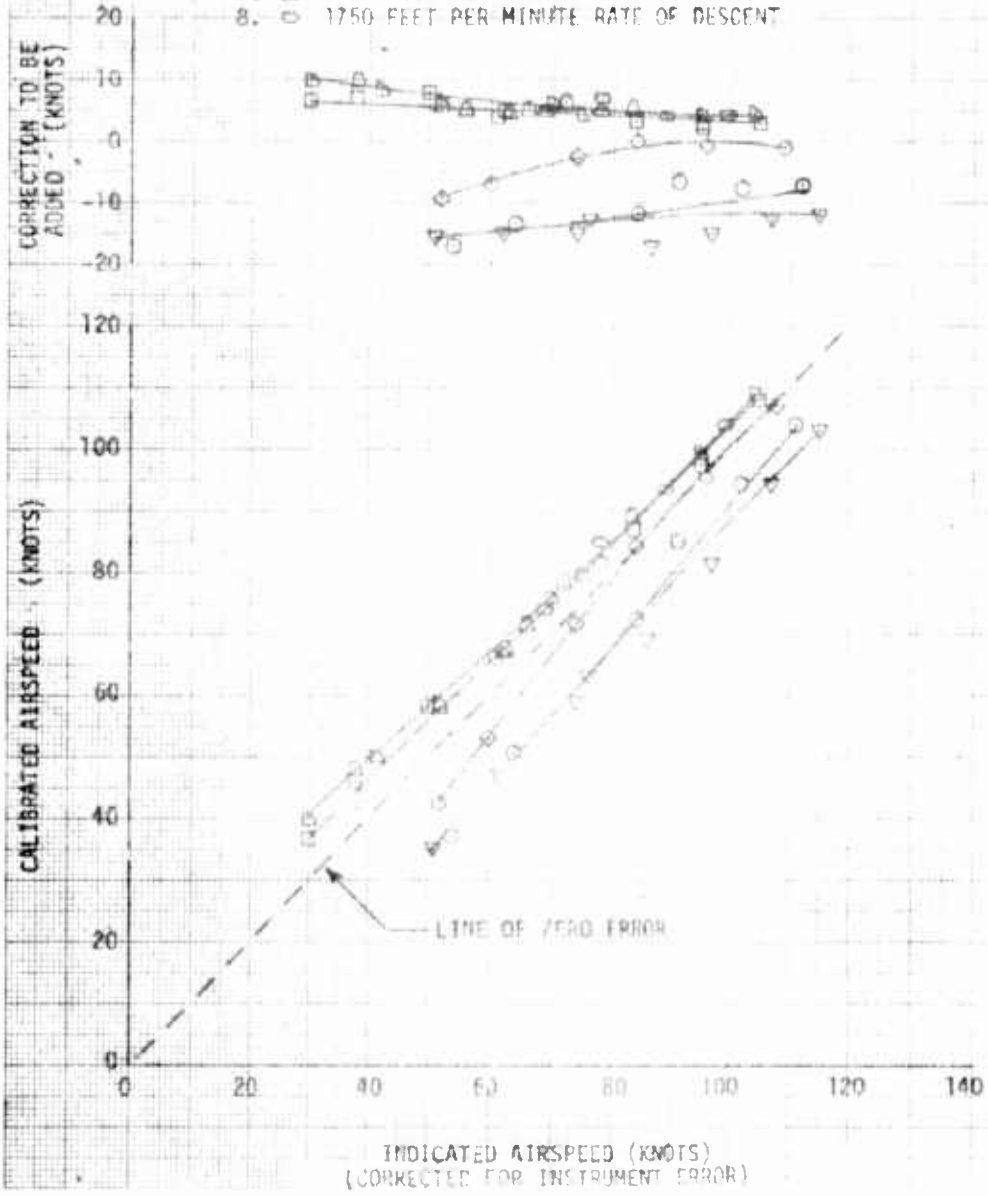

APPENDIX F. IN-FLIGHT ACOUSTIC TESTS

IN-FLIGHT ACOUSTIC COMPARISON OF THE 540 AND K747 MAIN ROTORS FOR THE AH-1S HELICOPTER

D. A. BOXWELL AND F. H. SCHMITZ
AEROMECHANICS LABORATORY
U.S. ARMY R&T LABORATORIES (AVRADCOM)
AMES RESEARCH CENTER
MOFFETT FIELD, CA

SUMMARY

This report presents comparative results of in-flight acoustic testing of the Army AH-1S helicopter when configured with the standard Bell Helicopter Textron 540 rotor blades and with the Kaman K747 improved main rotor blades. The acoustic measurements were made in association with USAAEFA-conducted production validation tests of the Kaman main rotor blades. Acoustic testing was directed by RTL Aeromechanics Laboratory personnel using the Ames Research Center's YO-3A acoustic research aircraft. Far-field acoustic data defining the impulsive noise signatures of the AH-1S helicopter during high-speed flight and during partial-power descents were gathered for each rotor configuration. The Kaman blades were found to radiate a significantly lower amount of high-speed impulsive noise than the standard 540 rotor blades at high advancing-tip Mach numbers. The two rotor systems can exhibit comparable peak levels of impulsive noise due to blade-vortex interaction. A distinguishing waveform difference between the acoustic signatures does appear to exist during partial-power descents, suggesting that the K747 rotor radiates less blade-vortex interaction annoyance than the 540 rotor system.

INTRODUCTION

Helicopters are now appearing with new or redesigned rotor systems that incorporate a number of structural and geometric changes. New airfoil shapes, tip planforms that include taper and sweep, and thinning are but a few examples. Although many of these new rotor systems were developed to improve performance, aerodynamics, or vibration, some also have modified acoustic characteristics. An example is the improved main rotor blades developed by Kaman Corporation. At the request of AVRADCOM, the RTL Aeromechanics Laboratory undertook the quantification of the acoustic signature characteristics of the Kaman K747 improved main rotor blade by comparison flights, on the AH-1S helicopter, with the standard Bell Helicopter Textron (BHT) 540 rotor blades. This acoustic quantification testing was conducted in association with the government production validation test of the Kaman blades by USAAEFA (ref. 1).

The Kaman K747 rotor blade has a tapered tip planform with varying thickness and airfoil sections, and is constructed primarily of composite materials. The design utilizes Boeing-Vertol advanced VR-7 and VR-8 airfoil sections of 12% and 8% thickness respectively, with the root end thickened for improved structural stiffness. Transitions from one airfoil contour to another are linear. A technical description of the Kaman rotor system is given in reference 2. By comparison, the standard 540 all-metal rotor blade has a rectangular planform with a 9.33% symmetrical special section airfoil. Both rotor systems are a 44 ft (13.41 m) diameter, two-bladed teetering configuration that use the B-540 hub and its associated hardware. Rotor speed is 324 rpm (33.93 rad/sec); tip speed is 746 ft/s (227.38 m/s). Basic dimensions for both rotor blades are shown in figure 1.

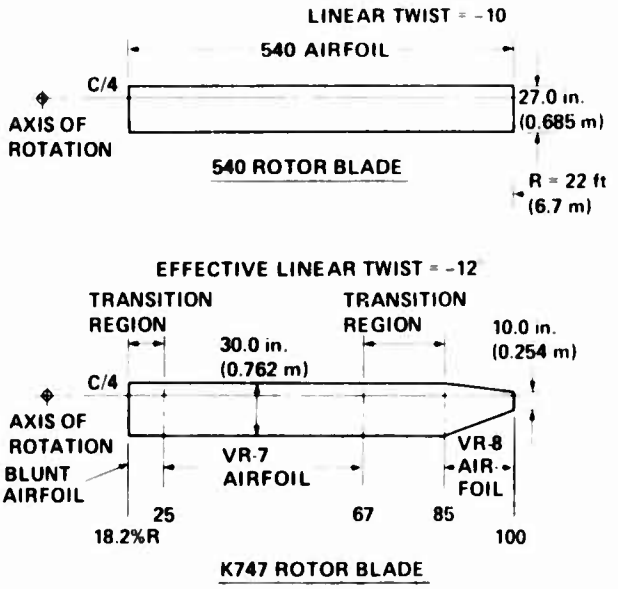

Figure 1.- Geometric comparison of the 540 and K747 rotor blades.

Most helicopters radiate two basic types of impulsive noise that are of primary interest to the Army. The first type is typical of a helicopter in high-speed flight, and is often called "high-speed" impulsive noise. The second is characteristic of helicopters experiencing blade-tip vortex interactions, and is appropriately labeled blade-vortex interaction impulsive noise. These tests, therefore, were conducted to investigate the radiated far-field noise during high-speed and partial-power descent flight conditions. Selected records were analyzed in order to report notable or overall acoustic characteristics of each rotor configuration at several controlled and comparative flight conditions.

TEST TECHNIQUE

A systematic and controlled measurement of each rotor's far-field acoustic signature was accomplished using an in-flight technique developed at the RTL Aeromechanics Laboratory. The technique and its advantages are well documented (refs. 3, 4); it has been used to investigate a number of helicopters in a manner similar to that reported here. For these comparative tests, the measurement technique utilized the YO-3A quiet, fixed-wing aircraft, which was flown to maintain fixed relative positions with respect to the AH-1S helicopter (shown, in general, in fig. 2). The YO-3A was instrumented with three externally-mounted microphones: one on the vertical stabilizer and one on each wing tip. Acoustic signals from each microphone were monitored on an oscilloscope in the YO-3A prior to and during recordings

Figure 2. In-Flight far field acoustic measurement technique with YO-3A and AH-1S.

on FM magnetic tape. A radio signal, transmitted once during each revolution of the main rotor, was used to trigger the oscilloscope; it was also recorded on the FM magnetic tape with the microphone acoustic signals. Instrumentation gains were adjusted for each flight condition in order to optimize the acoustic signal-to-noise ratio. Boom data indicating the YO-3A aerodynamic state and attitude were recorded simultaneously with the acoustic data. During each acoustic data run, the AH-1S on-board data system recorded selected helicopter parameters, including vehicle aerodynamic state, attitude, power train data, and rotor information (ref. 1).

TEST CONDITIONS

The in-flight acoustic measurement technique was used to measure and record the far-field acoustic signatures of each AH-1S rotor configuration in various flight conditions. Figure 3 shows the flight envelope that was tested; it is primarily defined by the YO-3A low-speed and high-speed flight limitations. This envelope, however, was sufficient to explore those flight conditions under which impulsive noise is known to occur as a result of either blade-vortex interactions or high-speed rotor aerodynamics. Acoustic data were obtained at intervals for descent rates between zero and 1000 ft/min (5.08 m/s), and for indicated airspeeds between 60 and 130 knots, with the YO-3A power limit dictating the high-speed boundary, as shown in figure 3.

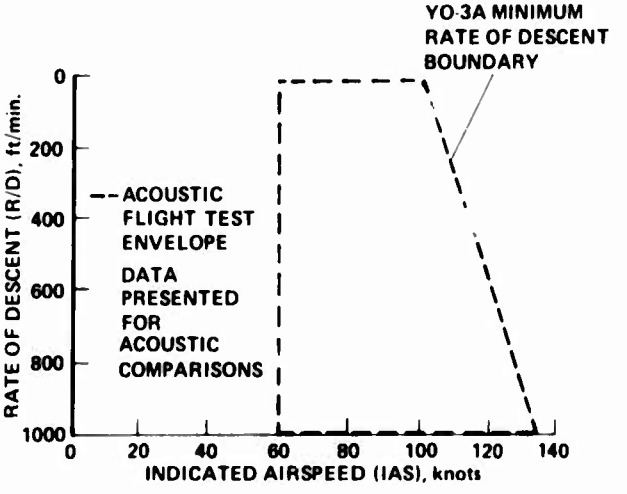

Figure 3.- Flight envelope for far-field acoustic measurements.

To facilitate an accurate comparison of the noise generated by each rotor system over a wide range of flight and atmospheric conditions, particular attention was given to acoustic flight testing based on non-dimensional parameters. It is known that for blade-vortex interactions, wake parameters such as advance ratio, thrust coefficient, and tip-path-

plane angle are important. Additionally, for impulsive noise, advancing-tip Mach number is a first-order parameter. The flight testing was conducted by calculating, in flight, the important parameters to be matched and by adjusting the flight variables for comparative data runs.

The in-flight test technique outlined previously allows the microphones to be spatially oriented in any desired direction from the helicopter rotor. It is known that high-speed impulsive noise radiates most strongly in-plane and ahead of the rotor, and that advancing blade-tip-vortex interaction impulsive noise is strongest below and generally forward of the rotor plane. Figure 4 shows two relative orientations of the microphones with respect to the rotor that were flown while impulsive noise was measured. Figure 4(a) illustrates the formation used to measure high-speed impulsive noise. This formation places the YO-3A tail microphone in-plane with the rotor hub at a nominal microphone-to-hub separation of 80 ft (24.38 m). Visual flight references and a copilot-operated (AH-1S) rangefinder were used to hold distance within ±5 ft (1.52 m) of the nominal position. Figure 4(b) shows the orientation used primarily for blade-vortex interaction noise measurements. This formation places the YO-3A left wing tip microphone 30° below

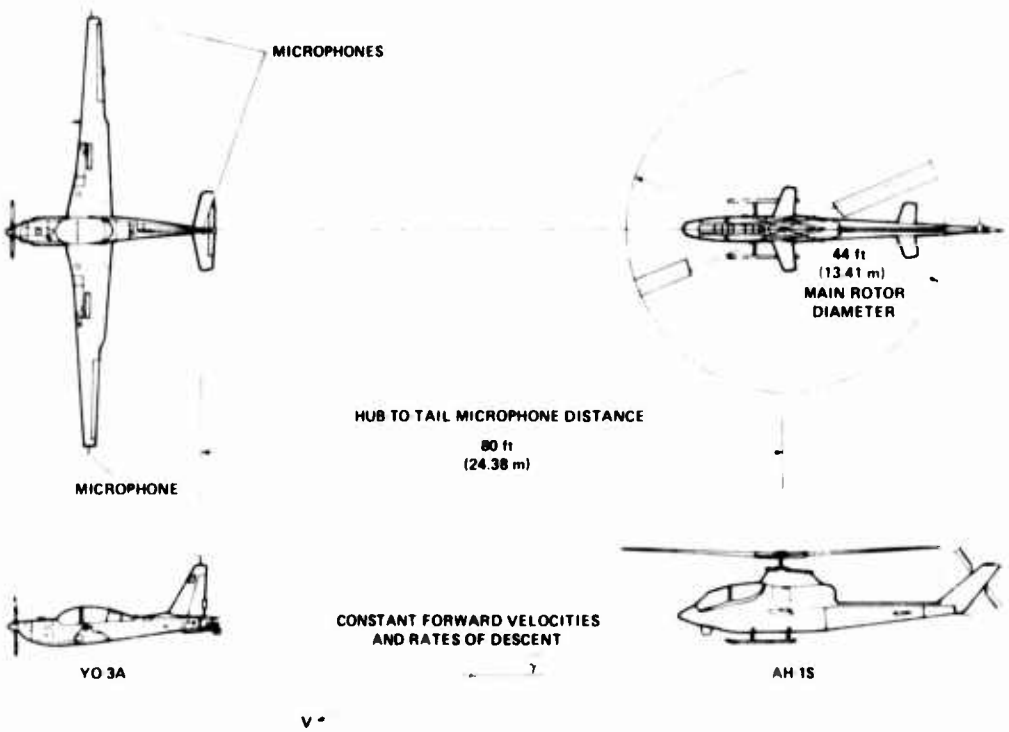

(a) High-speed impulsive noise.

Figure 4.- Relative orientation of aircraft for acoustic measurements.

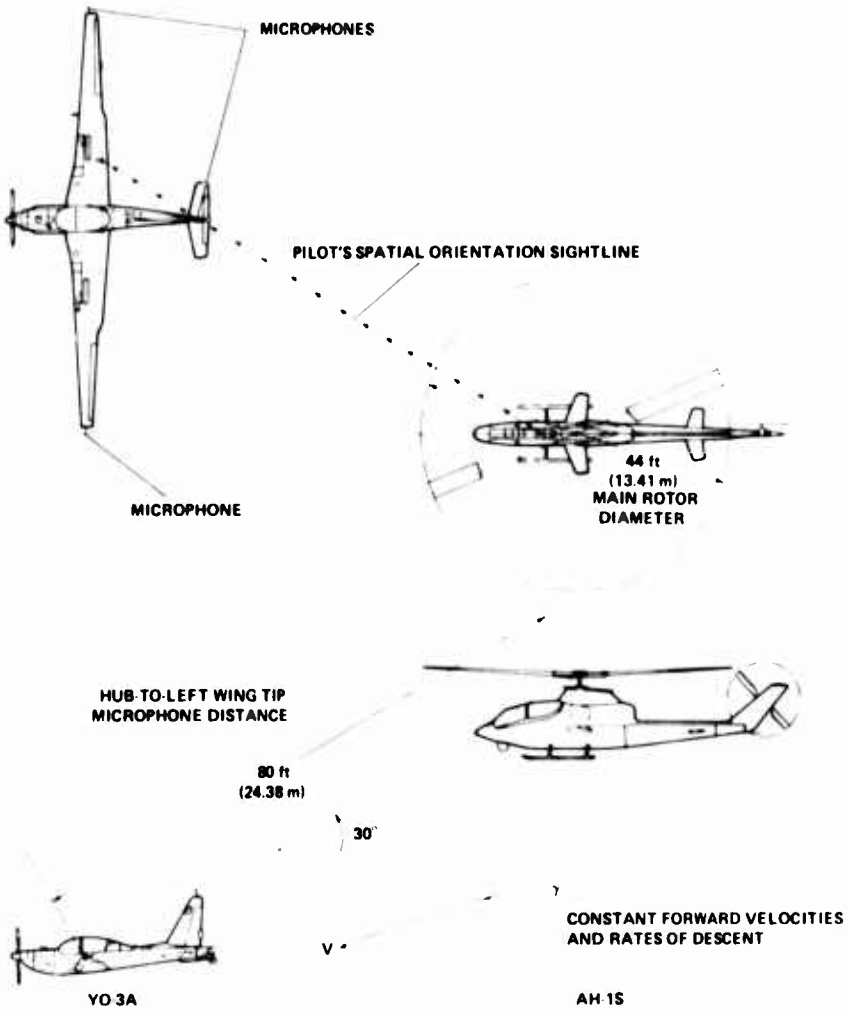

(b) Blade-vortex interaction impulsive noise.

Figure 4.- Concluded.

the rotor plane and 80 ft (24.38 m) from the rotor hub. The side position was used so that the AH-1S pilot could maintain good visual references on YO-3A orientation markings by looking through the canopy side window. Flight test acoustic data presented in this report were taken using the two orientations shown in figure 4, and are based on acoustic signatures measured by the microphones on the tail and left wing tip. Directivity information of the radiated noise was also recorded using the three widely spread microphones. At the present time, these results have not been analyzed and are not presented in comparing the two rotor configurations.

ROTOR ACOUSTIC SIGNATURE

The rotor acoustic measurements are presented here primarily in the form of acoustic pressure-time histories. These acoustic signatures are unaveraged, unfiltered "snapshots," representing the nature of the radiated noise for a nominal flight condition and nominal microphone-to-rotor orientation. These snapshots of the radiated noise were taken at a point during the 1-min data runs where the signature appeared to be most steady, and where taped comments indicated that the pilots were satisfied with flight conditions and orientation. Performance data recorded on both aircraft were used as a cross-check.

An idealized composite drawing is presented in figure 5 for identification of the waveform; it shows the general character of the measured acoustic signatures. In this figure, peak-pressure amplitude of the signal is illustrated for two blade passages, with time increasing from left to right. The negative pressure pulse is indicative of high-speed impulsive noise and the predominantly positive pressure pulses depict impulsive noise resulting from blade-tip vortex interactions. The waveform features shown in figure 5 are, at times, less clear in the actual acoustic signatures, due to

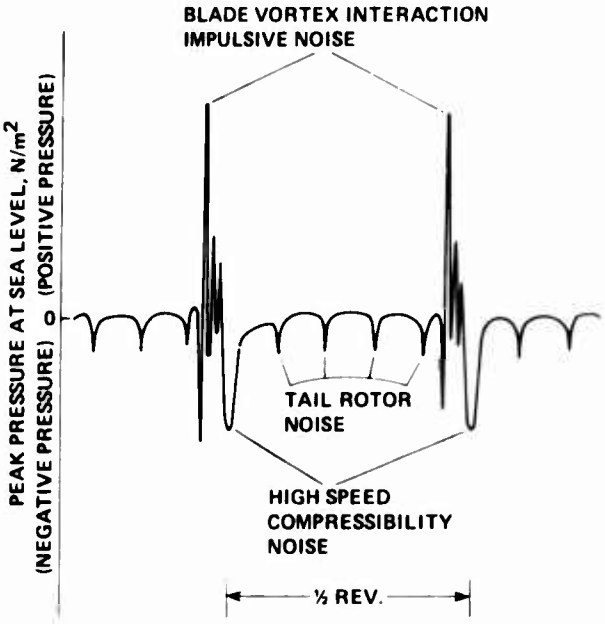

Figure 5.- Composite drawing showing dominant AH-1S acoustic waveform features.

contamination from sources such as background noise and the tail rotor acoustic signature. By adjusting instrumentation gains in flight, the signal-to-noise ratio and instrumentation dynamic range were optimized. Also, every effort has been made to present main rotor acoustic signatures that are minimally contaminated by the tail rotor impulsive noise. One final observation should be considered when viewing the rotor acoustic signatures presented here. The advancing blade-tip vortex interaction noise is phased in time, very close to the high-speed impulsive noise in the measured far-field acoustic signature. This means that one noise source can possibly disguise the waveform and true amplitude of another. Since the two types of noise have different directivity patterns, a judicious choice of microphone location can help amplify one source while minimizing the other. For example, the 30°-up position (fig. 4(b)) was chosen because blade-vortex interaction noise is a maximum and high-speed impulsive noise amplitudes are reduced. Although more optimum locations are probable, testing time prohibited their exploration.

HIGH-SPEED IMPULSIVE NOISE

From previous rotor acoustic testing, it is known that high-speed impulsive noise can exhibit substantial changes in both peak amplitude and waveform as a function of advancing-tip Mach number. Figures 6 and 7 show some of these measured high-speed impulsive noise characteristics for both of the AH-1S rotor systems. As previously explained, these data represent far-field amplitudes and waveforms as measured ahead of and nearly in-plane with the rotor tip-path-plane (fig. 4(a)). In figure 6, the peak negative pressure amplitude (corrected to sea level) of the high-speed acoustic pulse versus advancing-tip Mach number is shown. The graph in figure 6 was generated from simultaneous time histories of peak pressure level and advancing-tip Mach number during the data runs. Individual data points represent "time slices" taken during individual data runs and the shaded areas depict the degree of unsteadiness or signal-to-noise level in the measured data. At the lower Mach numbers (0.76 to 0.80) the data uncertainty tends to mask any significant difference between the two rotor systems; however, the peak level of the K747 blades appears to be slightly lower. Above a Mach number of about 0.85, significant reduction in high-speed noise peak pressure level is observed for the K747 configuration — approaching a peak-level reduction by a factor of 2 at $M_{AT} = 0.90$. Also shown in figure 6 are pressure-time histories of the acoustic signatures for both rotor systems at nearly similar flight conditions. The signatures show two blade passages in time (slightly more than one-half revolution) and illustrate the degree of impulsiveness of the radiated waveform as well as relative levels with tail rotor and background noise sources.

Again, previous rotor acoustic research for the UH-1H rotor (refs. 5, 6) has indicated that the rapid rise in peak pressure amplitude above a Mach number of about 0.88 can be accompanied by a waveform change that varies in character from somewhat symmetrical to sawtooth. In figure 7 the acoustic signature for a single blade passage has been expanded in time, illustrating

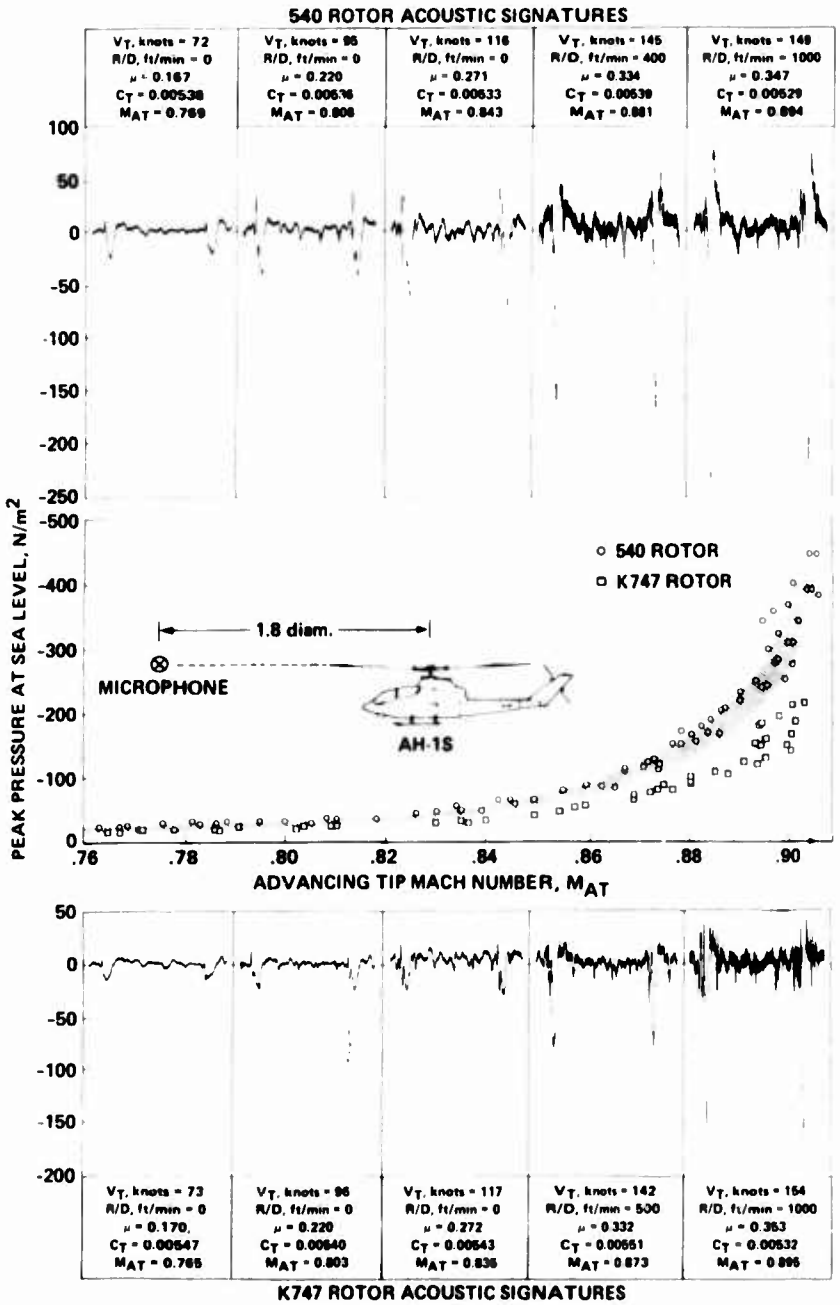

Figure 6.- Comparison of AH-1S high-speed impulsive noise for 540 and K747 rotor configurations.

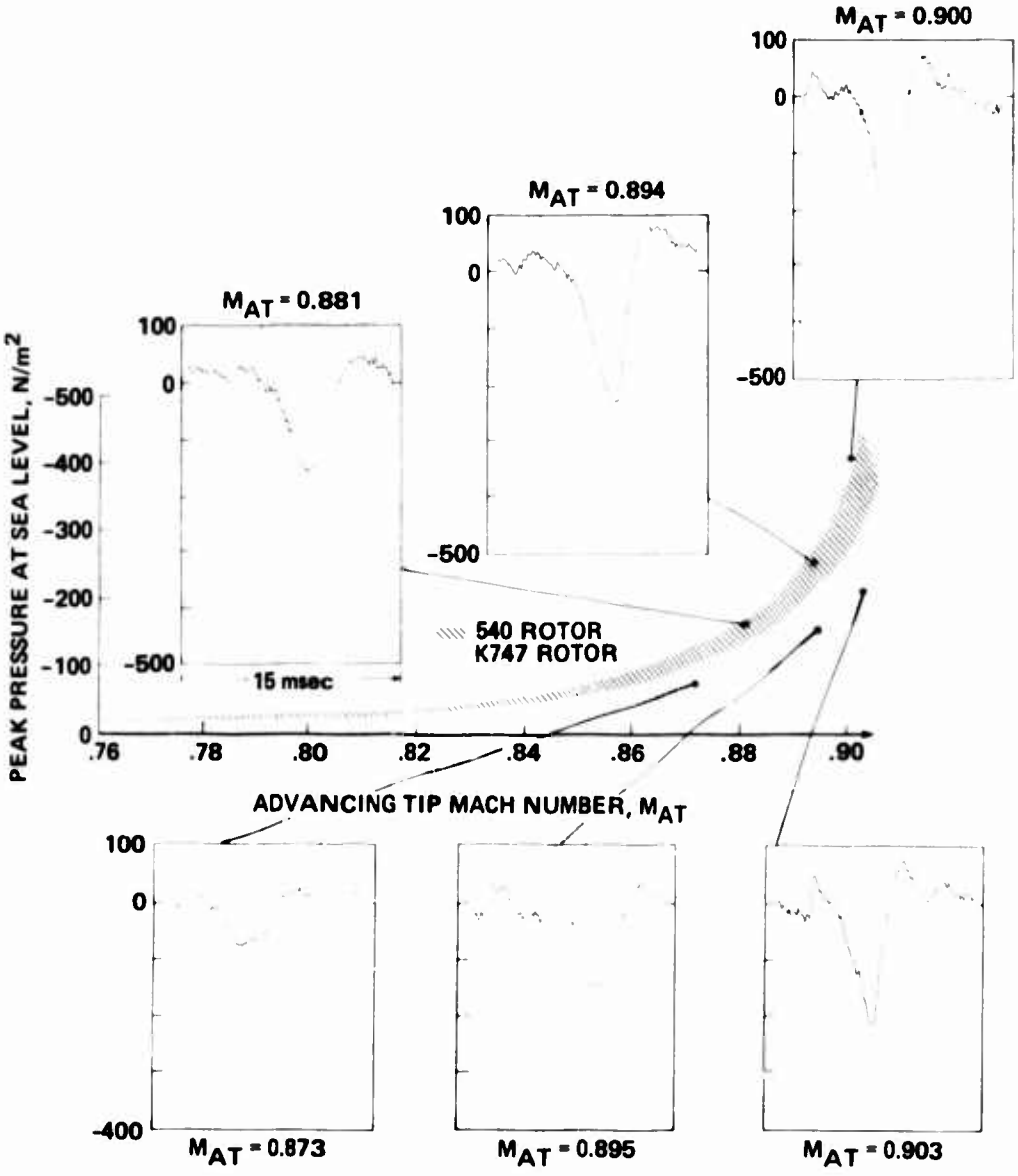

Figure 7.- Waveform change of high-speed impulsive noise for 540 and K747 configurations.

waveform change as advancing-tip Mach number is increased. For the 540 rotor blade system, the waveform transition from symmetrical to sawtooth is present and dominates the changing acoustic signature for advancing-tip Mach numbers of 0.88 to 0.90. This is not the case for the K747 blades which still exhibit a nearly symmetrical acoustic waveform near M = 0.90. This transition event of high-speed impulsive noise is delayed by the K747 blades, with the result that the radiated noise is substantially decreased. It should be noted that the relatively large uncertainty in the peak level of the 540 acoustic signature, shown at a Mach number of about 0.90, is due partly to the onset of waveform transition. This transition has been observed in previous measurements to be highly unsteady, even under well-controlled rotor test conditions (ref. 6). Some scatter is also attributed to the increased difficulty in maintaining steady flight conditions in high-speed descents.

BLADE-VORTEX INTERACTION NOISE

Noise generated by blade-tip vortex interactions from each rotor system was measured in the far-field using the rotor/microphone orientation illustrated in figure 4(b). The directivity characteristics of this type of impulsive noise produce maximum peak levels of the radiated noise generally below and in front of the rotor. Both rotor systems were tested in level flight and partial-power descents, the latter being a flight condition well-known for generating this type of noise.

Time histories of the blade-vortex interaction data are shown in figure 8 for the standard 540 blades, and in figure 9 for the K747 configuration. The flight conditions shown are nominal 60, 80, and 100 knots (IAS) forward velocities during descent rates of 0, 400, and 800 ft/min (0, 2.032, 4.064 m/s). This matrix was found to be representative of the noise radiated by each rotor. Listed with each acoustic signature in the flight matrix is the mean value of true velocity (V_T), advancing-tip Mach number (M_{AT}), advance ratio (μ), and thrust coefficient (C_T) for each run as derived from the AH-1S data system. Therefore, the acoustic signatures presented are representative of these nominal conditions. All signatures are shown to the same peak pressure scale (corrected to sea level) for direct-level comparison.

Several prominent features of the pressure-time histories in figures 8 and 9 are notable. Most general is the observation that noise due to blade-vortex interaction occurs with both rotor systems over the flight matrix presented here. In fact, this noise, characterized by distinct and primarily positive pressure acoustic pulses, was found to exist continuously at the rotor repetition rate throughout the flight envelope shown in figure 3. Although no attempt is made here to identify and relate each discrete pressure pulse with the local aerodynamic environment of the rotor and near-wake geometry, it is known from many previous studies that the number of blade-vortex interactions is directly related to the epicycloid pattern of the tip-vortex structure. Thus, the advance ratio plays the major role in determining how many blade-vortex interactions are possible, and rate of

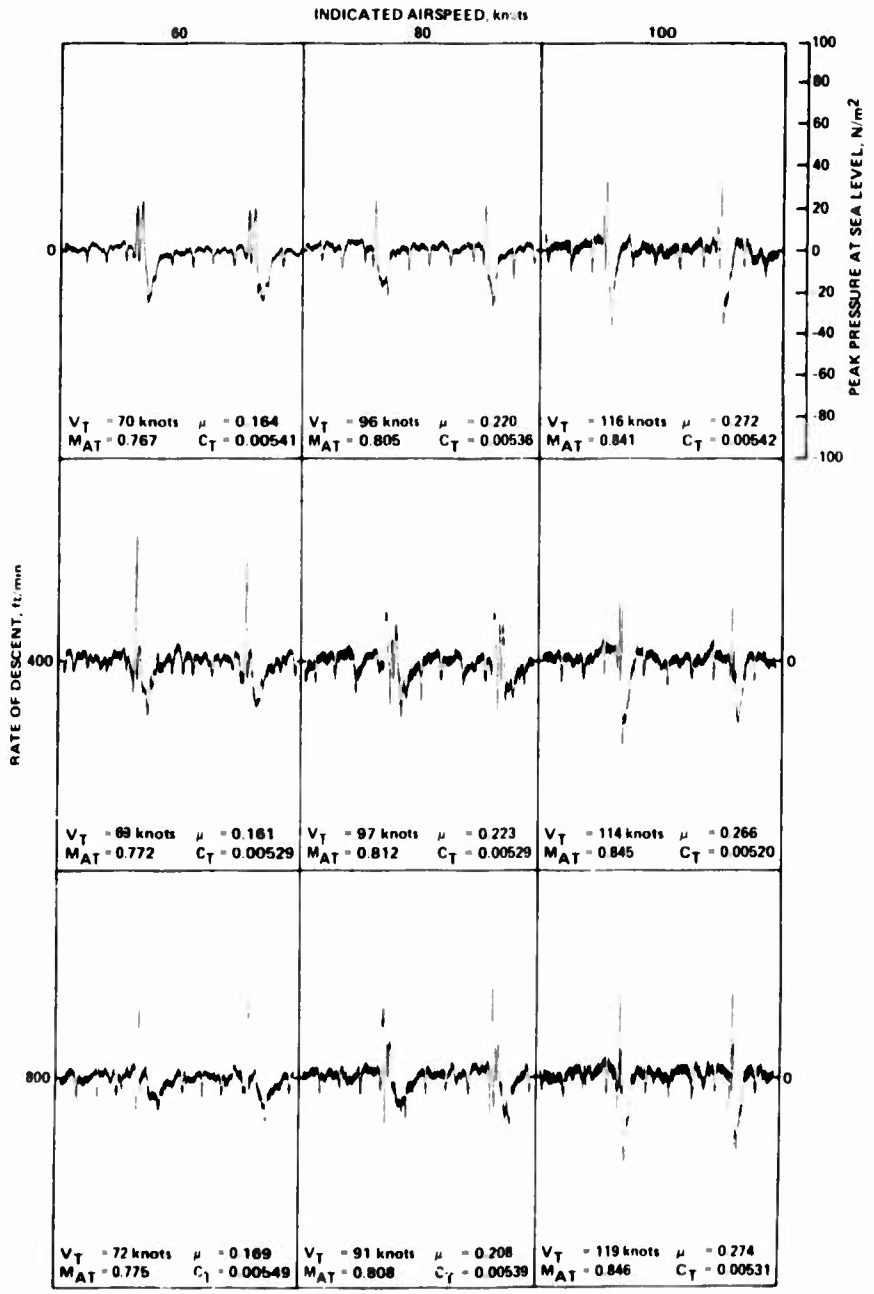

Figure 8.- Unaveraged acoustic signature of AH-1S with 540 rotor vs forward airspeed and rate of descent.

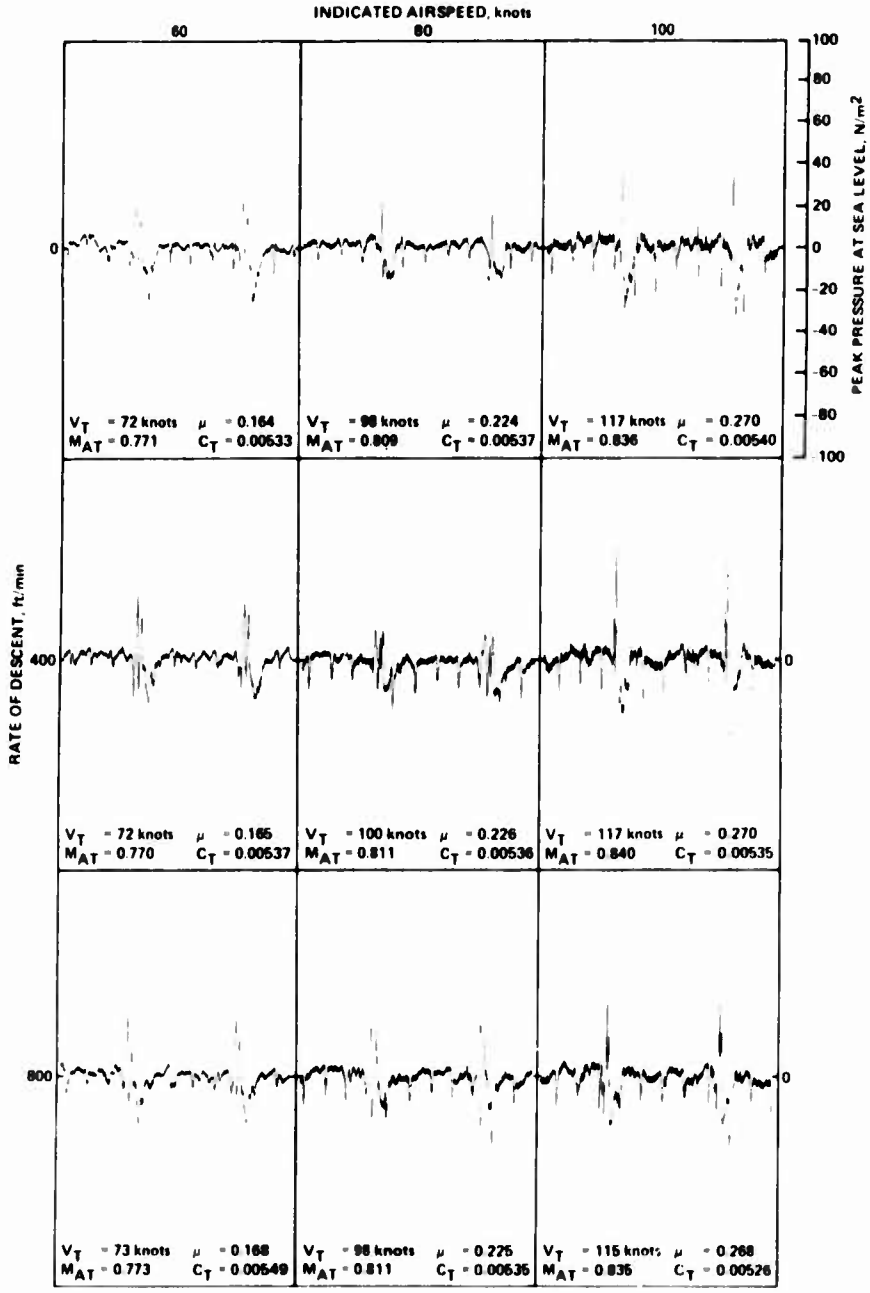

Figure 9.- Unaveraged acoustic signature of AH-1S with K747 rotor vs forward airspeed and rate of descent.

descent causes some of these candidate vortices to pass near the advancing blade, generating different patterns of impulsive noise. In terms of peak pressure, the interactions shown in figures 8 and 9 are comparable. In other words, one rotor system can produce acoustic pressure peak levels due to blade-vortex interactions that are not grossly different in peak level from the other system. There does appear to exist, however, a notable difference in the noise character during partial-power descents. As mentioned previously, the character of the blade-vortex interaction noise is governed to a large extent by descent rate. In general, as the descent rate is increased, a rotor blade is more likely to interact with other tip vortices. This trend is only qualitative however, and will tend to reverse as the rate of descent becomes so large as to force these older tip vortices above the interacting blade. This trend can be seen, for example, in figure 8 for the 540 rotor system at an IAS of 60 knots. As the rotor changes from level flight to a rate of descent of 800 ft/min (4.064 m/s), the noise signature radiated by two prominent interactions changes. The older (earlier in time) interaction signature becomes stronger, and the newer (later in time) one becomes weaker as the rate of descent increases. By comparison, the K747 configuration in figure 9, at nominally the same flight condition, does not exhibit the rotor-blade/tip-vortex interaction development with descent, as described above for the 540 system. Generally, the radiated noise signature seems much less dependent on rate-of-descent. This comparative observation also appeared at the higher advance ratios, but seemingly to a lesser degree (at least with this unaveraged matrix of acoustic signatures). This may imply that the tip vortices of the K747 blades are slightly more diffused or are in slightly lower positions than the 540 rotor tip vortices.

There are many important questions about the acoustics of full-scale blade-vortex interaction noise that the preceding snapshot approach has left unanswered. For example, what characteristics of the impulse govern low- and high-frequency noise? How do these characteristics influence the resulting annoyance? How steady and repeatable are the impulses? To attempt to answer these questions, a procedure analogous to one developed for analyzing UH-1H helicopter blade-vortex interaction noise (ref. 7) was used for these AH-1S rotor acoustic comparisons. The procedure involves frequency analysis techniques in conjunction with "time-windowing" of the measured acoustic signature and is outlined in figure 10 using the AH-1S/540 rotor acoustic signature. Figure 10(a) shows one rotor revolution (2 blade passages in time) of the acoustic pressure-time history within a 200 ms time window and the resulting 5 Hz wide resolution power spectrum. To obtain narrowband analyses, however, this classical technique averages more than one blade passage and thus can smooth the individual character of a single event of interest, such as blade-vortex interaction. The first step in refinement, therefore, was to take a power spectrum (still 5 Hz wide resolution) of one-half a revolution of data as shown in figure 10(b). The pressure-time history has been expanded in time for graphical clarity. Here, sound power from blade-vortex interaction, high-speed compressibility, tail-rotor, and some broadband noise sources are all still included, but variability from blade-to-blade in the acoustic signature has not obscured the power spectral character of the actual acoustic signature. Variability can now be dealt with, statistically, later in this analysis.

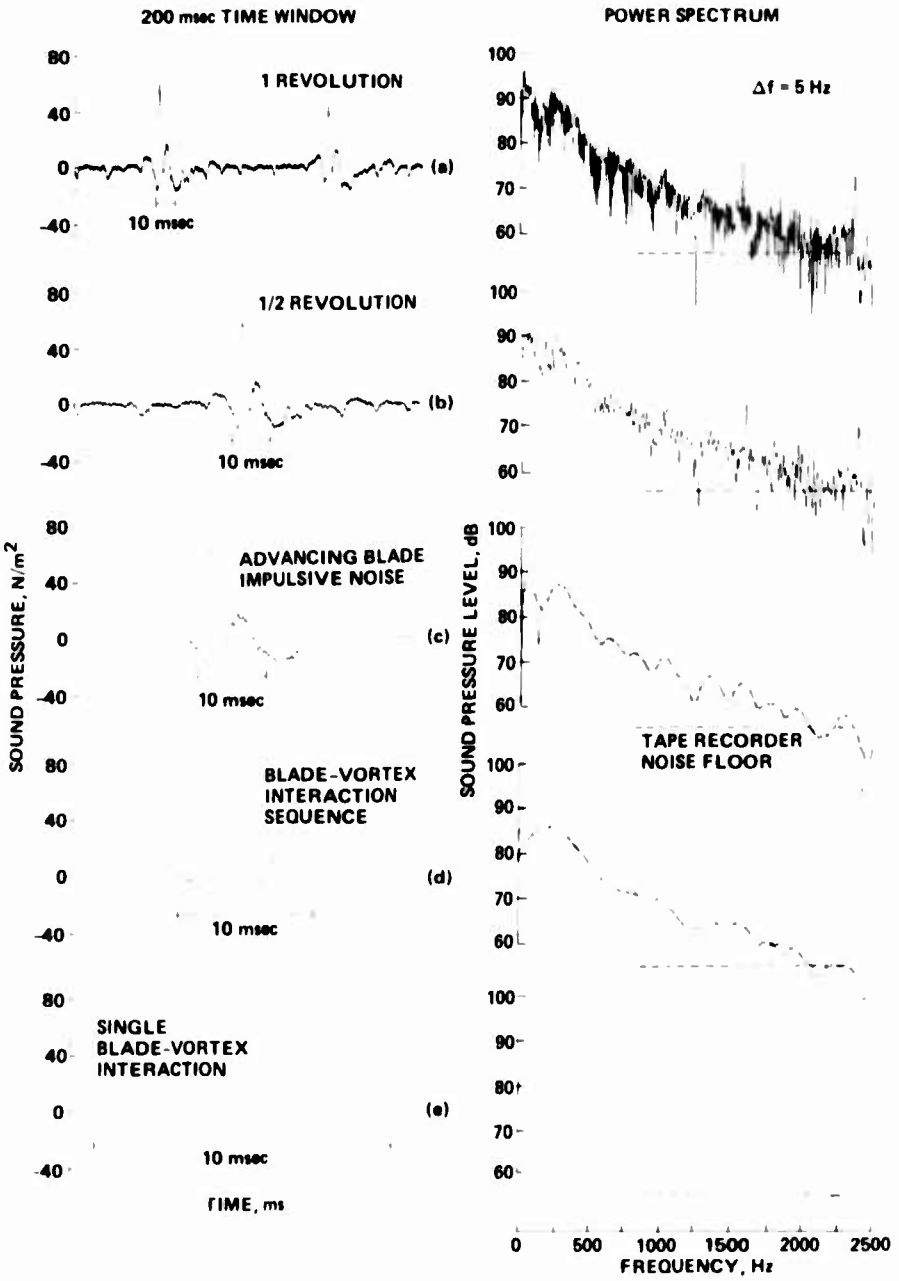

Figure 10.- Time filtering (windowing) of impulsive noise.

Next the data were further "time-windowed" by setting the measured pulse equal to zero everywhere except during that part of the half-period dominated by advancing blade-impulsive noise. The result is shown in figure 10(c) in both the time and frequency domains. In essence, much of the power contributed from broadband and tail-rotor noise sources has been eliminated, thus improving the signal-to-noise level of the resulting impulse. In fact, as shown in figure 10, the noise floor of the remaining high-frequency data (>2500 Hz) is set by the signal-to-noise ratio of the tape recorder. The lobed character of the resulting frequency spectrum is typical of a multi-impulse event without discontinuous first derivatives. It is also noteworthy that the largest sound pressure levels of this impulsive event are in the 200 to 750 Hz range.

The frequency content of blade-vortex interaction by itself is shown in figure 10(d). It is apparent that the only difference between this spectrum and the previous one is in the very low-frequency range of 0-100 Hz. This difference represents the energy content of the high-speed compressibility noise.

Finally, when all but the largest blade-vortex interaction is nulled, a definite change in power spectrum results (fig. 10(e)). The many-lobed character of the spectrum disappeared, replaced by a wide smooth-lobed curve with noticeably less energy in the 200 to 750 Hz range. This result shows that much of the blade-vortex energy in the 200-750 Hz range is a result of the multi-pulse character of the impulse.

By now the similarity of these techniques to Fourier transforms of discrete events is probably apparent. In essence, the technique of "time-windowing" a portion of the acoustic time history is another method of evaluating the power spectral density of the event. The power spectral density of one pulse is the envelope of the power spectrum of that same pulse, repeated at the characteristic periodic interval.

As mentioned above, a significant degree of variability or unsteadiness was observed in the measured blade-vortex interaction noise signatures for both the 540 and K747 rotors. This is illustrated in figure 11 for two "windowed" time histories for the 60 knot, 400 ft/min rate-of-descent case. The time histories have been expanded greatly to enhance the character of the acoustic impulses and it is observed, for both rotors, that the peak amplitude and detailed shape of the pulses do change for different blade passages. It is especially interesting to note that the time history of the AH-1S 540 rotor signature (fig. 11(a)) can be far from symmetrical and exhibit large positive pressure gradients in the oldest (earliest in time) blade-vortex interaction pulse. In contrast, the expanded time histories of the K747 rotor signature (fig. 11(b)) are predominantly symmetrical, triangular waveforms and not as substantially different from blade-to-blade as the 540 rotor.

Power spectra of the same "windowed" time histories are given in figures 12(a) and 12(b). It is apparent from these figures that measuring the power spectrum of one pulse sequence is not a good measure of frequency

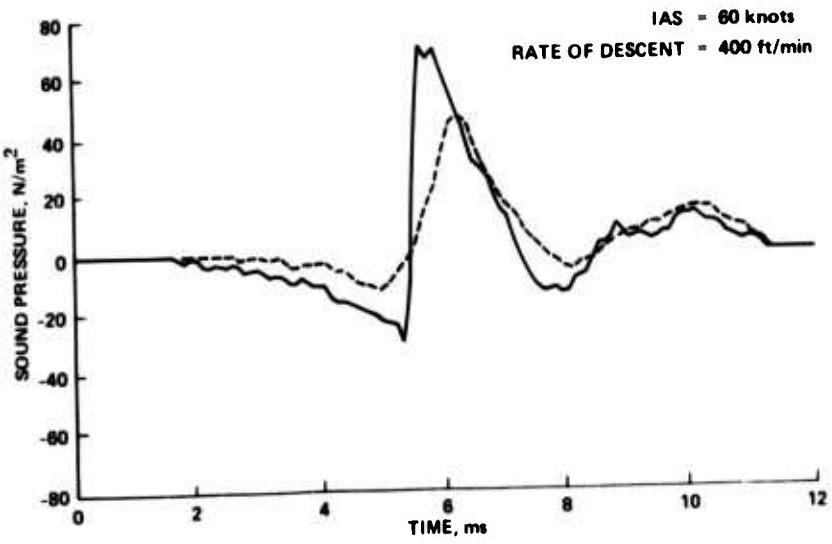

(a) 540 rotor.

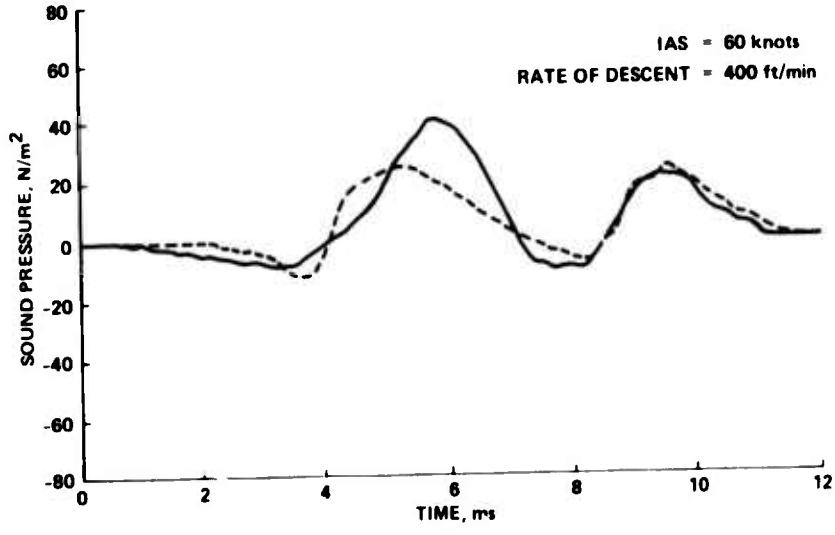

(b) K747 rotor.

Figure 11.- Typical waveform variability for measured AH-1S blade-vortex interaction signatures.

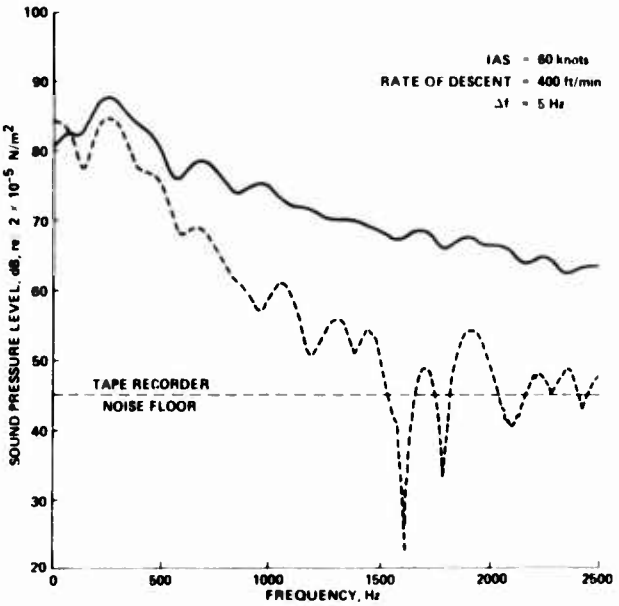

(a) 540 rotor.

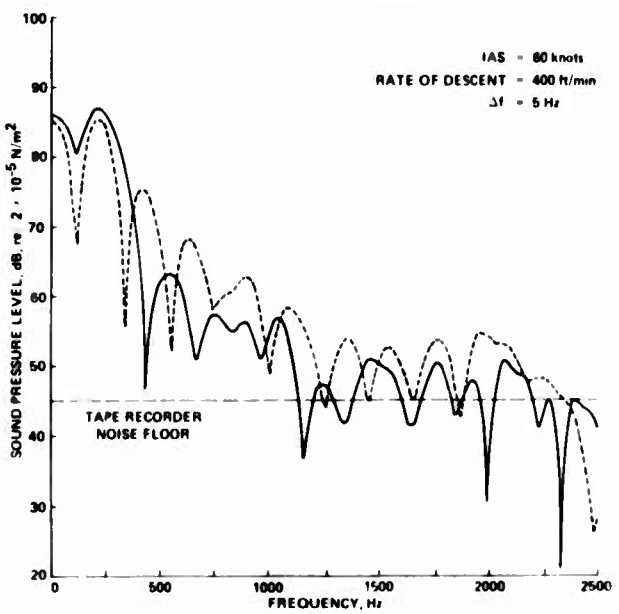

(b) K747 rotor.

Figure 12.- Power spectrum variability for blade-vortex interaction signatures shown in Fig. 11.

content — there is too much uncertainty. To help this situation, the power spectra of 16 time-windowed pulses were averaged for each rotor. The result and standard deviation (rms) are shown in figure 13. In general, for both rotors the resulting curves are not too surprising. From 0 to 750 Hz the standard deviation is less than 2 dB; above 750 Hz, a 3 dB standard deviation is typical.

For both rotors, the power spectrum of a typical pulse is essentially like the average power spectrum at the lower frequencies (<750 Hz), where the standard deviations that do exist are most probably due to amplitude variations in the pulse time history. The firm details of pulse shape plus other uncertainties govern the higher frequency character of the interaction, and are not as well accounted for in this analysis. It is also observed that the most intense energy content of the blade-vortex interaction for the AH-1S helicopter is in the frequency range of 200 to 750 Hz. Above 750 Hz, the energy content decays, as shown in figure 13.

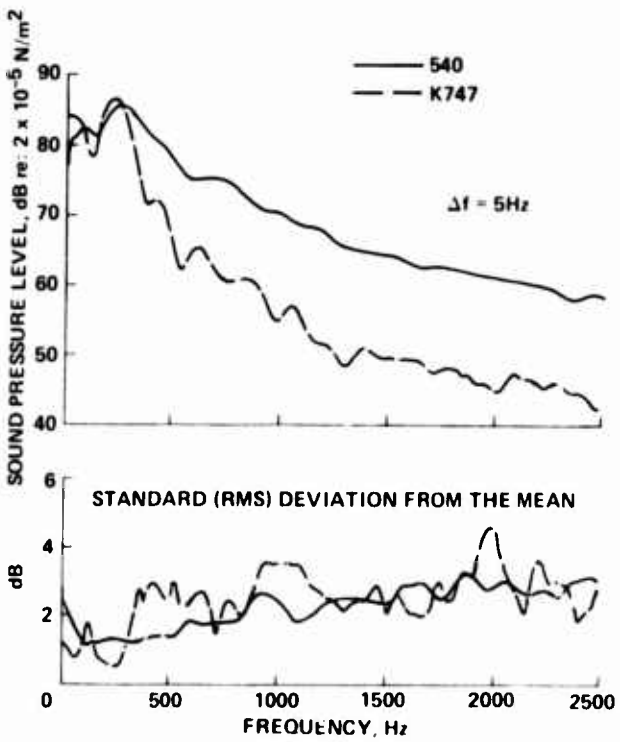

Figure 13.- Power spectrum statistical analysis of AH-1S blade vortex interaction noise for two rotors at IAS = 60 knots, rate of descent = 400 ft/min.

The most striking feature of figure 13 is the notable differences in the rate of falloff of the sound pressure level power spectra of the K747 blades when compared with the 540-rotor system. The latter has a very slowly decreasing amplitude with frequency, which tends to emphasize the higher frequency harmonics of the blade-vortex interaction acoustic signature.

It is interesting to note that measured acoustic data for the UH-1H helicopter reported in reference 7 exhibited similar slowly decreasing higher harmonic falloff. It was shown for the UH-1H that this spectral characteristic could be related to the impulse waveform by using a simple analytical model. This procedure led to an assessment of the rotor's annoyance. The same development is used here in comparing this more subjective aspect of the two AH-1S rotor acoustic signatures.

From the foregoing analysis of the two-bladed impulsive noise data, some commonality of the pulse shapes and basic periodicity of blade-vortex interaction noise is evident. To gain some idea as to the relative importance of some pulse-shape parameters, an analytical model has been developed (fig. 14). This simple analytic pulse, when repeated at twice the rotation rate of the main rotor blades, represents a single blade-vortex interaction encounter.

The pulse itself is made up of two triangles whose general characteristics are described by the pulse width of the positive-going pulse τ, the amplitude of the positive-going pulse H, the ratio β of the amplitude of the

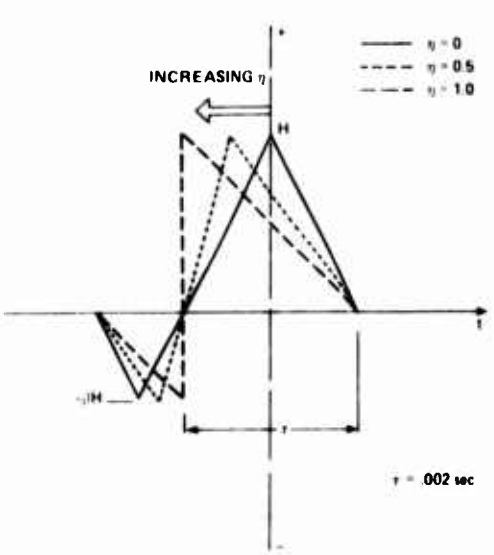

Figure 14.- Idealized analytic pulse.

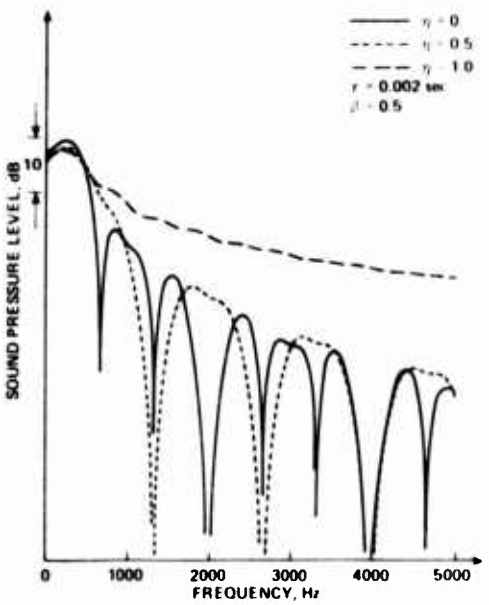

Figure 15.- Power spectral density of the simple analytical pulse.

absolute value of negative-going pulse to H, and the shape factor η. As shown in figure 14, $\eta = 0$ represents a sequence of two triangular pulses of opposite sign (negative pulse first), and $\eta = 1.0$ is a simple sawtooth wave of the same amplitude and overall pulse width. The unique feature of this simple analytical pulse is that its shape can change to represent local aerodynamic effects, but its peak amplitude and overall energy are constant. (This implies that the crest factor is also constant.) The symmetric ($\eta = 0$) triangular weaveform is representative of incompressible blade-vortex interaction phenomena, and the sawtooth (near infinite positive pressure gradient) is indicative of radiating shocks. If we now pretend that the aerodynamic designer has control over these effects, we can estimate how eliminating compressibility problems in the waveform structure might help reduce the annoyance of the blade-vortex interaction.

An important step in this estimation is the subjective evaluation of annoyance for helicopter impulsive noise. The FAA, in its role as the developer of the United States Noise Rules for Helicopters, (ref. 8), has chosen to describe helicopter annoyance with the effective perceived noise level (EPNL). The basic unit of measure of this subjective criteria is the perceived noise in decibels (PNdB). Because PNdB was originally developed for broadband noise sources typifying jet aircraft sounds, its applicability to low-frequency modulated helicopter noise has been questioned especially when impulsive noise is present. Attempts to improve or modify PNdB to account for helicopter impulsive noise have yielded conflicting results (ref. 9) — about which there is much technical controversy. However, because PNdB is currently used in the FAA notice (ref. 8) and is soon likely to become law, it will have tremendous influence on the helicopter design process. For this reason, it is used as the evaluation for helicopter blade-vortex interaction impulsive noise in these rotor comparisons.

A power spectrum of this single analytical pulse is shown in figure 15 for three different values of positive pressure gradients. The values of τ and β were chosen to be representative of the AH-1S and are noted. The $\eta = 0$ case indicates a highly lobed frequency distribution of power with a rapid harmonic falloff. This near symmetrical pulse shape is typical of many of the observed blade-vortex interactions for the K747 rotor, and indicates that most of the sound power is below 1000 Hz. The $\eta = 0.5$ case shown in figure 15 represents a wave with a positive pressure gradient that was present in many of the 540 rotor encounters. The more rapid increase in pressure is thought to be related to local compressibility effects. The power spectrum contains more energy at the higher frequencies, as would be expected. Finally, the power spectrum of the sawtoothed waveform ($\eta = 1.0$) shows much more of the pulse energy distributed toward higher frequencies. The spectrum is not flat, however, as it would be for an impulse, but falls as $1/(\text{frequency})^2$ at high frequency. This is the type of waveform that would be measured if shock waves were present in the radiating noise. As noted previously, no such waves were recorded during the AH-1S tests.

The relative annoyance of these simple pulse shapes was calculated by assuming that each blade of a two-bladed rotor generated the same basic waveform at the main-rotor rotational frequency (5 Hz). The resulting

narrowband spectra, whose envelopes are the power spectra of the simple pulse shapes, have been summed into one-third octave bands. The psychoacoustics results of reference 10 are then used to attach a relative value of "annoyance" to each octave band. This is illustrated in figure 16 for the $\eta = 0$ and $\eta = 1.0$ cases. In figure 16 the sound pressure level of the 1000-Hz, one-third octave band, which is equivalent in annoyance to the sound pressure level of the desired one-third octave band, is plotted vs. frequency. For the near symmetrical pulse shapes, the more important contributions to the annoyance occur in the 200 to 750 Hz range. As the pulse shape becomes more sawtoothed, high-frequency contributions become more important. At the extreme radiating shock conditions ($\eta = 1.0$), annoyances in the 200 to 750 Hz and the 1600 to 6300 Hz bands are of near equal importance.

Figure 17 summarizes the effects of pulse shape on annoyance of this simple repeated pulse. A maximum increase of 4.7 PNdB can be expected if radiating shock waves are generated during the one-blade, one-vortex encounter modeled here. Thus, compressibility effects can be responsible for large increases in annoyance. However, in our tests of the AH-1S, the maximum value of η was about 0.90, which corresponds to an increase in annoyance of 3.0 PNdB over the basic triangular pulse shapes.

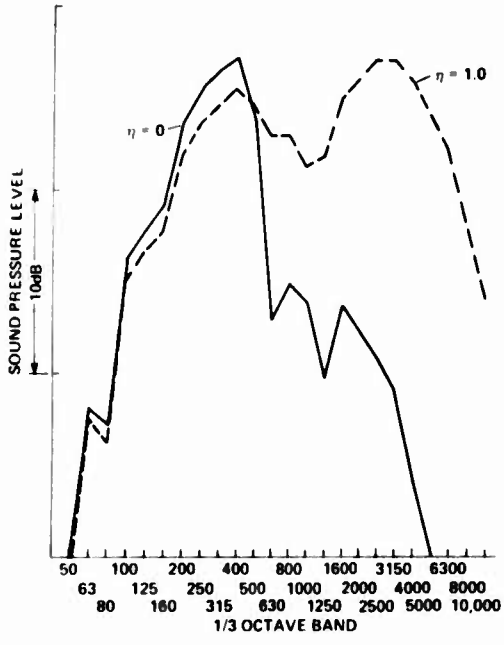

Figure 16.- Equivalent sound pressure level for equal annoyance in the 1000 Hz band.

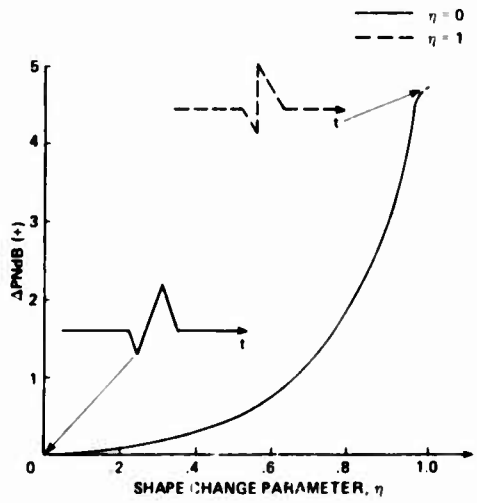

Figure 17.- Waveform steepening effects vs PNdB.

An interpretation of these analytical results in terms of the measured AH-1S blade-vortex interaction signatures can now be summarized. For the 60-knot, 400-ft/min rate of descent case, the acoustic signature of the 540 rotor is more sawtoothed than triangular. In fact, the positive pressure gradient of the 540 rotor is large for almost the entire length of the compression portion of the acoustic wave. In contrast, the expanded time histories of the K747 blades are nearly symmetrical, triangular pulses that the analytical model would suggest create very little "pulse-shape" impulsive annoyance. As subjectively noted in the previous analytical development, a large asymmetric character of the pulse can increase annoyance up to 4.7 PNdB while crest-factor and overall sound pressure level remain constant. The PNdB weighting procedure was also directly applied to the narrowband measured data (fig. 13) for the two AH-1S rotor systems. As was done previously for the idealized analytic pulse, these AH-1S averaged acoustic spectra were summed at the blade-passage frequency into one-third octave bands, and a perceived noise level calculated for each rotor. These measured data showed that the 540 rotor exhibited an increase of 4.0 PNdB over the K747 rotor, thus verifying that the simple analytical model does approximate the phenomena of interest. Again, no definite shocks were measured in any of the acoustic signatures — only quite large increases of pressure over short time intervals with the 540 rotor. Because these shock-like disturbances exist, they do generate substantial amounts of annoyance.

CONCLUSIONS

Comparative acoustic tests were conducted in flight on the Army AH-1S helicopter configured with the standard Bell Helicopter Textron 540 rotor blades and with the Kaman 747 improved main rotor blades. Far-field acoustic data defining the impulsive noise signatures of the AH-1S helicopter during high-speed flight and during partial-power descents were gathered for each rotor configuration.

High-speed impulsive noise was found to be considerably lower with the K747 blades. In terms of peak pressure levels, the K747 configuration showed significant noise reduction above an advancing-tip Mach number of about 0.85, and approached a peak-level reduction, by a factor of 2, at $M = 0.90$. For the 540 rotor blade system, an acoustic waveform transition from symmetrical to sawtooth dominated the acoustic signature for advancing-tip Mach numbers of 0.88 to 0.90. This transition event of high-speed impulsive noise was delayed by the K747 blades, with the result that radiated noise was substantially decreased.

These full-scale acoustic measurements have shown that there are many complicated, unsteady aerodynamic and acoustic events that govern blade-vortex interaction noise. Both rotors produced comparable amounts of noise due to blade-vortex interaction, if only peak pressure levels are of concern. Each configuration exhibited a different rotor-blade/tip-vortex interaction during descent, with the noise signature for the K747 blades less dependent on rate of descent. Compressibility effects were found to be important for the 540 rotor blades. These effects manifest themselves as sharp positive

pressure gradients in the blade-vortex interaction signature, but do not appear to steepen enough to become radiating shock waves. The resulting influence on annoyance appears to be significant. If the PNdB measure of annoyance is employed, the K747 rotor radiates significantly less blade-vortex interaction annoyance than the 540 rotor system.

REFERENCES

1. Kaman K747 Improved Main Rotor Blades. Production Validation Test - Government, United States Army Aviation Engineering Flight Activity (USAAEFA) Report, Project 77-38, Oct. 1979.

2. Fitzpatrick, J. E.: Technical Description Data for the K747 Improved Main Rotor Blade for the AH-1Q Helicopter. Kaman Aerospace Corp. Report P-83, Nov. 1975.

3. Schmitz, F. H.; and Boxwell, D. A.: In-Flight Far Field Measurements of Helicopter Impulsive Noise. J. American Helicopter Soc., Oct. 1976.

4. George, R. E.; and Duffy, V.: In-Flight Measurements of Aircraft Acoustic Signals. Advances in Test Measurement - Volume 14, Proceedings of the 23rd International Instrumentation Symposium, Las Vegas, Nev., 1977.

5. Schmitz, F. H.; Boxwell, D. A.; and Vause, C. R.: High-Speed Helicopter Impulsive Noise. J. American Helicopter Soc., Oct. 1977.

6. Boxwell, D. A.; Yu, Y. H.; and Schmitz, F. H.: Hovering Impulsive Noise - Some Measured and Calculated Results. VERTICA, vol. 3, no. 1, 1979, pp. 35-45.

7. Boxwell, D. A.; Schmitz, F. H.: Full-Scale Measurements of Blade-Vortex Interaction Noise. AHS Paper 80-61, May 1980.

8. Noise Standards for Helicopters in the Normal, Transport, and Restricted Categories. Notice of Proposed Rulemaking, FAA Notice 79-13, July 1979.

9. Galloway, W. J.: Subjective Evaluation of Helicopter Blade Slap Noise. Proceedings of an International Specialists Symposium on Helicopter Acoustics. May 22-24, 1978. (NASA CP-2052)

10. Pinker, R. A.: Mathematical Formulation of the Noy Tables. Journal of Sound and Vibration, vol. 8, no. 3, 1968, pp. 488-493.

APPENDIX G. EQUIPMENT PERFORMANCE REPORTS

The following EPR's were submitted during this test.

EPR Number	Date	Description
77-38-1	15 Sep 78	Skin void development and progression on K747 IMRB Maintenance procedures for K747 IMRB.
77-38-2	16 Sep 78	Skin voids on K747 IMRB.
77-38-3	28 Nov 78	Overheating of tailboom internal electronics compartment (insulation blanket found to be charred).
77-38-4	28 Nov 78	Mast bearing failure inspection requirement.
77-38-5	21 May 79	Excessive airspeed variations in climbs and descents.

DISTRIBUTION

Assistant Secretary of the Army (RDA)	1
Deputy Chief of Staff for Logistics (DALO-SMM)	1
Deputy Chief of Staff for Operations (DAMO-RQ)	1
Deputy Chief of Staff for Personnel (DAPE-HRS)	1
Deputy Chief of Staff for Research Development and Acquisition (DAMA-PPM-T, DAMA-RA, DAMA-WSA)	3
Comptroller of the Army (DACA-EA)	1
US Army Materiel Development and Readiness Command (DRCDE-DH, DRCQA-E, DRCRE-I, DRCDE-RT)	4
US Army Training and Doctrine Command (ATTG-U, ATCD-T, ATCD-ET, ATCD-B)	4
US Army Aviation Research and Development Command (DRDAV-DI, DRDAV-EE, DRDAV-EG)	10
US Army Test and Evaluation Command (DRSTS-CT, DRSTS-AD)	2
US Army Troop Support and Aviation Materiel Readiness Command (DRSTS-Q)	1
US Army Logistics Evaluation Agency (DALO-LEI)	1
US Army Materiel Systems Analysis Agency (DRXSY-R)	1
US Army Operational Test and Evaluation Agency (CSTE-POD)	1
US Army Armor Center (ATZK-CD-TE)	1
US Army Aviation Center (ATZQ-D-T, ATZQ-TSM-A, ATZQ-TSM-S)	3
US Army Combined Arms Center (ATZLCA-DM)	1
US Army Infantry Center (ATSH-TSM-BH)	1
US Army Systems Center (IGAR-TA, IGAR-Library)	2

US Army Research and Technology Labo- tories/	
Applied Technology Laboratory (DAVDL-ATL-D,	
DAVDL-Library)	2
US Army Research and Technology Laboratories/	
Aeromechanics Laboratory (DAVDL-AL-D)	1
US Army Research and Technology Laboratories/	
Propulsion Laboratory (DAVDL-PL-D)	1
US Army Troop Support and Aviation	
Materiel Readiness Command (DRCPM-CO-T)	5
Kaman Aerospace Corporation	5
Bell Helicopter	5
Defense Technical Information Center (DDR)	12